DETECTION OF SUB-MILLIMETER SCRATCHES IN TABLETS FOR FORENSIC ANALYSIS USING STRUCTURED LIGHT IMAGING

Graduation thesis by
Jitteke Struik
August 2003

Delft University of Technology
Faculty of Applied Sciences
Department of Applied Physics
Pattern Recognition Group

Supervisors
Prof. dr. ir. L.J. van Vliet
Dr. P.W. Verbeek

The Netherlands Forensic Institute
Departments of Digital Technology & Drugs

Dr. ing. Z.J.M.H. Geradts
A. Poortman-Van der Meer

Voorwoord

De belangrijkste reden voor mij om bij het NFI mijn afstudeerwerk gaan te doen was naast het feit dat ik dan eindelijk na al die jaren eens een keer de andere kant op kon fietsen, dat ik erg benieuwd was naar wat er hier allemaal gebeurt. Ik denk dat ik hier inmiddels wel lang genoeg rond gelopen heb om daar een redelijk beeld van te krijgen, hoewel ik me afvraag of dat wat er zich hier allemaal in de kelder van DT afspeelt nou wel zo representatief is voor hoe het er op de rest van het NFI aan toe gaat.
Maar goed, er was nog een tweede reden voor mijn komst naar het NFI ik had namelijk op een of andere manier de illusie dat als ik een contract van een jaar had om af te studeren dat ik dan ook binnen een jaar afgestudeerd zou zijn…
Dat het allemaal niet helemaal volgens planning is verlopen moge duidelijk zijn, over de redenen daarvoor is alles wel gezegd en zijn ook alle grappen al gemaakt. Maar hoewel er door sommigen tot op het laatste moment nog aan getwijfeld werd gaat dit meubelstukje toch echt niet mee verhuizen want na verscheidende malen kennisgemaakt te hebben met het fenomeen contractverlenging is het dan nu toch echt zo ver.
Ik wil dan ook van de gelegenheid gebruik maken iedereen te bedanken die er aan bijgedragen heeft dat Maarten eindelijk z'n pc's weer terug krijgt. Om te beginnen natuurlijk Lucas, Piet en Zeno voor de begeleiding van het project, de hulp op inhoudelijk en het vele geduld en begrip op persoonlijk vlak.
Voor het leveren van de benodigde middelen, allereerst Maarten voor 2 pc's 3 harde schijven 2 muizen, een paar (en nog een paar..) kleurenprintjes en een heleboel geduld, de gehele afdeling VM voor de thee, de pillen en de "vrijdagmiddagopvang", Caty voor de gezelligheid, steun en woordenboeken en tot slot Mapper voor het verstrekken van 2 laptops, 1 memorystick en 1 directielid...
Dan zijn er natuurlijk nog de mensen die de randvoorwaarden gecreëerd hebben waardoor er onder alle omstandigheden doorgewerkt kon worden zoals mijn trouwe personal assistant Marguerite. Mijn dank is groot voor de 3x daagse massages, de vitamineshots, de 10-daagse spoedcursus "presenteren op hakken" en vooral de lol. Vooral ook niet te vergeten Ief voor alle hulp, ijsjes en de mooie uitnodigingen.
Uiteraard wil ik ook mijn lieve vriendje BJ bedanken voor de continue steun op alle vlakken maar vooral voor het op zeer originele wijze wegnemen van de afstudeerstress door me er precies op tijd even aan te herinneren dat er ergere dingen zijn in het leven dan splitsende tabellen en onthoofde justitie logo's. Over de manier waarop valt te twisten maar de boodschap was duidelijk.
En dan, last but not least, in de categorie humor ende vermaak, Kees en Kees die naast het saboteren van m'n pc, boobytrappen van m'n kamer en de monsters op het toilet, er voor me waren op het enige moment in dit jaar vol rampen dat ik het echt niet meer zag zitten. Net toen ik me zat af te vragen of het op zou vallen als ik gewoon lekker niet meer terug zou gaan stonden daar ineens die twee "enge mannen" voor de deur..
Onwijs bedankt allemaal! Ga jullie stiekem toch wel een heel klein beetje missen.

Abstract

At the Drugs department of the Netherlands Forensic Institute XTC tablets are compared to identify common sources of manufacture. This is currently done by comparing the chemical profiles of the tablets. In this thesis it is investigated whether it is possible to identify which tablets have been manufactured with the same punch. Tablets that are compressed using the same punches are not recognized through chemical analysis when their chemical compositions differ. Punches may contain characteristic marks or damages, which are pressed into the tablets and can be used for identification. This report describes how these marks can be detected using a depth-image of the tablets obtained through structured light imaging. In chapter 2 the production process of XTC tablets, the manufacturing of punches, their characteristics and what specific problems they bring to the imaging process is discussed. Chapter 3 contains a theoretical description of triangulation systems, the structured light approach and a characterization of the specific setup present at the Forensic Institute. Triangulation systems are known to suffer from occlusion, chapter 4 starts with a theoretical analysis of the situation for the imprints in tablets. Based on the worst-case imaging scenario, a groove that is positioned parallel to the projected stripes, it is concluded that it is not possible to obtain reliable depth information of an entire tablet using a single recording. To make sure that all possibly present damages are detected, it is concluded that it is necessary to rotate the tablet and make multiple recordings in different positions. This way it is possible to obtain reliable depth information of an entire tablet. Experiments show that recording the tablets in steps of 20 degrees is required to properly image grooves of any orientation.

In chapter 5 the diameter and height of the smallest detectable bumps are determined to be 6μm and 10μm respectively. This is sufficient for this purpose while smaller marks on the punches will not be recovered in the tablets due to the grain size of the XTC mixture. In case there are no identifying bumps detected, the depth-images can be used for exclusion purposes. Large differences between the entire depth-images or features of the tablets that can be extracted from these depth-images indicate that the tablets under investigation were not manufactured with the same punch.

A listing of such features is given together with the questions involving their discriminating powers that must be answered in further research before they can be used to draw conclusions about the used punches.

Before the images of different tablets can be compared, they are matched using a Matlab routine that matches their Fourier-Mellin transforms through symmetric phase only matched filtering. Several experiments were conducted on paracetamol tablets as well as XTC tablets to determine the performance of this routine and to examine the possibility of comparing the recordings of the tablets through their Mean Square Error (MSE) values. The results show no overlap between MSE values of recordings of tablets that were manufactured with the same punch and the ones that were manufactured with different punches. No forensic conclusions can be drawn from experiments conducted on just a few tablets. Therefore it is recommended to fill databases with depth-images of XTC-tablets to obtain more statistical data in order to determine the relevance of differences in depth-images of tablets.

Table of contents

1 INTRODUCTION

"Controlled drugs are supplied to the illicit market in a variety of forms, including tablets, capsules, powders and solutions. The role of the forensic chemist is directed towards not only identifying the actual drug present but also to providing intelligence information for further use in demonstrating common sources of manufacture" [1].

This statement made in 1974 regarding amphetamine and in particular LSD, which were the most widely abused drugs at the time, holds now, almost 30 years later, due to the rise and exponential growth of XTC, more then ever. At the drugs department of the Netherlands Forensic Institute hundreds of XTC-tablets are submitted for analysis every week. Besides demonstrating the presence of substances that are under the regulations of the Dutch Opium law, more and more requests for comparison analysis come up. The results of these comparisons are used to prove relations in sources of manufacturing between tablets confiscated at different locations. These relations can indicate connections between suspects or reveal the extent of an organization. They can be used directly as evidence in court or as information for the police to give direction to an investigation.

At this moment the comparison of XTC tablets is done by chemical analysis, the conclusions are based on their chemical characteristics. Using different detection methods, like gaschromatography, mass spectrography and infraredspectrography the presence and concentrations of the different ingredients is examined.
The tablets can be distinguished based on differences in concentrations of the active ingredient MDMA, or on the presence and concentrations of different fillers and expedients. Syntheses-pollutes, by-products that are formed during the synthesis of MDMA are, if they are detected, also very useful for comparison purposes.

These chemical analysis are time consuming and therefore only performed in case it is expected to be very likely that the tablets in question are related. These suspicions of relations between tablets are based on appearance, physical features like size and shape. To give the tablets an innocent look and make them recognizable for consumers, the illicit manufacturers make tablets with an imprint of for instance animals or cartoon figures. The comparison starts with a visual inspection of these imprints, referred to as logos, if they are similar and the size and shape of the tablets are too, the chemical analysis can begin.
Now the question has risen whether it would be possible to identify common sources of manufacturing based on physical characteristics instead of chemical. If possible, physical methods will have several advantages. The most important one being that physical methods contrary to chemical are non-destructive. Chemical methods are not able to identify the use of the same punch in case of different compositions, therefore another great benefit will be that physical methods will recognize the use of the same punch regardless of composition, assuming the differences in composition do not result in large differences in physical features.
This report describes an investigation of the possibilities of this option. Besides using features as size and shape this study examines the discriminating powers of features that can be compared if depth-information of the surface of the tablets is available. This depth-information is obtained using an optical 3D- measuring system that is present at the Netherlands Forensic Institute.

The possibilities of the 3D measuring system, how it operates and what adjustments have to be made to make it applicable for this purpose are described in this report. The problem with

occlusion that was expected to occur using this kind of measuring systems, based on the literature and theory, did indeed occur. The consequences for this research and the solutions that will be implemented are also described in this report.

2 INTRODUCTION TO FORENSIC ANALYSIS OF XTC TABLETS

This chapter contains an inventory of the features of the tablets and punches that have to be explored. To determine the features and the measurements that have to be done, to be able to compare them properly, an extensive study was done on the production process of the XTC tablets as well as the punches that are used to compress them. Mutual dependencies between the different features are revealed and a proposal is done to determine their relevance.

2.1 XTC tablets

Figure 1 example of XTC tablets with different imprints

The tablets under investigation mostly contain MDMA, (3,4- Methylenedioxy-N-Methylamphetamine) commonly known as Ecstasy. The MDMA powder is mixed with some fillers and coloring agents and compressed into tablets. The illicit manufacturers often make use of punches resulting in tablets that bear an imprint consisting of all sorts of registered trademarks and fantasy figures. Figure 1 shows some examples of these logos.
For the selection of features that can be used in the comparison, it is important to know what aspects play a role in the determination of these features. To find out what these aspects are, the whole course that the tablets follow must be studied. The lifecycle of a tablet can be divided into three phases:

2.1.1 Phase 1: production of the XTC powder

Besides the actual drug, MDMA, several other ingredients are added for different reasons.
For starters if the drug is very potent and the dose required in the tablet is very small, the tablet may need to be bulked out with filler such as starch, to prevent the tablet from being unacceptably small. Secondly it's rather unlikely that the drug itself will possess the physical characteristics needed to compress it into a satisfactory tablet that does not crumble when handled. It is usually necessary to add a stabilizer (i.e. another material, such as cellulose) that does have these desirable compression characteristics.
In addition to direct compression another method to make tablets that is widely practiced is called wet granulation in which the tablet powder undergoes a special granulation process before being compressed. In wet granulation, a wet mass of the powder is formed using a granulating solution containing a binding agent. This is then "chopped" into small granules and dried prior to compression into a tablet. A benefit of this method is that the active substance will be well spread.
Disintegrants, traditionally maize starch, which swell when they come into contact with body fluids, can be added to a tablet to promote its disintegration after it is taken.
It might also be necessary to add a lubricant to the tablet powder, such as talcum, to improve powder flow in the tablet machine and finally to prevent the tablets from sticking to machine components Magnesium stearate can be added as well.

This shows that a tablet is not really a simple dosage form and the drug itself ends up being just one of many ingredients in the tablet.
Obviously this will have important implications for the forensic chemist while different manufacturers might use different fillers or stabilizers. Thus in case tablets from two different manufacturers contain the same dose of the actual drug, they might still be distinguished based on the presence and concentrations of these added substances. The exact consequences for the physical comparison methods need to be determined, but it is clear that in this first phase the chemical composition of the XTC-powder is determined and therefore it influences the features through density, sticky-ness and bulk modulus.

2.1.2 Phase 2: production of the tablets

Tablets are made from a powder that has been compressed so that it forms a coherent mass. This is done by feeding the powder into a metal well (die) in a tablet machine and compressing it between two steel rods (punches). The simplest type of tablet press is the single-station machine, having only one pair of punches, [15]. A rotary tablet machine will contain many such dies and punches and a hopper containing the powder fills the dies as the machine rapidly rotates. Figure 2 shows an example of a confiscated tabletting machine.

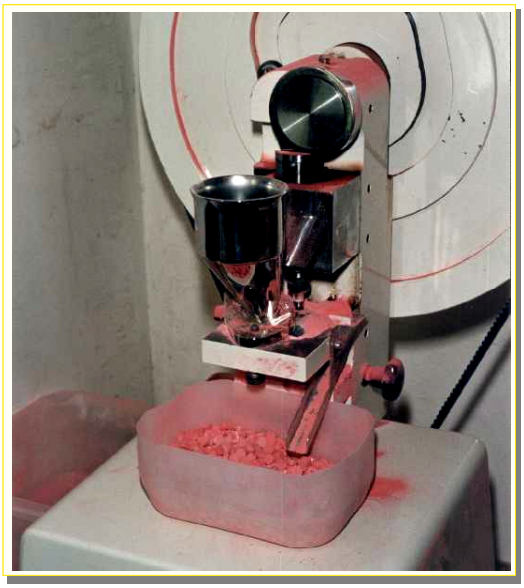

Figure 2 picture of a confiscated tabletting machine

In this phase choices for the upper and lower punch are made as well as choices for the thickness and the used pressure. Therefore this phase has great influence on the features that depend on the used pressure. Another very important aspect in this phase is the influence of wear and tear on the machine, the dies and punches. How many tablets are made with the same punch before it is worn out? How do the features of the tablets change over time due to this wear and tear process?

2.1.3 Phase 3: Time period between the moment the tablet was produced and the moment that it is being examined.

The aspects that play a role in phase 3 are the most difficult to define, because anything can happen in this period, the tablet can deform due to absorption or changes in temperature. It can be damaged during transportation or in someone's pocket etc. Important to realize though is that any kind of damage that is done to the tablets in this phase will result in "less tablet". Scratches or missing parts of the tablet in any shape or form are clearly distinguishable from deviations in the tablets due to damages on the used punch. Damages on the punch will result in "more tablet". A scratch on the punch will create a heightening on the tablet during tabletting that can never be the result of damaging after production

2.2 Punches

Figure 3 examples of punches

To find out more about the manufacturing process of the punches in general a legal punch maker was visited. Turns out that the lifecycle of a punch can be divided in different periods as well in which choices are made that have an effect on the features that can be used in the comparison process. Figure 3 shows some examples of different shaped punches.

2.2.1 Phase 1: the manufacturing of the Master

A single punch can be manufactured directly but another widely used method is to produce multiple punches from one master. First the steel master punch is shaped on a turning lathe. To make sure that the punches can be easily removed from the dies during tabletting they are shaped a bit conical, how much exactly depends on the tablets that have to be made with it but it's usually in the order of 15 seconds. The steel is then solidified, it is heated in a furnace up to 800-1000 degrees and cool down again in oil at 100 degrees. The tension that was built up in the steel by suddenly cooling it off is released by tempering it at 250-300 degrees. To smoothen the surface of the punch the steel is not just honed but lapped as well. Lapping is prepared by smearing a bit of lapping paste that contains diamond powder onto a stick and rub it over the steel punch.
Three possible machining methods to create the logos in the punches are milling, engraving and spark erosion. When using one of the first two techniques the punch will have to be smoothened again afterwards. Polishing the punch with lapping paste can smoothen possible cutter scratches but will not remove them entirely.

2.2.2 Phase 2: making multiple punches out of a single master

The punches that are actually used to make the tablets are impressions of the master punch. These impressions are made with a hobbing press. The hob master that was made of hardened steel is pressed into a mould of unhardened steel creating thereby a negative of the engraved logo in the mould. By repeating this process multiple punches with the same logo can be manufactured. Before using them to make tablets the moulds will have to be hardened as well in the same way as described above for the master punch.

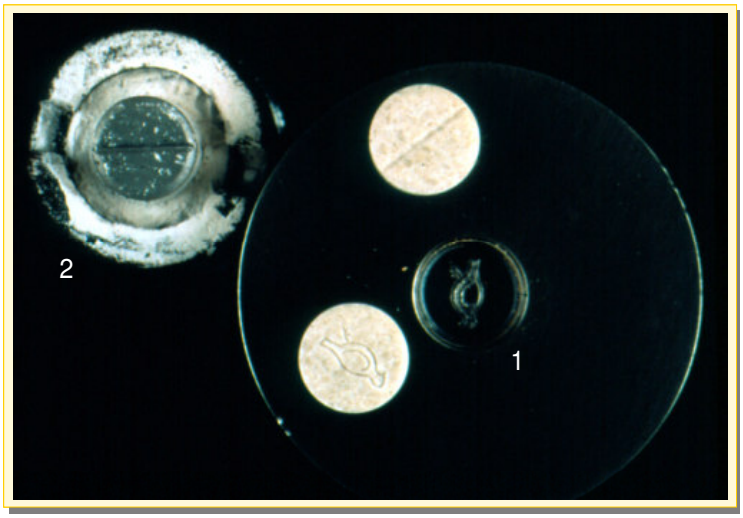

Figure 4 example of both upper and lower punch used to compress XTC tablets with a pelican logo

2.2.3 Phase 3: the period in which the punches are actually used to make tablets.

In this phase the punches will start to wear off, they can be damaged during production or might be dropped by someone. Rusting can occur due to poor storage conditions in the presence of acids or other nasty substances. The same reasoning as for the tablets holds here as well, the damages done to the punches or their imprints in this phase must be distinguished from deviations due to slovenliness during manufacturing. Contrary to the first, the last category scratches cannot automatically be classified as unique. It depends on the techniques that were used to manufacture the punch and the specific scratches whether they are reproducible or not. More information about the characteristics of the used production methods is necessary to determine whether present scratches can be used to identify a certain punch and belonging tablets. In this thesis this aspect is not studied further its focus was on the detection of the damages the conclusions about their source and thereby discriminating powers is left for further research. Relevant for this thesis is the fact that the scratches that are searched for are most likely to occur on the edges of the punch and its imprint. The parts that are sticking out are most vulnerable to damaging. The same areas on the tablets are contrary to the ones on the punches the least vulnerable to damage while parts that are sticking out on a punch are not on the tablet. Thus because the scratches in these areas are most likely to survive phase three of the life of the tablets they are most interesting for this research.

2.3 Feature Selection

The selection of the features that can be used in the comparisons is a complex process, starting with a list of all the features that one can think of. Then a specific measurement must be defined to determine each of the features. For each measurement, the uncertainties, and possible problems of the used measuring method must be documented. Besides knowing how precise the measurements can be done, it is also important to know how relevant the features are. When for example the uncertainties that come with the measurements are greater than the differences among tablets or punches themselves, there is no point in using this feature for comparison, because it is impossible to identify matches based on this kind of measurements. Another type of useless features are the ones that depend on too many steps in the manufacturing process so that the consequences of the different steps are untraceable, making it impossible to draw conclusions about matching or non-matching.
If for example it turns out to be impossible to determine whether differences in measurements result either from the use of different punches or the use of different pressures during compression, then a definite conclusion has to be made based on other features. All these aspects need to be examined so the selection process can be summarized as follows:

- List of all measurable features
- Determine for each feature how precise it can be measured, how relevant it is and where it depends on.
- Draw conclusions about the utility of each feature based on the answers of the three questions above.
- Determine final list

In this chapter only the first bullet is treated and the second is described in the form of a plan. The plan describes what measurements need to be done to determine the uncertainties of the features listed below and what questions involving their relevance need to be answered in the future. The third and fourth steps were not performed in this project while the main focus was on the imaging process. This report describes the investigation of the possibilities of the measuring method and whether reliable measurements of the features are even possible with the available system.

2.3.1 Features

When the tablets arrive at the drugs department they will be submitted to visual inspection first. Shape and color are the principal features that assist in the initial identification of tablets from a common source. The collection of confiscated tablets shows that a large variety of shapes is used, including round, oval, hexagonal and even animal shapes. The faces can be flat, convex or concave and the edges plain, rounded or beveled. Designs or lettering on the faces can be imprinted and break lines may be applied to afford an easy means of dividing the tablet into halves or quarters. Color is added to tablets for the aesthetic appeal together with a funny logo it gives the tablets an innocent look. A visual or low power microscopic inspection can detect a mismatch based on shape of the tablets or the shape of the imprint on the tablet. The next step in the comparison process is the measurement of the diameters and thickness of the tablets using an electronic micrometer.

In case the tablets are not circular the longest and shortest sizes of the tablet are measured. After this the only physical feature that is left that can be determined is the weight of the tablets, using an analytical balance. The results of these measurements are documented and used to support the conclusions that result from chemical analysis, but they are not sufficient to lead to hard conclusions about the used punches on there own.
However, using the depth-image that can be obtained with the MicroCad measuring system many more physical features can be determined so that it might be possible to draw more definite conclusions about the used punches. Especially in case that the production of the MDMA was done by different people while for the tabletting the same machine and punch was used chemical analysis can only detect the mismatch in source of the XTC powder. However by doing a physical examination a match in used punches can be detected no matter what tablets were made with it.

2.3.2 List of features

- Position of the logo on the tablet and its position with respect to the break line
- Diameter or comparable parameters in case the tablet is not circular.
- Thickness of the tablet
- Depth, width and angle/slopes of the break line
- Depth and angles of the logo
- Several roughness parameters
- Angle of the edges of the tablet in case they are beveled or the radiuses in case they are rounded

2.4 Determination of uncertainties in measuring angles, depths and widths.

2.4.1 Break line:

Take 10 recordings of the same tablet. To avoid problems with occlusion and shadows, the tablet should be positioned in a way that the break line lies in the direction of the projector. Before each recording, replace the tablet, refocus and readjust the lightning, to simulate the situation of recording the tablets at different points in time. Take a cross-section perpendicular to the break line in each of the recordings. Match the images with each other beforehand to assure that the cross-sections are taken at the same position. To rule out accidental deviations use the mean of 10 neighbouring pixels for these cross-sections. Calculate in all recordings the slope, depth and width of the break line and determine their means and standard deviations
To make sure the same distances are measured always take the two points with the largest distance between them.

2.4.2 Logo characteristics

Take 10 recordings of the same tablet but now with the logo side up. Again readjust the lightning, refocus and replace the tablet before each recording to try to simulate the future situation when

comparing tablets, as good as possible. Be aware of occlusion problems, it might be necessary to take more then one recording to be able to image the whole tablet properly.

2.4.3 Tablet characteristics:

Depending on the shape of the tablet certain measurements can be done. In case the edges are bevel, the angles of the edges can be determined, or the “roundness” in case of rounded edges. The uncertainties of these angles can be determined following the same kind of procedure as with the angle of the break line, only both sides of the tablet have to be recorded. The tablets have to be positioned in such a way that the angle that is under observation is recorded properly, meaning, be aware of occlusion.

2.4.4 Diameter of the tablet

First check if there is indeed a diameter, the tablet might not be circular. Measure the diameter 10 times and calculate the mean and standard deviation of these measurements.

2.4.5 Thickness of the tablet:

Uncertainties can be determined in the same way as for the diameter. Care should be taken in case of ‘difficult’ tablets, tablets with shapes and logos that make it difficult to decide where to measure the thickness.
The thickness can probably be determined easier using an electronic micrometer but it is recommended to use the Microcad system in case of these ‘difficult’ tablets, while with the Microcad it is possible to measure heights on exact locations.

3 MEASURING SYSTEM

To find out what the uncertainties, limitations and possible problems of the measuring system are, it is necessary to understand exactly how it operates. The theory behind this kind of systems will be explained first and after that there is a description of the specific setup at the Netherlands Forensic Institute. The possibilities of the software that is used by the MicroCad system will be described shortly. The chapter ends with the characterization of the system.

3.1 Triangulation systems using active illumination

The calculation of the height values is done by triangulation. Triangulation systems are based on the method that is used by the human visual system to obtain depth information, see [2]. The two eyes image an arbitrary point on different locations of their retinas. The difference in location is called disparity. For the human brain is it a simple problem in trigonometry to identify the position of the observed point from this disparity. But in stereovision, where two cameras are used as eyes, it turns out to be rather difficult to find the corresponding points in the two camera images. This correspondence problem can be solved by replacing one of the cameras with a projection unit which projects known light patterns or another kind of light source such as a laser that projects a controllable beam. Because a system like this creates its own illumination as a part of the measuring technique it is a form of active triangulation whereas stereovision is a passive triangulation method.

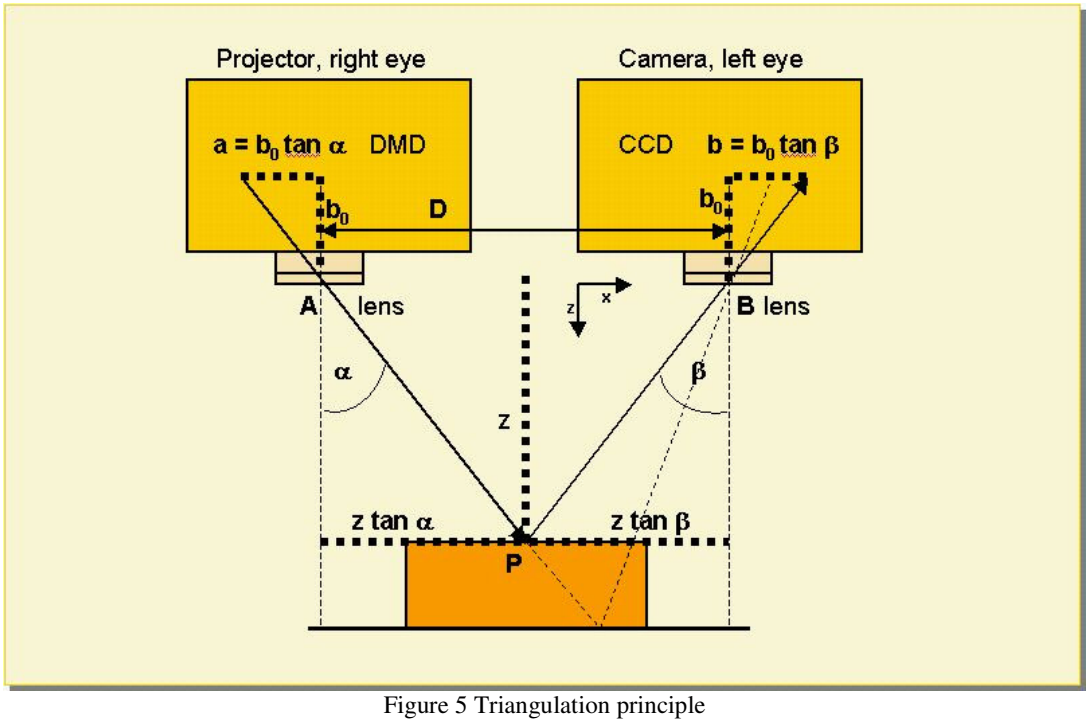

Figure 5 Triangulation principle

The principle of triangulation is presented in Figure 5. When the exact geometry of a setup is known, it is possible to calculate the height at every position of the examined surface. In this example a CCD camera and a DMD projector are used as “eyes” and their optical axes are

assumed to be parallel. Furthermore, their image planes coincide, their image distances b_0 are equal and their lens centers are in the Figure 5 indicated by points A and B. If now the points P that have to be measured are assumed to be in the plane through both optical axes the following expressions can be defined:

- Eye distance $\equiv D = z \tan \alpha + z \tan \beta$
- Triangulation angle $\equiv \gamma = \alpha+\beta$
- Disparity $\equiv a + b \equiv b_0 \tan \alpha + b_0 \tan \beta = b_0 D/z$

The expression for the disparity can be rewritten into an expression for the depth z

- Depth $\equiv z = b_0 D/(a + b)$ [1]

Because the depth is inversely proportional to the disparity $\equiv a + b$, the measuring error of depth dz depends on the errors made in the determination of the image positions a and b, da and db and this error can be found by partial differentiation

- Depth measuring error $\equiv dz = \delta z/\delta a\, da + \delta z/\delta b\, db$
  $= -(z^2/b_0 D)\,(da + db)$ [2]
  $= -(D/z)^{-2}\,(D/b_0)\,(da + db)$

To minimize this measuring error the eye distance D must be large compared to the measured depth z and because

- $D/z = \tan \alpha + \tan \beta$ [3]

a small measuring error demands a large triangulation angle γ.

In the configuration that is used for the MicroCad the CCD camera is positioned perpendicular to the object that is under observation so in this case the angle β is zero. The choice for a specific configuration defines the possibilities of the system with respect to the visible regions. The consequences for this particular setup in terms of occlusion problems will be discussed in the section problems and solutions.

3.2 Structured light

There are many active range imaging techniques that use different kinds of illumination, see [2]-[5]. The simplest realization is scanning a scene by a laser beam and detecting the location of the reflected beam. This location is determined in the presence of the object under examination and in the recording of the reference plane. The difference in location of the spot in both situations is used to calculate the height of the object. Thus in order to obtain an M x N image using a single spot illumination, the spot has to be scanned in two directions and M x N measurements have to be made. In sheet-of-light range imaging a sheet (or line) of light is projected onto the object resulting in range data along that line. To extract dense range data this line needs to be scanned across the scene, but because scanning takes place in only one direction, in this case only N measurements are needed for an M x N image. The projection of multiple lines in each image can

speed up this process by making scanning unnecessary but it also introduces a dilemma, how many lines should be projected simultaneously? When projecting too little important height differences might be missed if they lie in between consecutive lines but projecting too many introduces an ambiguity problem. If there are too many lines projected, they lie so close together that large height differences might cause them to shift so much that they cross over each other making it impossible to determine which of the projected lines is under observation.
A solution to this problem is found in the structured or coded-light approach, in which the projected stripes are encoded. If each beam has a unique coding as many stripes as needed for good resolution can be projected without causing identification problems. There are many different encoding techniques, the MicroCad system uses a form of time encoding.

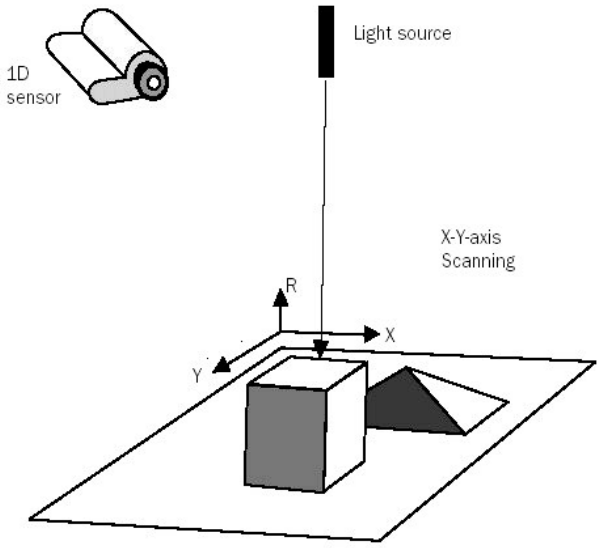

Figure 6 Single-spot range imaging, 2-axis scanning is required for complete 2D range image acquisition.

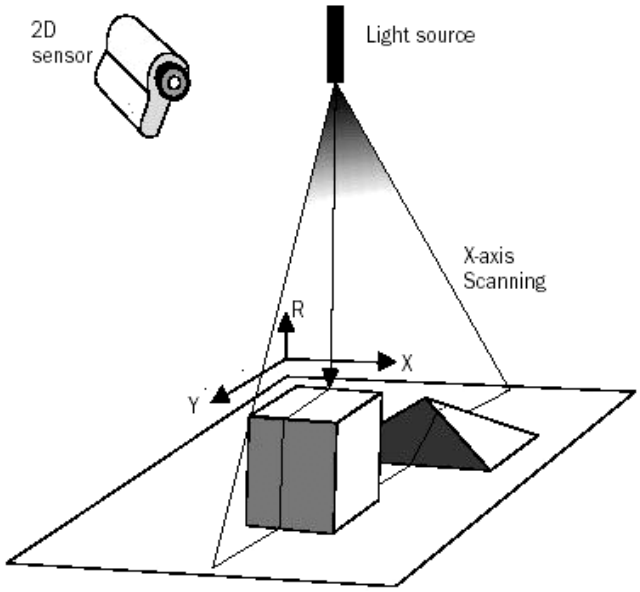

Figure 7 Sheet of light range imaging, 1-axis scanning is required for complete 2D range image acquisition.

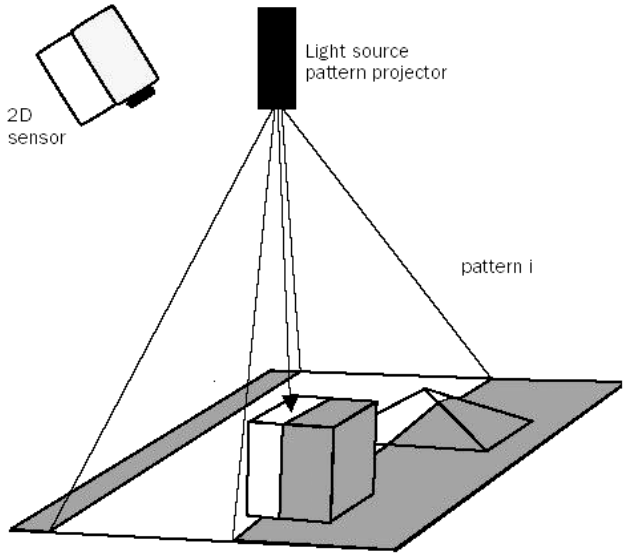

Figure 8 Range imaging with coded light, no scanning is required for complete 2D range image acquisition

3.2.1 Time encoding

Using n-bit binary numbers 2^n beams can be distinguished, these numbers can be added to the beams as a time series. When this is done for each beam simultaneously, a total of n patterns is projected successively.

The patterns that are projected consist of black and white stripes. The dividing line between the white, illuminated bands and the black, non-illuminated bands, is used as contour line. If the surface that is under examination is not flat, the reflected patterns which are recorded by the camera will be distorted. The location of the distorted lines is detected and compared to the location of the lines in the recording of the reference plane, the relative displacement of the contour lines is then used to calculate the height difference.

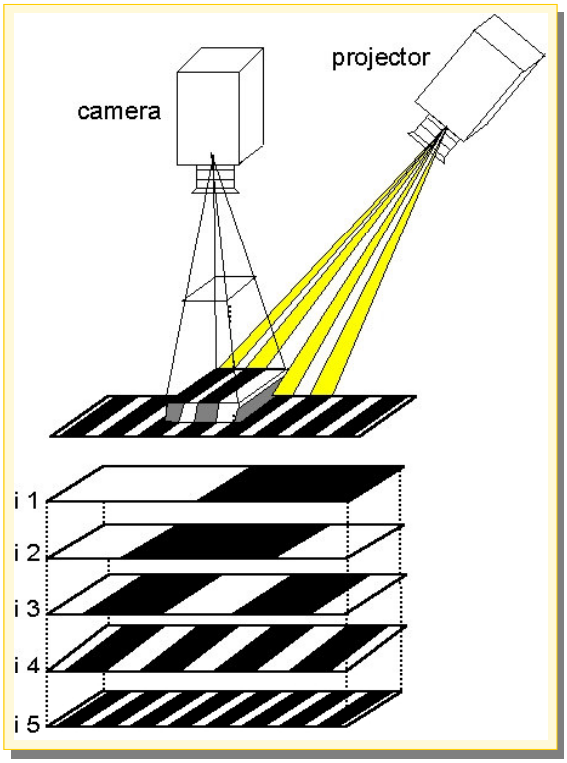

Figure 9 Gray code patterns

The patterns that are projected are chosen in such a way that no two patterns have the same contour lines and a contour line is uniquely identified by the illumination levels at the same point in the previous patterns.
Each of the patterns is actually projected as a differential pair, that is, each of the images and its complement: stripes that are on in the first of a pair are off in the second and visa-versa. The use of differential pairs reduces the sensitivity of the system to background illumination levels and to changes in surface reflectivity.
For the encoding the Microcad system makes use of Gray code, which is a special form of binary code. A Gray code is a way of encoding binary numbers so that only a single digit changes from one number to the next. That means that only a single 0 can change to a 1, or a single 1 can change to a 0, both Gray and binary encoding are shown in Figure 10. If one of the projected patterns is shifted by accident, the resulting error in case of gray encoding will be small while for binary encoding this error can be significant. As can be seen on the right of Figure 10 a shift of one of the projected patterns will result in a change of the position of black and white transitions for the belonging column. This change will result in an erroneous code for the line at the position of the black and white transition. The code tables on the left of Figure 10 prove that when the lines are gray coded the erroneous code will always be the one of a neighboring line while for

binary coded lines the erroneous code might be the one of a few lines further leading to much larger errors.

Line	Binary			Gray		
1	1	1	1	1	1	1
2	1	1	0	1	1	0
3	1	0	1	1	0	0
4	1	0	0	1	0	1
5	0	1	1	0	0	1
6	0	1	0	0	1	1
7	0	0	1	0	1	0
8	0	0	0	0	0	0

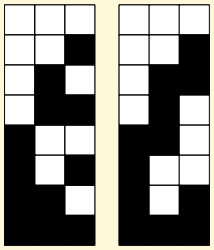

Figure 10 Gray versus ordinary binary encoding

Since measurements take place along the transitions between black and white stripes, the height resolution depends on the number of stripes that is being projected. N patterns are used to encode 2^N-1 transitions, the j-th pattern contains 2^{j-1} transitions. The more transitions the higher the resolution but in the gray code method the smallest stripes are still several pixels wide and the same height value is assigned to all these pixels, thereby making the limited resolution the major drawback of this method.

3.2.2 Phase-shift

Phase-shifting is another encoding technique that is also implemented in the Microcad system. The phase-shift method makes use of a sine-shaped intensity profile. This profile is shifted several times with a certain phase and the resulting profiles are projected successively. Again, the determination of the height on each position is done by comparing the recordings of the reflected patterns in the presence of the object of interest with the recordings of the reference plane. However in this case it is the difference in phase on each position in both situations that is used to calculate the height. To be able to determine the phase and thus the phase difference projection of at least 3 shifted patterns is required. Figure 11 shows an example of such shifted patterns. The Microcad system projects 4 sine shaped intensity profiles, the phases of these profiles are shifted over $\pi/2$ with respect to each other.

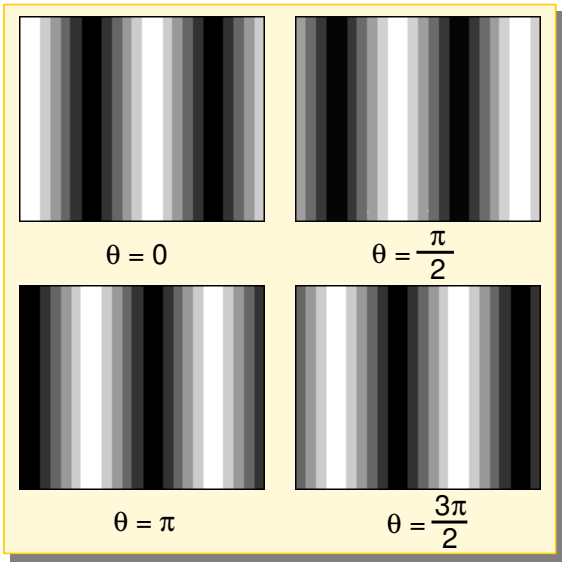

Figure 11 Phase-shift patterns

The four patterns are projected on both the reference plane and the object, the calculation of the phases in both situations is done using the following procedure. The intensity at every position with co-ordinates (x,y) can be represented by

$$I(x,y) = U(x,y) * \left[1 + C(x,y) * \cos(\varphi(x,y) + \theta\right] \qquad [4]$$

In this formula *U(x,y)*, represents the brightness of the background, θ the phase shift of the projected pattern and φ is the phase angle. The contrast *C(x,y)* is calculated using

$$C(x,y) = \frac{(I_{max} - I_{min})}{(I_{max} + I_{min})} \qquad \text{with } I_{max} = U + CU \text{ and } I_{min} = U - CU \qquad [5]$$

For every position four intensity values are measured in the reflected patterns, I_1, I_2, I_3 and I_4, using [4] they can be written as

$$\begin{aligned} I_1 &= U * \left[1 + C * \cos\varphi\right] \\ I_2 &= U * \left[1 + C * \cos\left(\varphi + \frac{\pi}{2}\right)\right] \\ I_3 &= U * \left[1 + C * \cos(\varphi + \pi)\right] \\ I_4 &= U * \left[1 + C * \cos\left(\varphi + \frac{3\pi}{2}\right)\right] \end{aligned} \qquad [6]$$

Because $\cos\left(\varphi+\frac{\pi}{2}\right)=-\sin\varphi$, $\cos(\varphi+\pi)=-\cos\varphi$ and $\cos\left(\varphi+\frac{3\pi}{2}\right)=\sin\varphi$, the formulas in [5] can be rewritten as follows:

$$\begin{aligned} I_1 &= U + UC * \cos\varphi \\ I_2 &= U - UC * \sin\varphi \\ I_3 &= U - UC * \cos\varphi \\ I_4 &= U + UC * \sin\varphi \end{aligned} \qquad [7]$$

Combining I_1, I_2, I_3 and I_4 gives:

$$\begin{aligned} I_2 - I_4 &= -2UC * \sin\varphi \\ I_3 - I_1 &= -2UC * \cos\varphi \end{aligned} \qquad [8]$$

together with the expressions in

$$\begin{aligned} \sin\varphi &= \frac{I_2 - I_4}{-2UC} \\ \cos\varphi &= \frac{I_3 - I_1}{-2UC} \\ \tan\varphi &= \frac{\sin\varphi}{\cos\varphi} = \frac{I_2 - I_4}{I_3 - I_1} \end{aligned} \qquad [9]$$

this finally results in an expression for the phase angle φ :

$$\varphi = \arctan\left(\frac{I_2 - I_4}{I_3 - I_1}\right) \qquad [10]$$

When this phase angle φ is calculated for both situations, reference plane and object, the difference in phase, $\Delta\varphi$ can be determined for each position. Using this difference in formula [10] the relative height can be calculated for every position on the object.

$$Z_{rel}(x, y) = \frac{\Delta\varphi(x, y) * \lambda}{2\pi} \qquad [11]$$

In this formula Z_{rel} represents the height of the measured object at position (x,y) with respect to the reference plane and λ, the period of the sine shaped profile that was projected.

Because the phase is continuously distributed within its range of non-ambiguity, a theoretically infinite height resolution can be obtained, actually limited only by the errors that are due to gray-level quantization and noise. The major drawback in the phase-shift approach results from the

fact that the range of non-ambiguity is limited to the interval of 0-2π, strongly reducing the height range.

3.2.3 Combination of Gray code and phase-shift

To exploit the positive features of each method and compensate for their drawbacks a combination of both methods was designed and this combination, the phase-code method is used by the MicroCad system. First, several patterns of the gray code method are projected to deal with the large height range, then the four patterns of the phase-shift method are projected to realize the desired high resolution. The phase-shift technique acts as a refinement on the Gray code technique. The period of the last projected Gray code pattern, the one with the smallest stripes is used as wavelength for the sine shaped intensity profiles. In this way the phase measurements are used to interpolate in the region in between the smallest height steps that resulted from the Gray code measurements. This can only be done under the assumption that the surface contains just gradual changes in height in these regions. The determination of the phase differences and the calculation of the heights is done by the procedure described above, but because in this case the period of the Gray code pattern is used as wavelength, formula [11] can be rewritten as follows:

$$Z_{rel}(x,y) = \frac{\Delta\varphi(x,y) * h_{\min}}{2\pi} \qquad [12]$$

with $Z_{rel}(x,y)$ the height difference with respect to the height determined by the gray code method at position with coordinates (x,y) and h_{min} the minimal observable height difference that results from the Gray-code measurement.

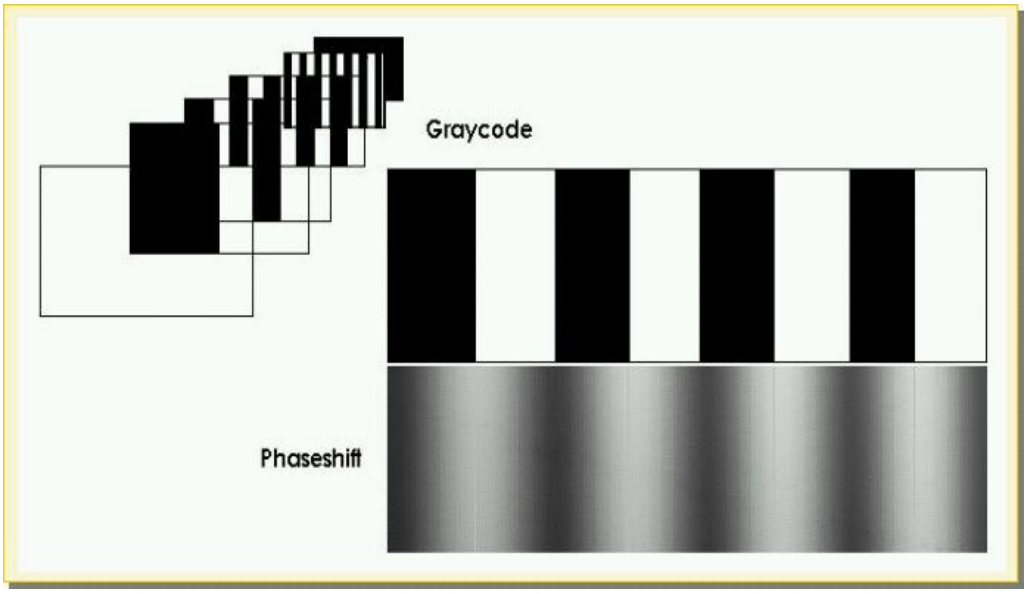

Figure 12 Patterns used by the Phase-shift and Graycode combination method

Besides the combination of the two methods it is also possible to use them both separately. The pure phase shift is the fastest method because only a few patterns are projected. Therefore it can be useful for moving, for example living samples. If the Gray-code method is applied greater height variations can be handled, but the resolution is not as good as with the phase-shift. For the examination of XTC-tablets it is necessary to be able to measure greater height differences. If also the best resolution possible is desired, then the combination method should be used, in this way the advantages of both methods are combined. The 15 seconds that it takes to do these measurements is not a problem in this case, because the tablets do not move.

3.3 The projection system

The system that is used to project these black and white patterns is based upon Digital Light Processing™ (DLP™), developed by Texas Instruments Inc, see [6]. DLP™ differs from the LCD projection based systems because it makes use of a Digital Mirror Device™ (DMD™). The DMD is a single chip containing a matrix of 800 x 600 aluminum square mirrors. Each mirror has an area of 16x16 mm^2 and acts as a binary light switch that can reflect the incident light into the aperture of the projector lens. The mirrors can be tilted over an angle of +/- 10 degrees to an "ON" and "OFF" state in less then 20 µsec. The light reflected from the "ON" mirror is directed to an image point, light from an "OFF" mirror is reflected away from the aperture. All micro mirrors move accurately to project a digital grayscale image at video rate (40 msec). If a micro mirror is always "ON" during a sequence of images, a maximum intensity will be produced. (in 8 bit grayscale; 255) A gray value of 128 for example can be produced by turning the mirror to the "OFF" state during half the time. In this way the whole image is directly built bit by bit for all pixels parallel.

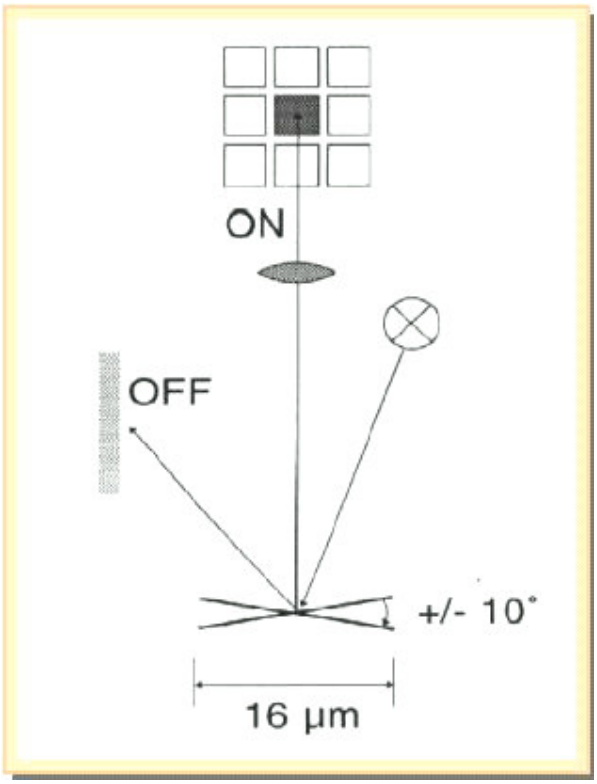

Figure 13 Function principle of a DMD

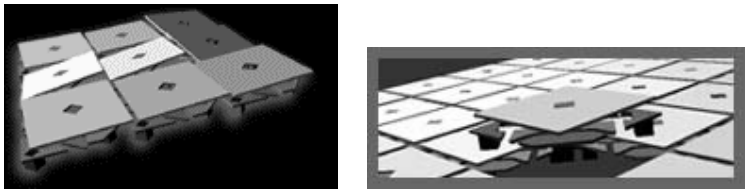

Figure 14 left: tilting of the mirrors, right: hinge-mechanism

Figure 13 demonstrates the principle of the Digital Mirror Device and two pictures in Figure 14 show the tilting of the mirrors and the hinge mechanism. Using DLP instead of LCD projection has several advantages:

- High light efficiency: The DMD pixel elements are highly reflective aluminum mirrors, using a hidden hinge technology the DMD is able to realize an active mirror area of 90%. Due to optical diffraction that occurs in practice, effectively 80% of the incident light is finally reflected. Compared to LCD based systems where the efficiency can be as low as 25% due to necessary polarization this very good.
- High contrast ratio: the high fill factor together with the large active area, (the gaps between the mirrors are small (2 µm)), result in a high signal to noise ratio.

3.4 Microcad system

Figure 15 is a picture of the Microcad system as it is present at the Netherlands Forensic Institute. The above described projection system (2) projects together with a variable light source (3) the black and white structures onto the object that is placed at the measuring-area (5). The digital camera (1) records the possibly distorted, black and white line structures that are reflected by the object's surface. The recorded data of the observed images is processed by the computer (4) and used to calculate the height-profile of the object under observation.

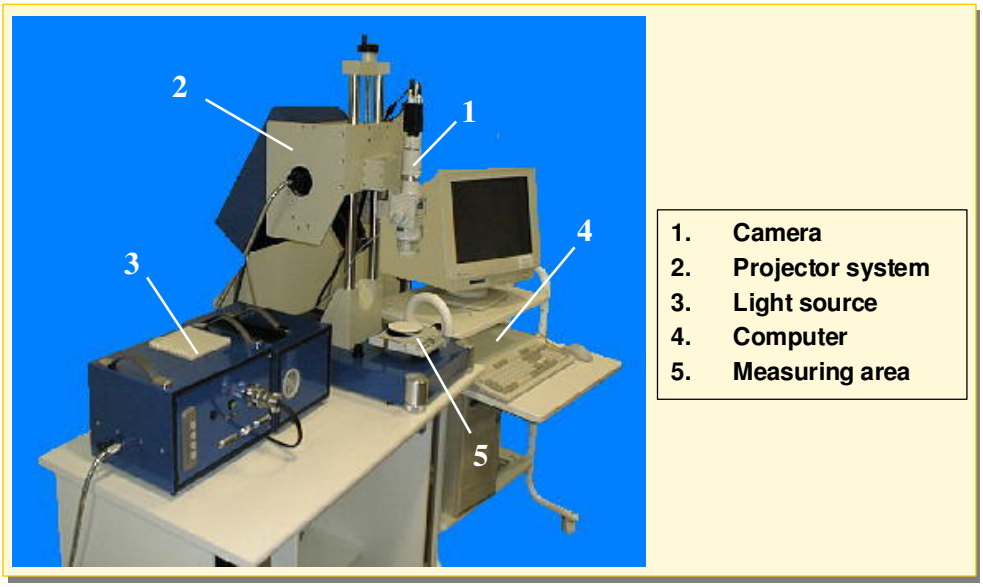

Figure 15 Microcad measuring system as it is present at N.F.I.

Besides understanding how the Microcad operates it is also interesting to know what it can do. To find out all the possibilities, a lot of experiments were performed using all the options presented by the software. Before measuring a few parameters have to be adjusted to the specific situation. One of these parameters is the illumination. Because the system can be used for different measurement tasks, the optical characteristics of the objects to be measured can be very different. In case of strongly reflecting surfaces and unfavorable angles, only a small quantity of light falls into the aperture of the camera lens. Opening up the aperture is possible up to a specific limit and has the disadvantage that in case of a wide opened aperture only a small focusing range is available. For this reason it can be necessary to use the possibility of the frame grabber to adjust the light amplification. This gain can be adjusted from the software.
The level of magnification can be chosen depending on a trade-off between desired magnification and desired size of the field-of-view.

3.4.1 Software

The windows-based software controls the measurement operations as well as the image processing and analysis operations. The standard output of a measurement is a 2D gray value image, the left picture in Figure 16 is an example of such an image. The height at every position

is represented by different gray values in such images. These 2D profiles can also be represented in 3D, the 3D representation of the image on the left is displayed on the right in Figure 16.

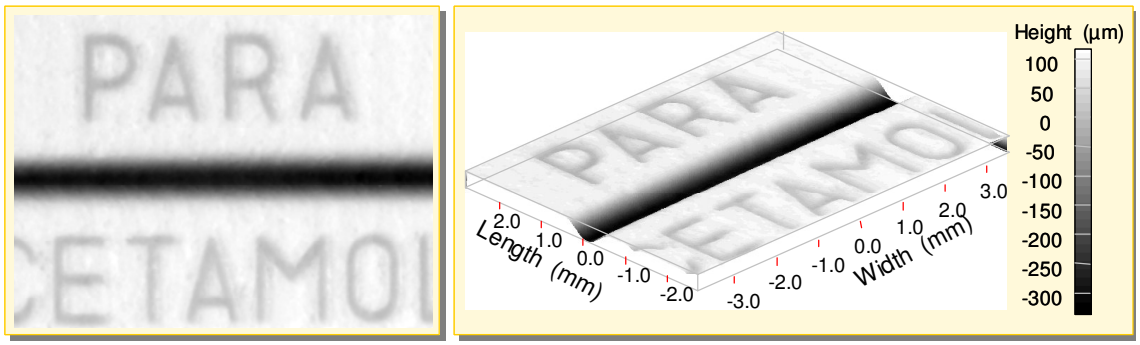

Figure 16 Example gray scale image, right: 3D representation of 2D profile on the left

The image can undergo many different operations, several different filters can be applied and the profiles may be leveled, zoomed or scaled. Cross-sections can be taken at every position in every direction. In these cross-sections it is possible to measure several kinds of distances, heights, widths and angles. Roughness parameters can be determined in the 2D profiles as well as in their cross-sections, and roughness or waviness profiles can be displayed. An example of a cross-section with calculated distance and angle is plotted in Figure 17.

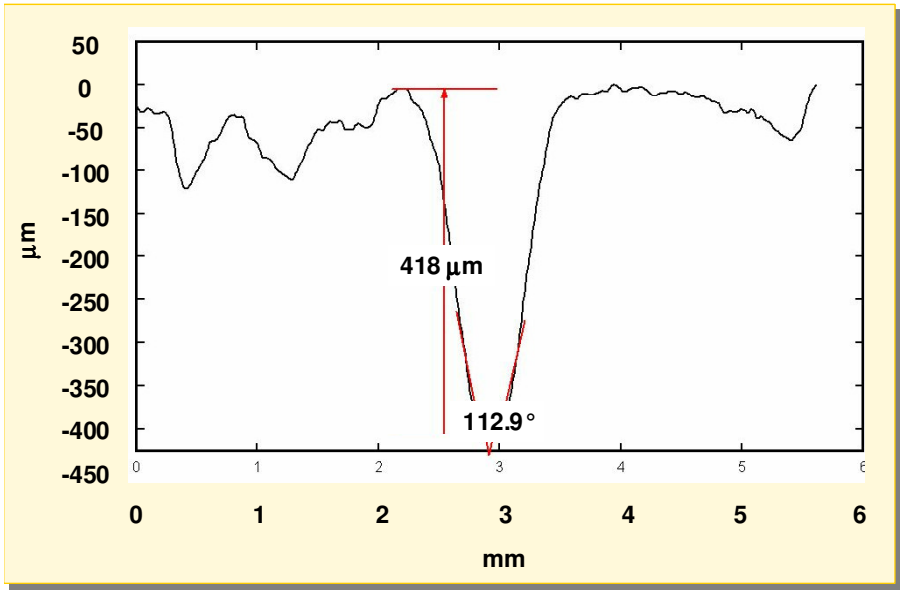

Figure 17 Example of a cross-section picture

For a listing of all the possible options, see Appendix B: . All measurement data may be stored on floppy or hard disk, printed or exported and transferred to another computer system for further image processing and analysis. Using Matlab and an image processing toolbox [7] even more operations can be done on the measurement data.

3.5 System parameters

3.5.1 Resolution

To determine the systems detection level a Silicon Standard with step-heights varying from 1 to 10 µm was developed by Dimes, the Delft Institute for Microelectronics and Sub-microelectronics. This standard was recorded 10 times without moving it in between and mean and belonging standard deviation values for all steps were calculated. Determination of the 95% confidence intervals for these mean values showed that only the largest step of 10 µm could be classified as actual height step because for this step there was no overlap between the confidence intervals. The calculation of these intervals was done using following approximation of the Student t-distribution definition for confidence intervals

$$\bar{x} \pm 2 * \frac{s}{\sqrt{n}} \qquad [13]$$

Where $\bar{x}$ represents the mean value s is the belonging standard deviation and n stands for the number of measurements. Figure 18 shows a picture with on the right the DIMES standard and on the left two mirrors that were used to determine the system noise, see section 3.5.3. The gray samples below are moulds of both standards. Figure 19 is an example of a cross section in one of the recordings showing the 10 µm step. To rule out accidental deviations the values in the curves that were used in the calculation of the confidence intervals were averaged over ten neighboring pixels.

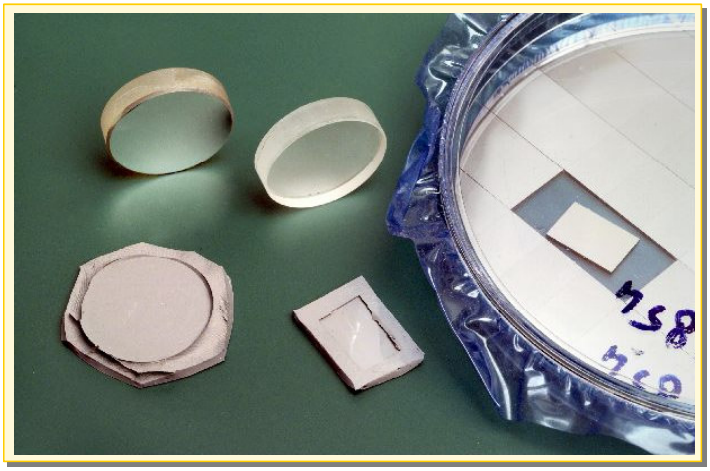

Figure 18 Picture of the DIMES standard and the mirror for the noise measurement

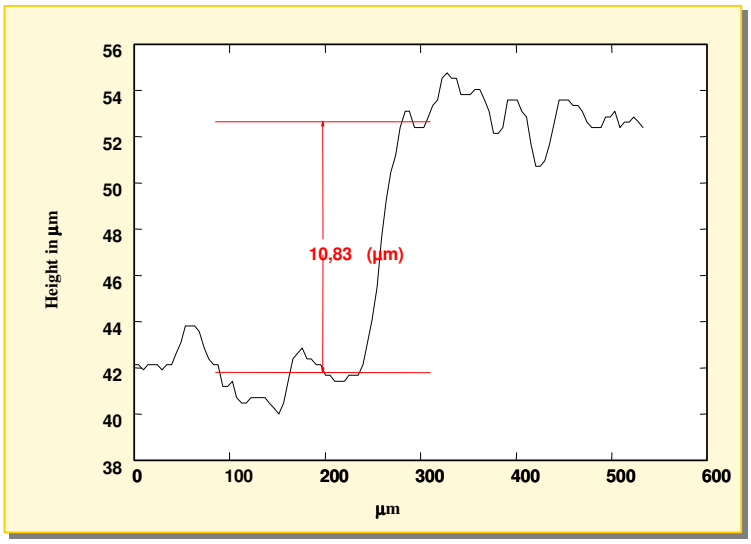

Figure 19 Cross section of the 10 µm step

The resolution for the x and y directions is determined using a test object shown in Figure 101 (which is described extensively in section 5.2) that contains a series of seven holes with increasing diameters (4µm, 6 µm, 10 µm, 20 µm, 25 µm, 40 µm and 50 µm). This test object was measured twelve times. Figure 20 is an example of a zoom of one of these recordings. Only the three largest holes are visible. As can be seen in Figure 21 that shows twelve cross sections through the holes, the other four disappear in the noise.

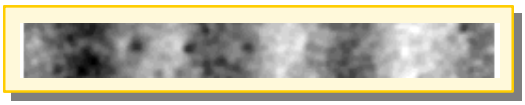

Figure 20 Zoom of series of holes

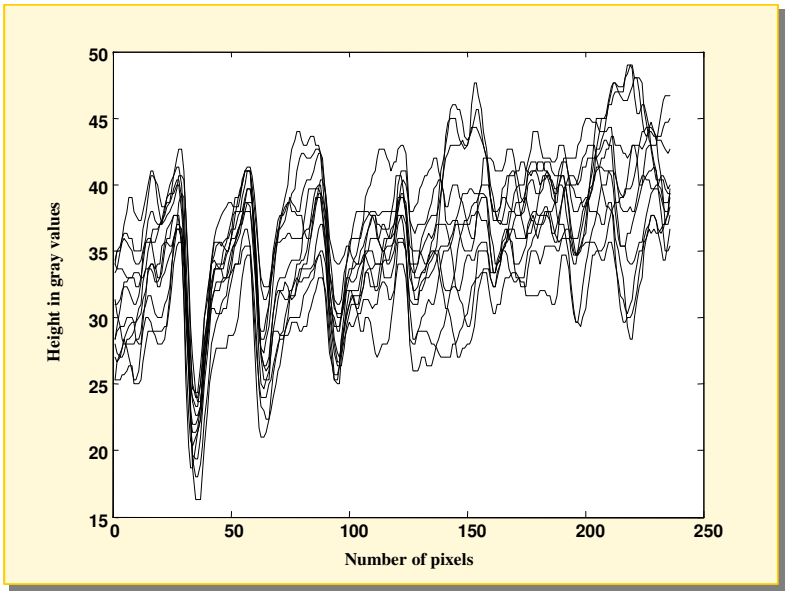

Figure 21 Twelve cross sections through series of holes

Figure 22 shows how after averaging the twelve recordings all seven holes appear. To determine whether the holes are actually there or are the result of noise the same procedure is used as described above. Calculating the 95% confidence intervals show that all height differences except the one with the 4µm diameter in the figure can be classified as holes.

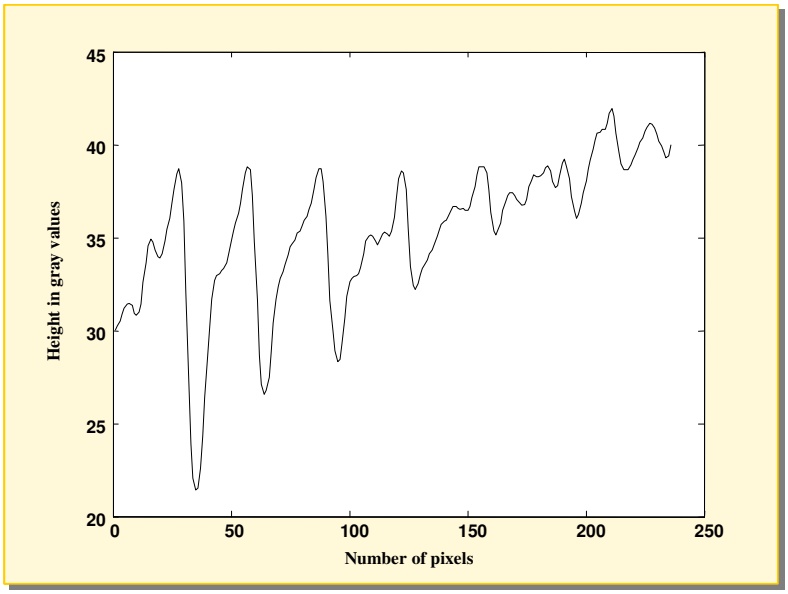

Figure 22 Mean of twelve cross sections through the holes

It can be concluded that holes with a diameter down to 6 µm can be distinguished. However their sizes are not measured correctly by the system.

3.5.2 Measuring area

The size of the measuring area depends on the level of magnification, the level that is used for the examination of XTC-tablets results in a measuring area of 6mm x 8mm.

The vertical measuring range was determined using a 5 mm and a 9 mm step. Cross-sections were made in both recordings and they are presented in Figure 23 and Figure 24. The 5 mm step is imaged properly but with the 9 mm step focusing problems start to occur. The low end of the profile is supposed to be flat but it is calculated as having height differences of hundreds of microns. A vertical range of 5 mm is more than enough though for this purpose while the height of XTC tablets usually about 3 or 4 mm.

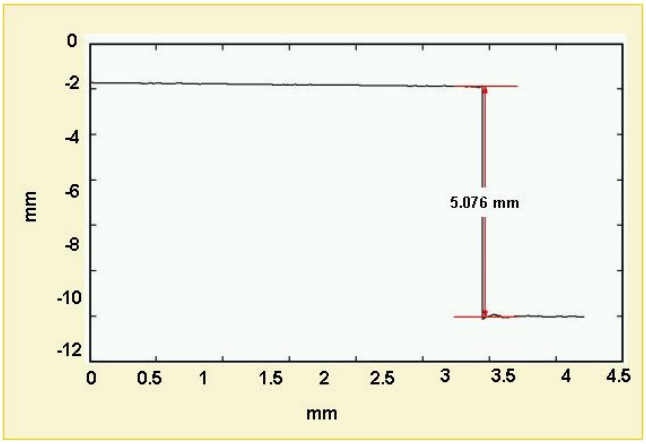

Figure 23 Cross section in the recording of the 5 mm step

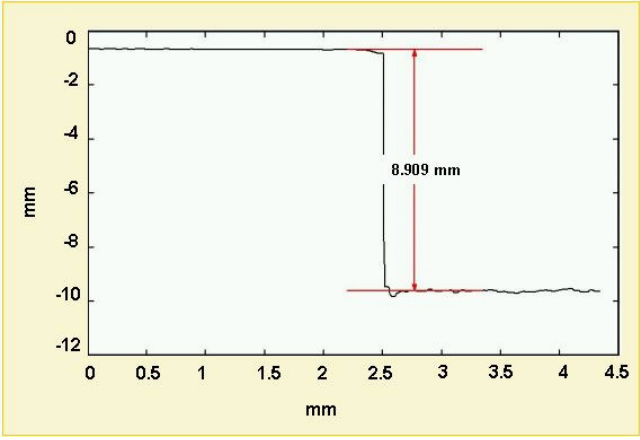

Figure 24 Cross section in the recording of the 9 mm step

3.5.3 System noise:

In systems that use a CCD-camera, the acquired images may be contaminated by several sources of noise, see [8], for example:

- Photon noise: inherent to the statistical nature of photon production and has a Poisson distribution.
- Thermal noise: originates from the stochastic effect that electrons can be freed from the CCD-material trough thermal vibration, causing a dark current which cannot be distinguished from the photo-current
- Quantization noise: occurs in the A-D converter and is due to the amplitude quantization process

In the MicroCad system the CCD camera is cooled and an 8-bit AD-converter is used. Therefore the main source of noise is the photon noise, see [8].

The system noise was determined using a ‘flat’ mirror, see Figure 18. Flat meaning in this case that the roughness of the mirror surface can be maximal a tenth of the wavelength of the light that

is used to examine the surface. This mirror was recorded ten times in a row and the system noise was calculated as the mean of the standard deviations of these ten measurements: $\bar{s} = 2.31\mu m$.

3.5.4 Reproducibility

The reproducibility is defined as the standard deviation of the mean of a series of measurements. The reproducibility of the system is determined as 1.6 µm using a 100 µm standard. No adjustments where made in between the ten recordings and the standard was not removed.

3.5.5 Calibration

Before these parameters could be determined, the system had to be calibrated. This calibration procedure consists of several steps, namely the adjustment of the reference level, the lateral calibration and the vertical calibration. For the reference plane a white flat plate is used and for the lateral calibration a well defined grating. The vertical axis is calibrated with a $500\mu m$ groove that was supplied with the system a picture of this groove is presented in Figure 25

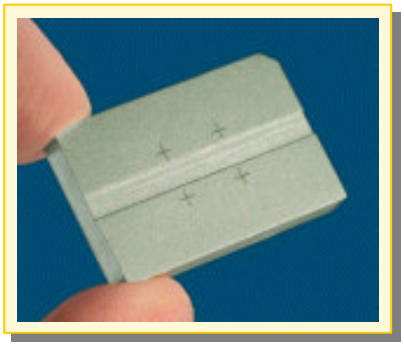

Figure 25 $500\mu m$ groove used for vertical calibration

To verify whether it is possible to use other planes for the adjustment of the reference level as well, tests were done using several different flat planes. In order to determine whether these calibrations were indeed done correctly a test object with known dimensions was designed and measured. The object, a plastic staircase with steps of 30 µm height and 500 µm width is shown in Figure 26. The results proved that it's very well possible to use other planes as reference level for the measurements. An example of a cross-section in which the measured height and width of the steps of the staircase are indicated is shown in Figure 27.

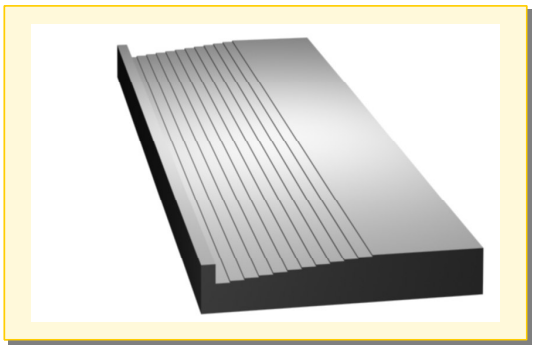

Figure 26: staircase test object

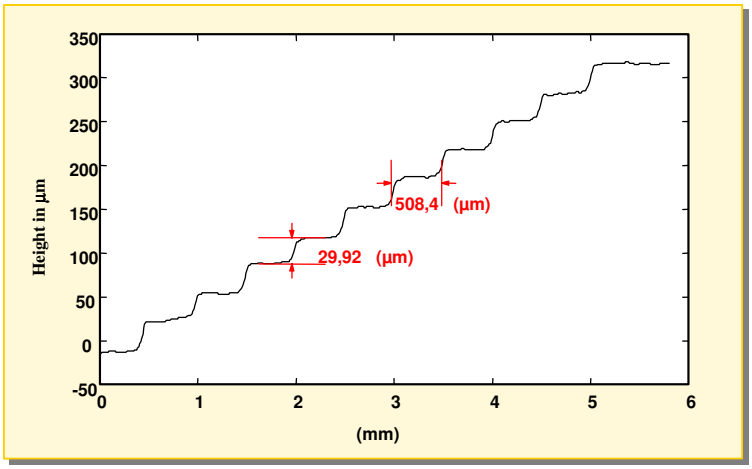

Figure 27 Cross section in recording of staircase

4 RESEARCH APPROACH

To determine the possibilities of the Microcad system for forensic analysis of drug tablets a plan was developed that will be described in this chapter. Following conclusions from chapter 2 were used as a starting point for this investigation:

- Damages of the punches are by far the most useful features to investigate because in forensics they are considered unique and therefore have great discriminating powers. Furthermore the resulting bumps on the tablets can be linked without a doubt to these scratches because whatever else happens to a tablet after production can never result in "more tablet" in the form of bumps.
- Damages are most likely to occur on vulnerable areas of a punch, like the edges of the logo or on top of the break line. Knowing that at the same time the bumps that are created in those areas are the ones that are most likely to be detected over time because they are the least vulnerable to wear of the tablets during transportation or storage, these areas can clearly be appointed as most interesting regions of the tablets.

4.1 Problems and solutions

The theory behind the Microcad system and its possibilities in general were described extensively in chapter 3 but to determine the possibilities for this specific application, measuring tablets and punches, a closer look at the problems that occur due to the shape and material of these objects is necessary before the actual measuring can start.

4.1.1 Reflection

Due to the geometry of the set up, highly reflective surfaces are hard or impossible to measure. The projected patterns will not be reflected into the aperture of the camera. Tilting the object so that the reflection is directed into the camera could be a solution in case of flat reflective objects. In this research the problem will occur measuring the punches, and because of their shape another solution is needed. Measurements will not be done on the punches themselves but on a cast that is made of the punches. The casting material that is used, Silmark low viscosity grey from BVDA, is a two component non-transparent material that is also used in the toolmark section of the Netherlands Forensic Institute. Results of a study described in [9] shows the good quality of this casting material,

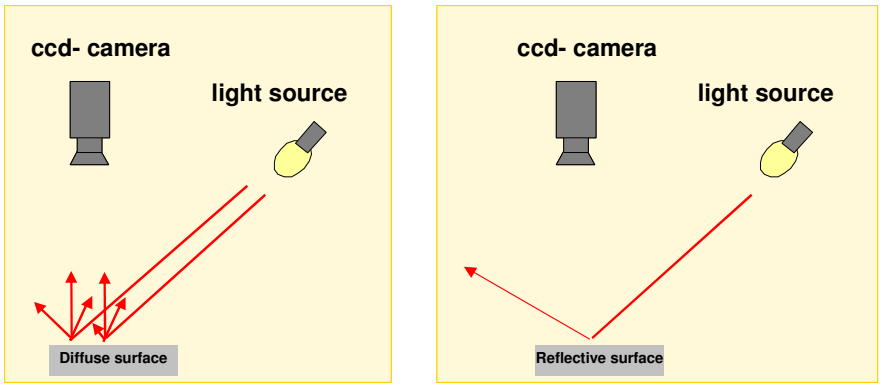

Figure 28 Difference in reflection from diffuse and reflective surface

4.1.2 Occlusion

One of the most common problems for this kind of systems is occlusion. An occlusion can occur either when the camera cannot read the reflected light or when the projector cannot reach the desired point on the surface because of intersection with surrounding objects or parts of the object itself.

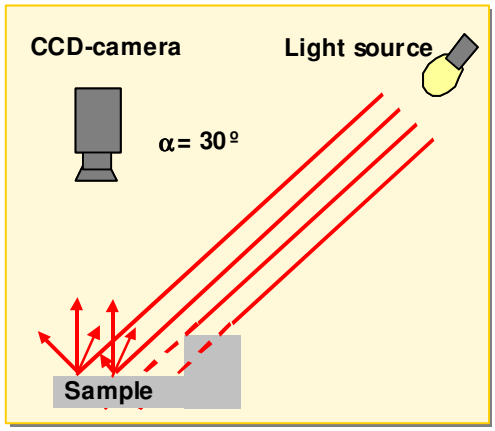

Figure 29 Example of occlusion: the light source cannot reach all points on the sample due to a blockade by the sample itself.

The amount of shadow effects or occlusions that occur depends on the geometry of the system as well as the properties of the object under observation. With sufficient knowledge of the relevant parameters of the system and the object such as triangulation angle and object height, the occurrence of occlusion becomes predictable. Figure 30 shows how by moving the camera and projector the amount of shadow effects can be controlled [10].

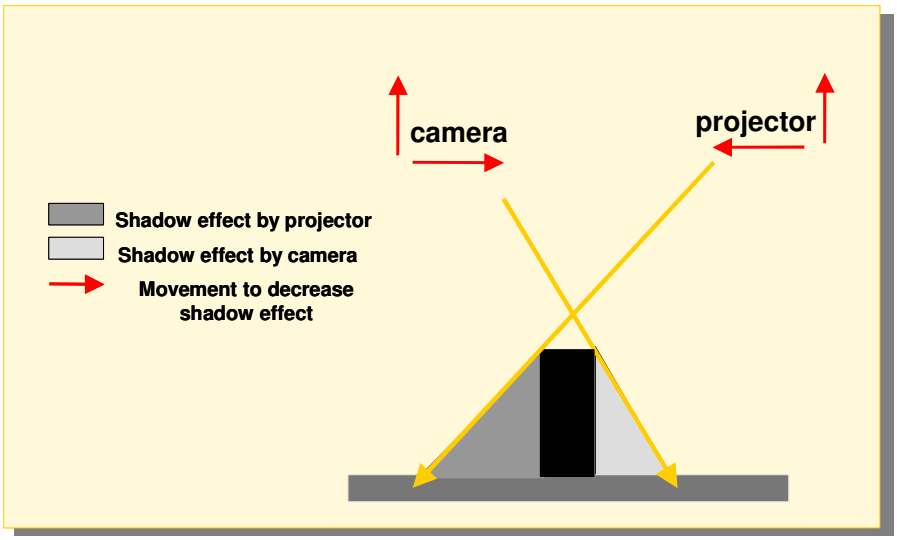

Figure 30 Shadow effects by projector and camera including ways to reduce these effects

Moving camera or projector in the indicated directions causes a decrease in triangulation angle and thereby a reduction of the occluded areas. But as was shown in section 3.1 a smaller triangulation angle also results in a larger error in the height measurements. Due to this larger error there are less distinguishable levels in other words a smaller triangulation angle leads to a lower resolution. These contradictory demands for the triangulation angle make it difficult to determine the "best setup", because it depends on the measurements that will be done with it whether it is necessary to sacrifice the resolution in order to minimize occlusion problems. To predict whether occlusion plays a role in the measurements on XTC tablets with the MicroCad system, a study of the relevant parameters was done. Besides studying the problem in theory, several experiments were done on paracetamol as well as XTC tablets to determine the magnitude of the problem and the outcome of both studies is described in the following sections.

4.1.2.1 Analysis of occurrence of occlusion

Because in the configuration of the MicroCad, the camera is positioned perpendicular to the object, only occlusions due to the blockade of the field of view of the projector can occur. The first series of measurements on paracetamol tablets showed that the part of the tablet that is most likely to cause problems is the break line. Figure 31 shows an example of the same paracetamol tablet that was shown in Figure 16 but now it is rotated over an angle of 90 degrees.

Figure 31 Example paracetamol with occluded areas on the right side of the break line

The white spot indicates that something has gone wrong. The tablet is now positioned in a way that the projector is blocked at some positions by the object itself. One of the sides of the break line is not visible for the projector, resulting in unreliable height calculations. As was already mentioned at the beginning of this chapter the break line and other areas of the logo containing edges are the most interesting regions for comparison therefore it's essential to find out what exactly is happening in these areas and what can be done to solve this visibility problem. The break line contains a V-shaped profile and because this is also the most difficult profile to image properly this V-shape was chosen as the basis for the analysis. Any adjustments made to the setup to optimize the imaging of the V-shaped profile will automatically result in optimal imaging of any other slopes that might be encountered while measuring XTC tablets. Figure 32 is a schematic drawing of such a V-shaped profile with angle β Figure 33 defines the triangulation angle α and combining these two figures results in Figure 34. From this figure it becomes clear that when measuring angles smaller than 30 degrees occlusions will definitely occur. The projector cannot reach all the points on one of the sides of the V-shape in case $\beta \leq 30°$

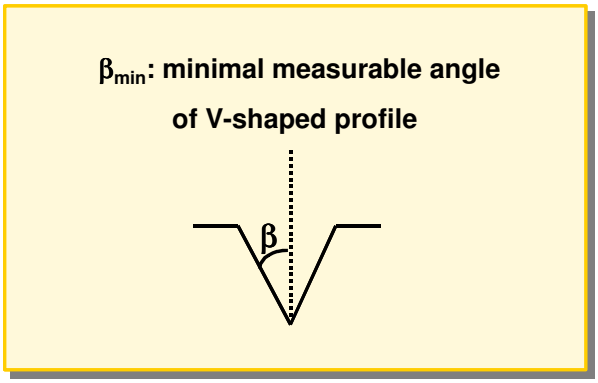

Figure 32 V-shaped profile, definition of β

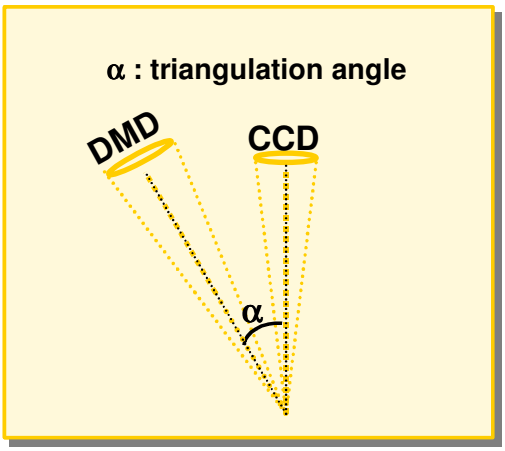

Figure 33 Definition of α

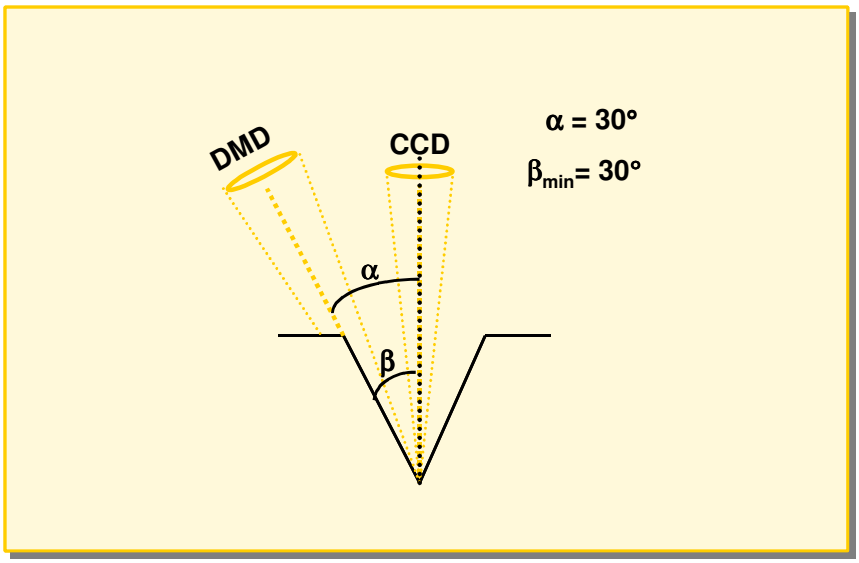

Figure 34 Occluded region for $\beta \leq 30°$ with $\alpha = 30°$

This situation makes it necessary to make more then one recording to image the whole tablet properly. In each recording the tablet is rotated in such a way, that when the images are combined, the calculated height on every position of the surface is reliable. In Figure 35 the angle of rotation is defined as φ and it's obviously desirable to reduce the number of necessary recordings to a minimum.

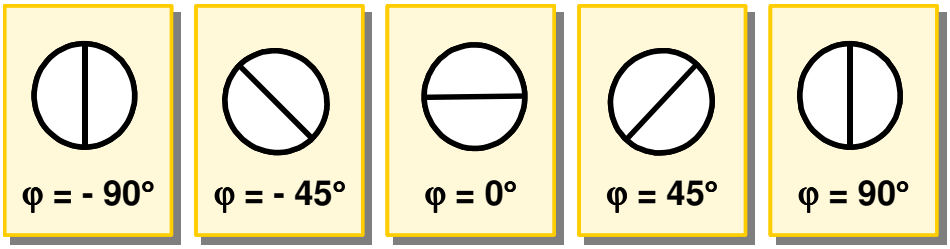

Figure 35 Definition of φ: the tablets have to be rotated several times to obtain reliable measurements for the entire tablet.

The best configuration to avoid occlusion problems is when the camera and the projector are positioned at the same angle to the normal. In this set up it is not possible to change the position of the camera or projector, the only option to realize this configuration is to tilt the object over the half of the triangulation angle. By tilting the object this optimal configuration is simulated and the number of necessary recordings is expected to reduce. Figure 36 shows schematically what the consequences of this tilt are in terms of minimal measurable angles.

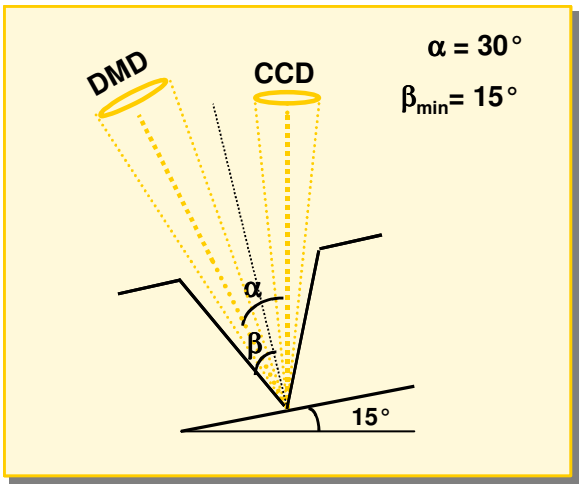

Figure 36 Consequences of a 15° tilt on the occluded region

Figure 36 shows that tilting the V-shaped profile over 15 degrees should make it possible to measure smaller angles up to 15 degrees properly. This improvement and resulting reduction of necessary recordings will be demonstrated by comparing the results of experiments with tablets that lie flat on the measuring plane and tablets that are tilted. This tilt is realized using a special designed holder, which is shown in Figure 37. While designing this holder attention was paid to problems with for instance the vertical measuring range that might appear as a result from this tilt.

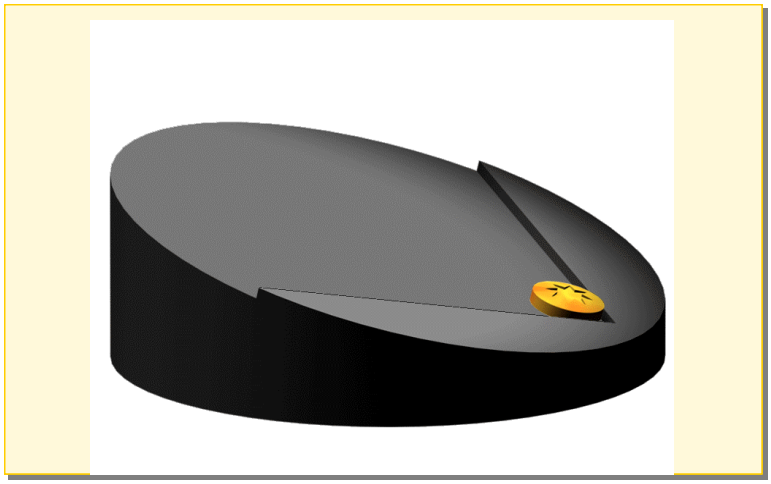

Figure 37 Holder with tilt of 15° used to simulate a configuration with projector and camera positioned at the same angle to the normal.

In section 3.5.2 the vertical measuring range was determined and assuming that the thickness of the XTC tablets varies between 2.5 mm and 4 mm, a tilt of 15 degrees will not cause any problems in that field.

4.1.3 Examples

Projection from the left

Figure 38 Panda logo recorded without holder, φ = 0°

Projection from the right

Figure 39 Same panda logo recorded without holder, φ = 180°

Projection from the right

Figure 40 Same panda logo recorded with holder, φ = 0°

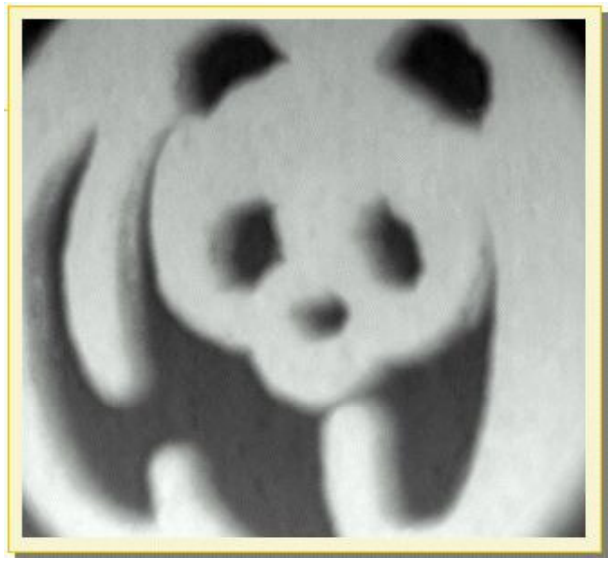

Projection from the left

Figure 41 same panda logo recorded with holder, φ = 180°

In the figures Figure 38-Figure 41 the occurrence of the occlusions and the effect of the holder on the occlusions is demonstrated using a XTC tablet with an imprint in the shape of a panda bear. Figure 38 is a recording of the tablet while it is lying flat on the measuring plane, in this series of measurements ϕ = 0° is defined as the position where the projector is on the left of the tablet. As can be seen from the white stripes on the left side of the panda's head and on his behind there are occluded areas, apparently these areas contain slopes with angles that are too small. Figure 39 is a recording of the same tablet lying flat on the measuring plane only now it is rotated, ϕ = 180°, in this figure the recording is rotated back over 180° so in the position it is presented here the projection came from the right. The occluded areas are now 'mirrored', the white stripes lie in the same grooves but when the tablet is positioned in this way the points on the other sides of the grooves cannot be reached by the projector. The same mirror effect can be seen in case of the

shadowed areas, as for instance in the panda's eyes, in Figure 38 the right side of the eyes is affected by shadows while in Figure 39 it is the left side of the eyes that is not imaged properly. The same holds for the panda's legs, nose and ears. This mirroring of the problem areas proves that we are indeed dealing with occlusion and the problems are not caused by some weird spot on the tablet. When the tablet is now recorded while lying on the holder with the slope of 15 degrees the white spots disappear. This is shown in Figure 40 where $\phi = 0°$ so the projection came from the left again. In Figure 41 the tablet was rotated again over 180° and for comparison purposes after recording it was rotated back. So the holder does seem to improve the situation but as can be seen from the paws, eyes, nose and ears, there are still shadowed areas. The differences between the two recordings in Figure 40 and Figure 41 show that even when the holder is used the height values that are determined in the grooves depend on the way the tablet was positioned while it was recorded. Due to this dependency on ϕ it might be necessary to make more then one recording when the shape of the logo makes it impossible to determine afterwards in which way the tablet that has to be compared was recorded. And to make sure that all damages that might be present in the grooves are in fact detected all orientations in the logos must be imaged properly.

Figure 42 paracetamol recorded without holder, projection from the right, $\varphi = -90°$

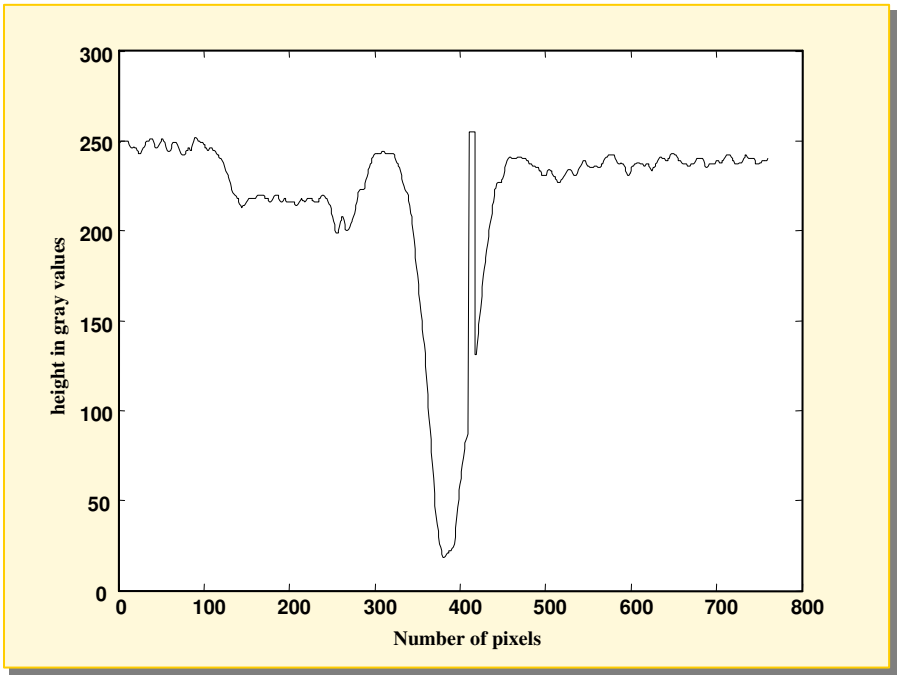

Figure 43 cross-section in Figure 42 through occluded area

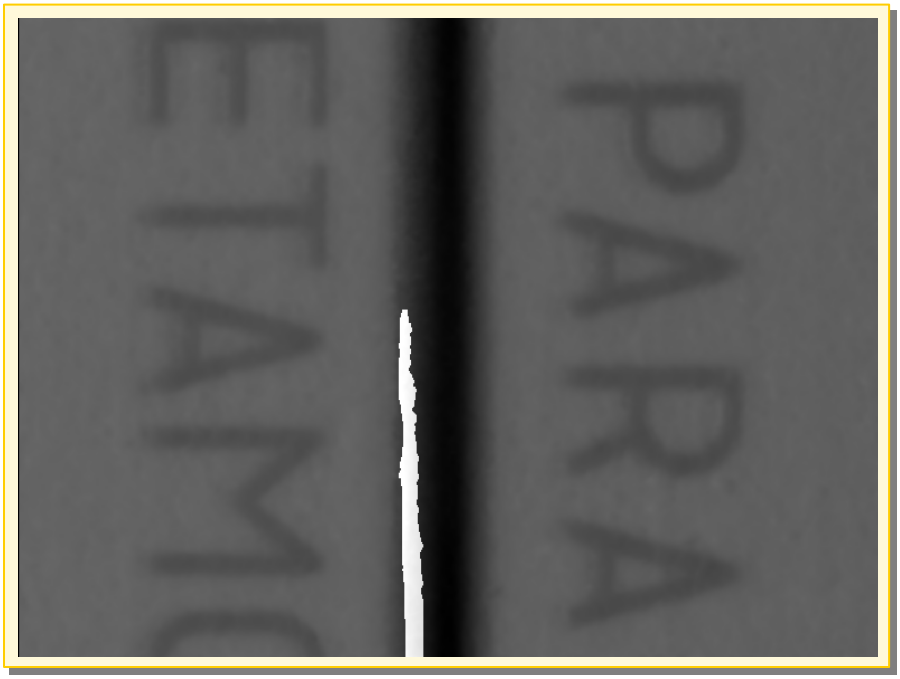

Figure 44 paracetamol recorded without holder, projection from the left, $\varphi = 90°$

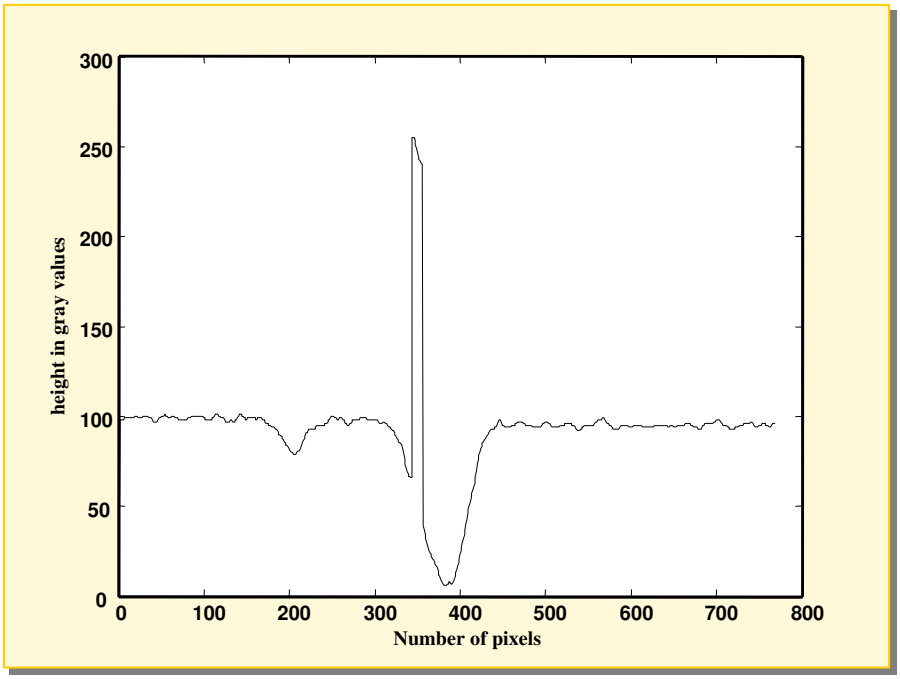

Figure 45 cross-section in Figure 44 through the occluded area

Figure 46 Paracetamol recorded using the holder, projection from the right, $\varphi = -90°$

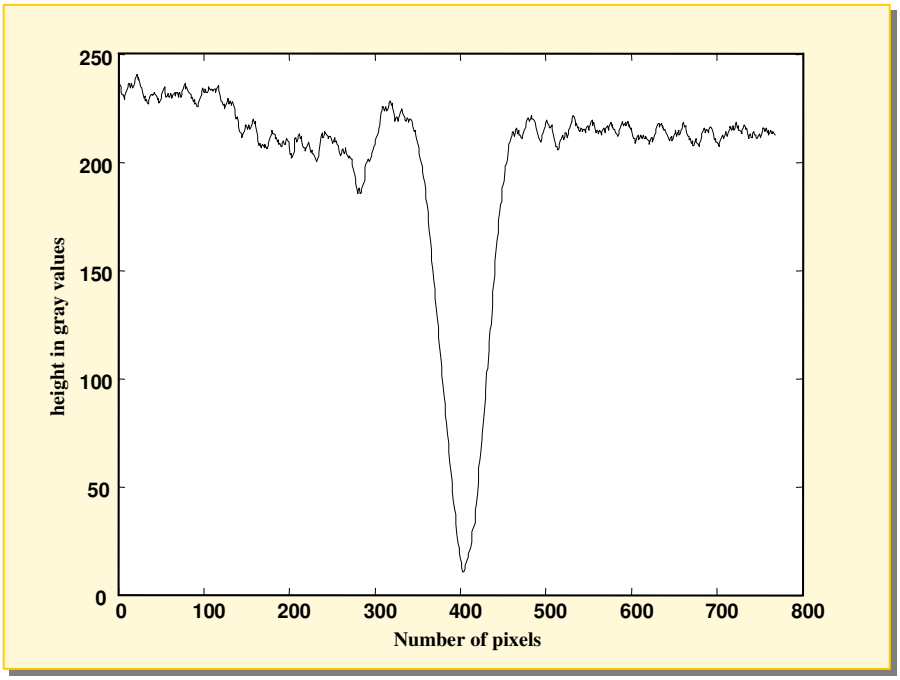

Figure 47 Cross-section in Figure 46 at the same location as in Figure 42

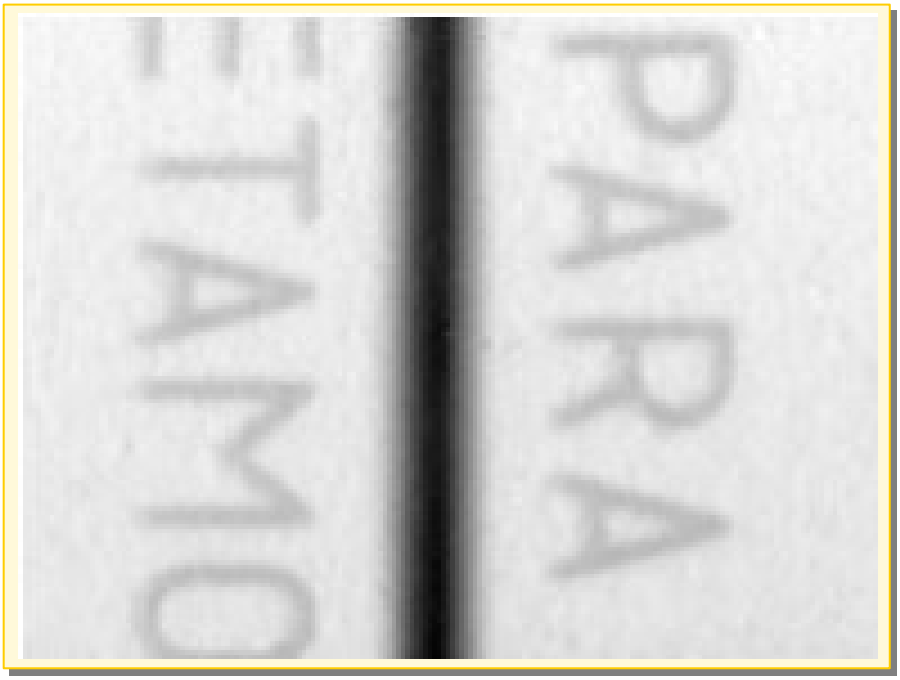

Figure 48 Paracetamol recorded using the holder, projection from the left, $\varphi = 90°$

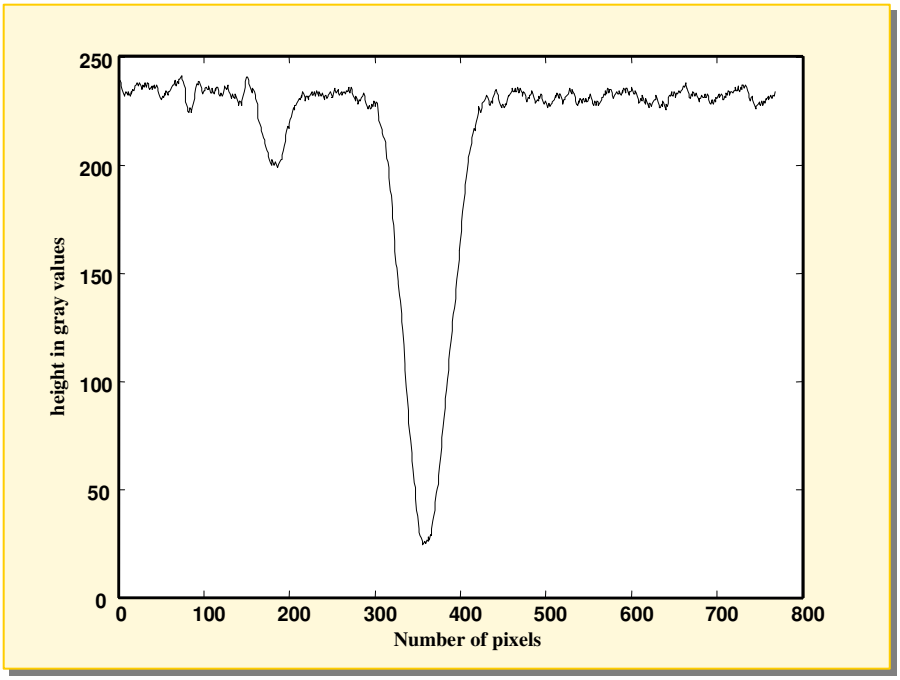

Figure 49 cross-section in Figure 48 at the same position as in Figure 44

Figure 50 Paracetamol recorded without the holder, projection from the right, $\varphi = 0°$

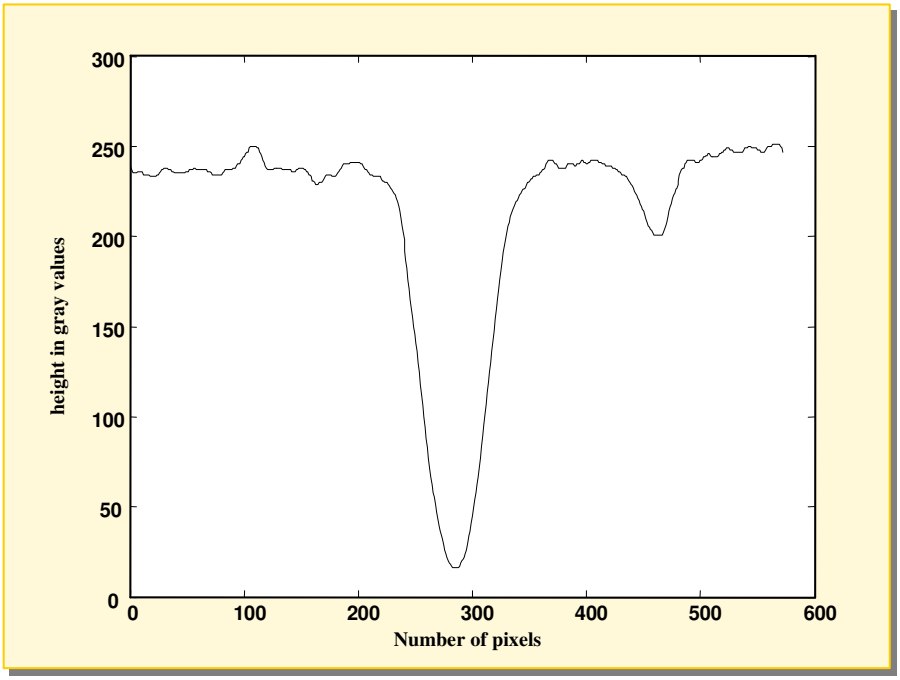

Figure 51 cross-section in Figure 50

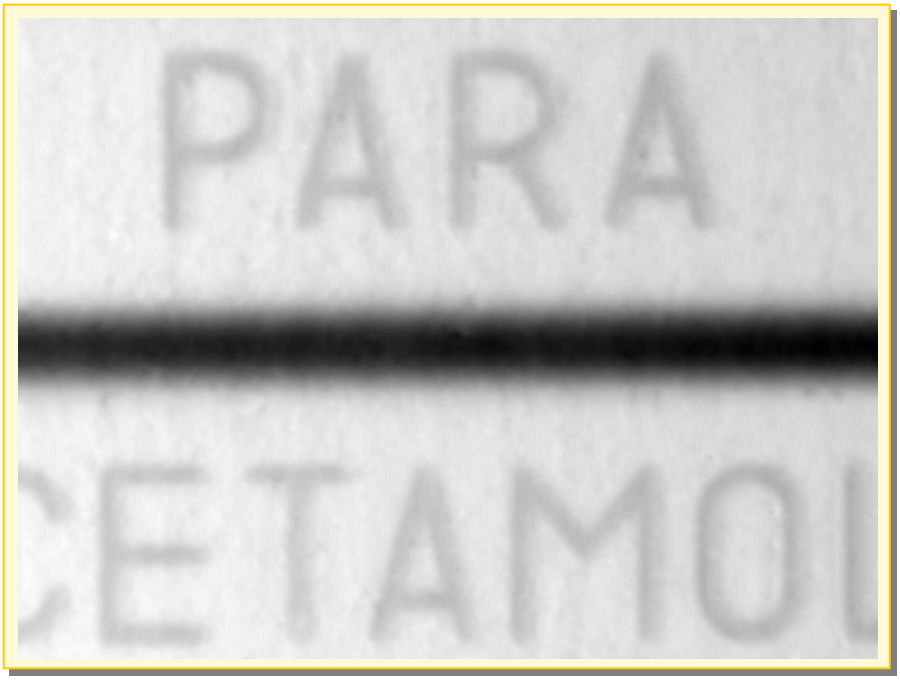

Figure 52 paracetamol recorded with holder, projection from the right, $\varphi = 0°$

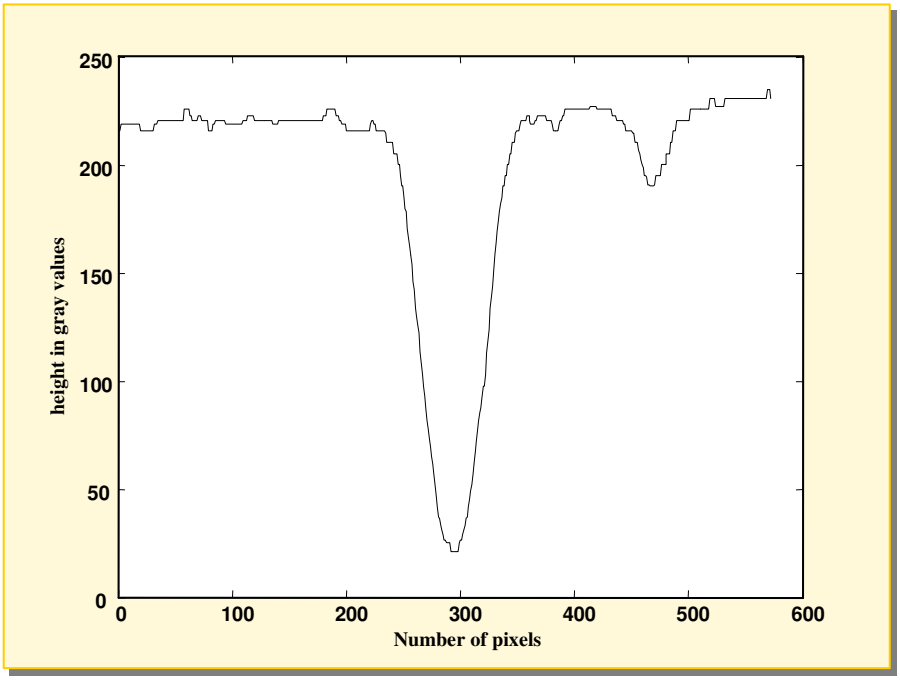

Figure 53 Cross-section in Figure 52 at same position as Figure 50

Figure 42-Figure 52 confirm the expected problems with the V-shaped profile of the break line and demonstrate the effect of the holder on the measurements of one of the paracetamol tablets that was examined. In Figure 42 the tablet was recorded without use of the holder. In this figure the tablet is recorded in a way that the projection came from the right, and this position is defined as the $\phi = 90°$ position. The beveled sides of the break line cause problems as was expected but

also the letters seem to be suffering from shadow effects, the right side of every groove is less sharp then the left one. Figure 43 is a cross-section taken horizontally through the T and the white spot, and it shows the extreme height values that are given for the points that could not be reached by the projector. Figure 54 shows the location of the cross-sections that were taken, on the left for Figure 43 and Figure 47 and on the right for Figure 45, Figure 49, Figure 51 and Figure 53. When the intensity of the reflected beam that comes from a certain point is below the tress hold level, an extreme height value is assigned to this point to indicate that the measurement was not reliable. The shadow effects on the letters result in non-symmetrical parabolas in the curve, the left sides of the parabolas are more steep then the right sides. Again to prove that the white area results from occlusion and is not caused by something on the tablet, it was rotated over 180 degrees and recorded again, the result is presented in figures Figure 44 and Figure 45. The mirroring effect that occurred in the recordings of the panda bear logo is observed here as well, rotating the tablet over 180 degrees results in a shift of the occluded area from the right to the left sides of the grooves. This shift is also visible in the picture of the cross-section. Figure 46-Figure 49 demonstrate the effect of the holder. Using the holder the tablet was recorded in the same positions, referred to as $\phi = 90°$ and $\phi = -90°$, as in Figure 42 and Figure 44 and the cross-sections were also taken at the same location as in Figure 43 and Figure 45. The results show that the use of the holder does lead to an improvement, the white area has disappeared and the other shadow effects are reduced. The shifting of the shadows from right to left still takes place when the tablet is rotated over 180 degrees and the course of the height profile in the break line is visible different in both recordings, the side of the V-profile that is closest to the projector is less steep than the other side in both situations. The cross-section pictures also show that the sides of the break line and the sides of the grooves of the letters are still not equally steep. Finally to check how well these recordings really are, they have to be compared to the recordings of the tablets when it is in the position $\phi = 0°$. This was done for both situations, with and without holder and the results are presented in Figure 50-Figure 53. When the tablet is in the position $\phi = 0°$, the break line is positioned perpendicular to the stripes that are projected so in this way both sides of the break line can be reached by the projector at the same time and no problems with occlusion are expected. Figure 50 and Figure 52 prove that this is indeed true, the entire break line is imaged properly and as also can be seen from the cross-section pictures that are given in Figure 51 and Figure 53, in this case the sides are symmetrical. The effect of the holder when the tablet is in position $\phi = 90°$ can be seen in the shadows that are appearing on the sides of the letters that are now positioned parallel to the stripes that are projected.

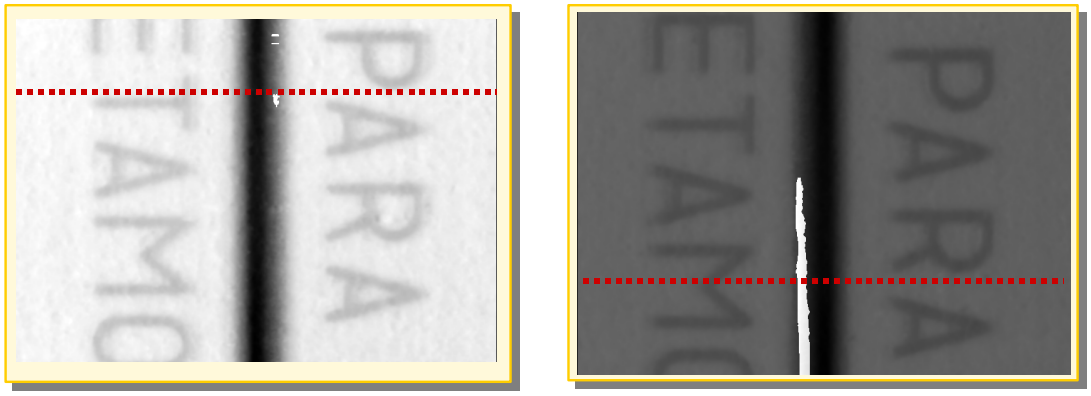

Figure 54 Location of cross-sections, left for Figure 43 and Figure 47 and right for Figure 45, Figure 49, Figure 51 and Figure 53

Conclusions:

The examples given above confirm what was expected from the theoretical analysis, tilting the tablets over an angle of $15°$ does improve the imaging. The occluded areas that result in erroneous extreme height values disappear and other areas that to a lesser degree suffer from shadow effects are also visibly reduced by the use of the holder. Anyhow more quantitative experiments must show whether the holder does indeed improve the measurements significantly enough that the differences between recordings of a tablet in $\varphi = 0°$ and $\varphi = 90°$ become negligibly.

4.1.4 Symmetrically imprints

The number of recordings that is necessary to properly image an entire tablet might be reduced when the holder is used but the final minimal number depends also on the characteristics of the logo that is imprinted. When it is difficult to determine in which position the tablet that has to be compared was recorded due to symmetrical shape of the logo it is necessary to try more then one position and search for the best match. Figure 55 shows some examples of tablets containing logos that are rotational symmetric such as the simple single or double break line imprints but also three-, four-, or fivefold symmetry logos are not uncommon in the large collection of confiscated tablets.

Figure 55 examples of logos with rotational symmetry

An assumed $0°$ recording of for instance a four-legged star logo should be matched with the $0°$ recording of the second tablet but also with its $90°, 180°$ and $270°$ recordings because they cannot be distinguished during recording. Figure 56 shows for example the situation that one of the legs of the star has been damaged in this case the $\varphi = 0°$ will definitely not match the $\varphi = 90°$ or the other two positions.

Figure 56 star logo with damaged leg

More general in case of a n-fold symmetry applies for the rotation step $\Delta\varphi$ between subsequent rotated recordings

$$m \cdot \Delta\varphi = \frac{2\pi}{n} \qquad m = 1,2,3.... \qquad [14]$$

A quick examination of a tablets surface that only contains a break line and no letters like in the paracetamol example, shows that there is indeed a clear difference between its $\varphi = 0°$ and $\varphi = 180°$ recordings. The results are presented in Figure 57-Figure 59. To compare both images and their cross-sections, the $\varphi = 180°$ image is rotated over 180°. The cross-sections were both taken at the same location on the tablet and show a good match after they were 'mirrored'. A more thorough experiment to investigate the symmetry situation is described in chapter 5.

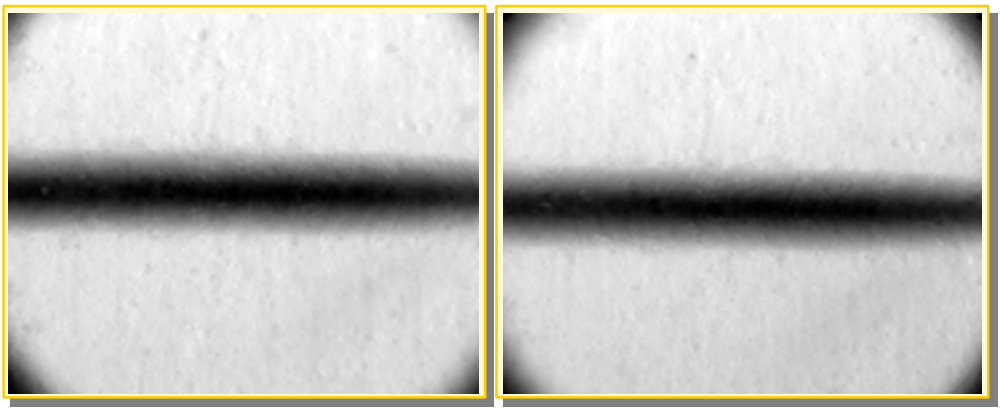

Figure 57 Break line in XTC tablet: recorded with holder, left ϕ = 0°, right ϕ = 180°

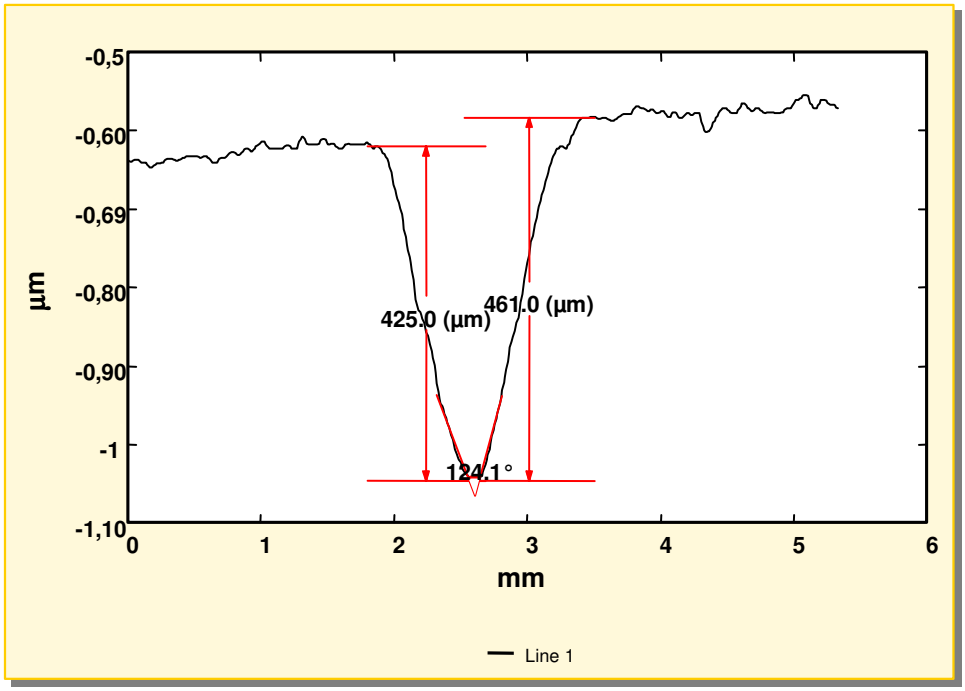

Figure 58 Cross-section in left picture of Figure 57, ϕ = 0°

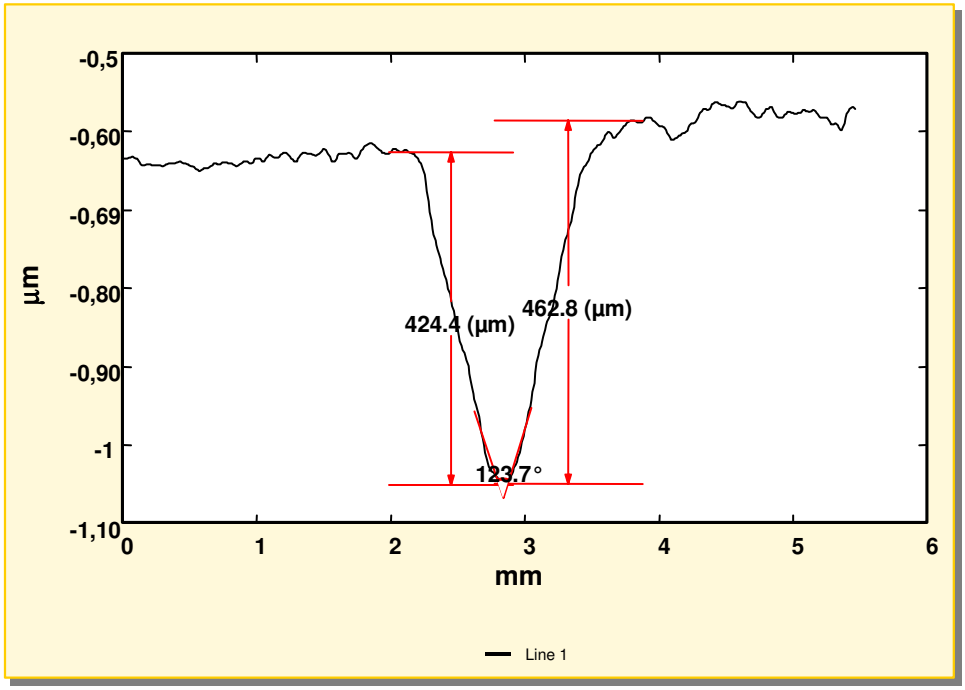

Figure 59 Cross-section in right picture of Figure 57, ϕ =180°, rotated back afterwards

4.1.5 Translation

Using the holder another problem is taken care of as well. The V-shaped holder makes sure that tablets with the same diameter have their centers at approximately the same position, therefore eliminating large translations from the recordings. The tablets that are recorded while lying flat, are also not translated in relation to each other, because a second holder was made, with the same V-shape but without the slope, see Figure 60.

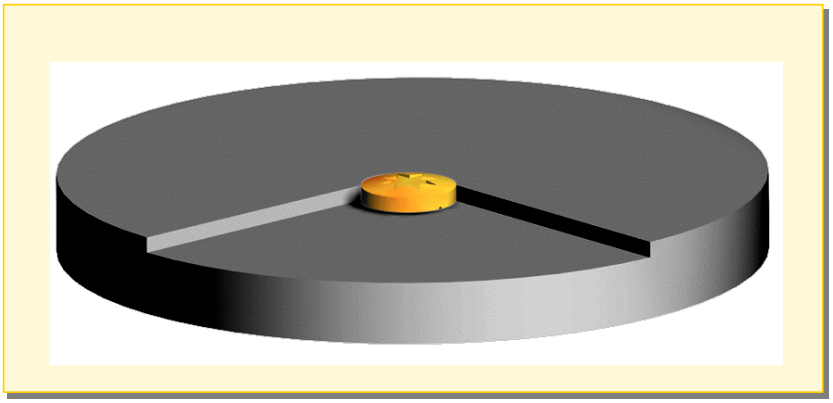

Figure 60 "pac-man" holder eliminates translations

4.2 Three-phase plan for comparison process

Based on the analyses of occlusion and symmetry problems can be concluded that the comparison of tablets cannot be done by simply recording two tablets and comparing the resulting images. Multiple recordings of each tablet even in the case of non-symmetrical imprints are inevitable. The developed procedure for the comparison can be divided into three phases that will be described in the following sections. For each phase the subsequent steps that must be taken are treated. The experiments that were done to either show the results of these steps or to decide between different options for each phase are mentioned briefly here but will be treated extensively in chapter 5.

4.2.1 Phase 1: recording the tablets

Depending on the symmetry and slopes of the imprints of the tablets under investigation a number of recordings of both tablets must be made. Both tablets must be rotated several times over the same angle until each orientation present in the logo is imaged properly. All recordings must be made in one series to assure constant conditions as much as possible. To improve precision in detection of the bumps multiple recordings of the tablets in each rotated position can be made and averaged. Figure 61 shows an example of such a series of recordings of a rotated paracetamol tablet

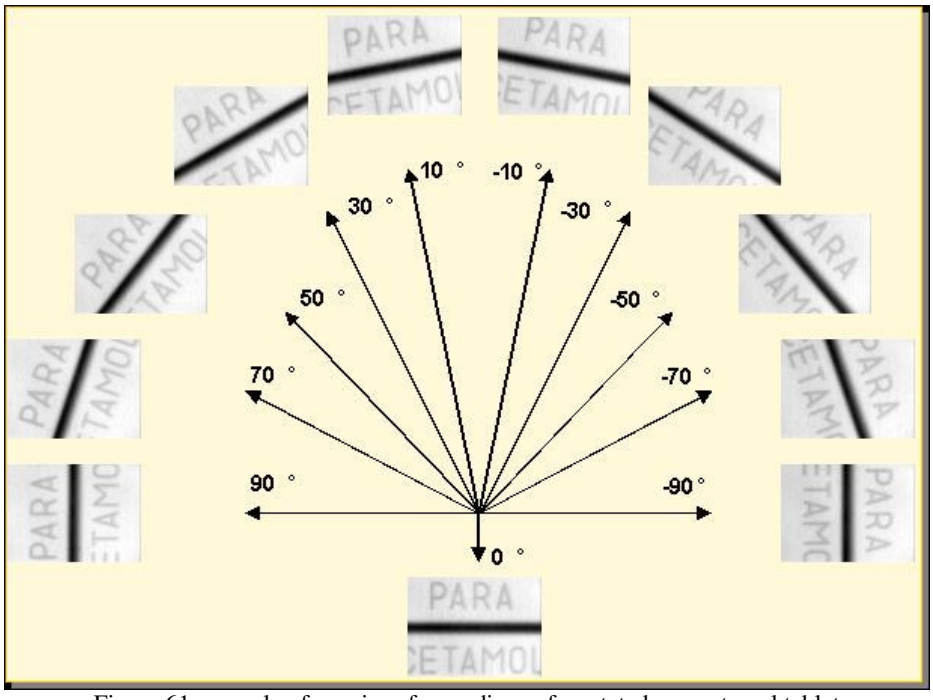

Figure 61 example of a series of recordings of a rotated paracetamol tablet

Experiments:

- Determination of the minimal number of required recordings
- Determine the dimensions of the smallest detectable bumps and show improvement of precision through mediation of multiple recordings of a tablet in the same position.

4.2.2 Phase 2: image processing

There are two ways to use the recordings of the rotated tablets to do the comparison. In the first option the recordings of the rotated tablets are investigated one by one, recordings of both tablets in the same position are compared mutually. In the second option all recordings of each rotated tablet are combined into one image. These combined images are then used to compare the different tablets with each other. Both ways require different image processing steps that will be described successively. Figure 62 and Figure 63 show the subsequent steps for both methods.

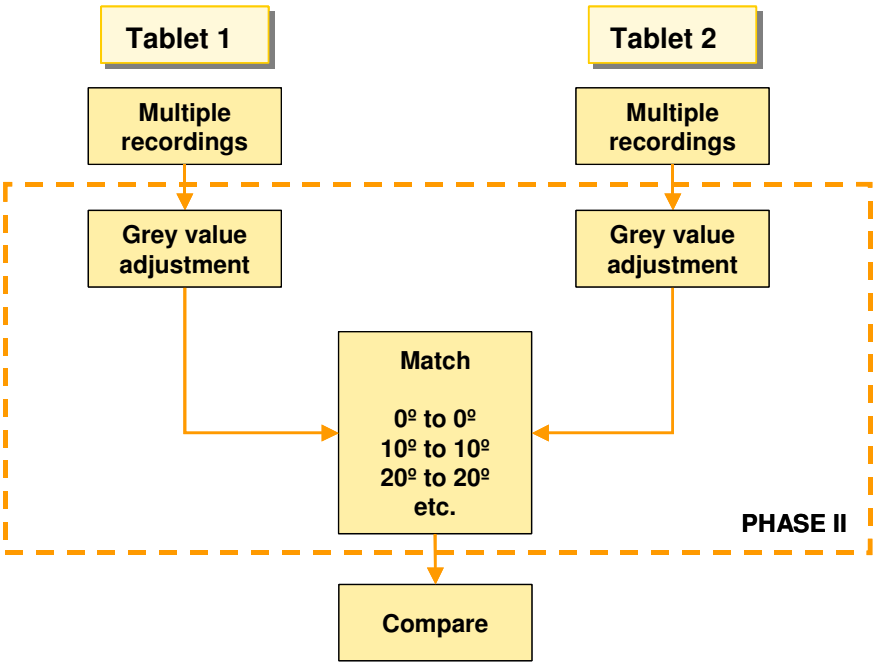

Figure 62 Flow diagram outlining method one

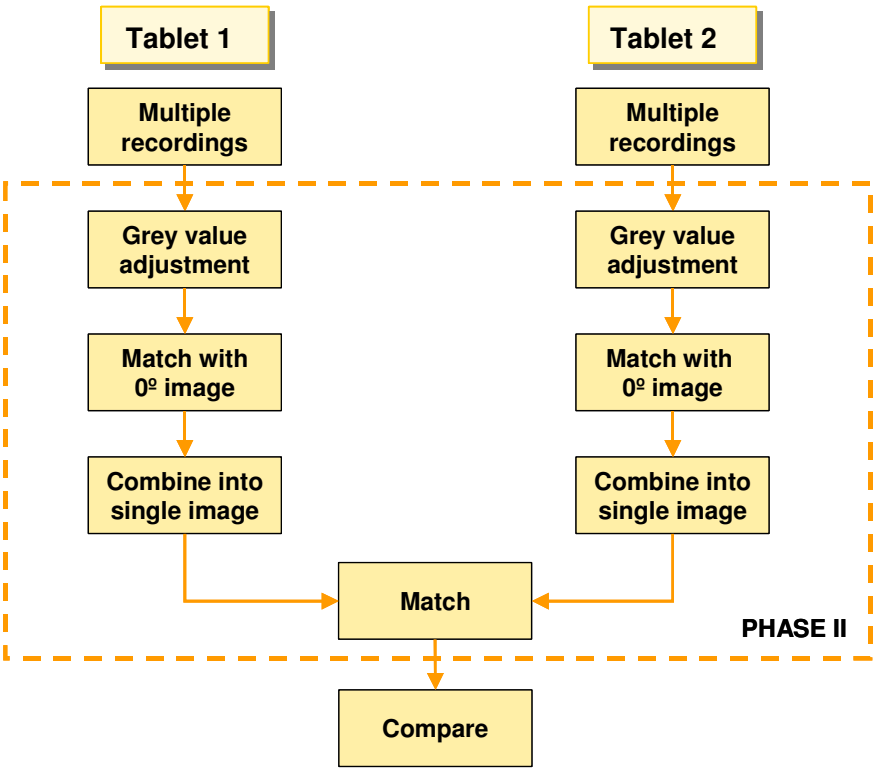

Figure 63 Flow diagram outlining method two

4.2.2.1 Method 1

Dependent on the holder that was used to record the tablets either the first or the first two steps are the same for both methods.

Step 1: Grey value scaling

Because it is not possible to compare images or cross-sections from different images in one figure within the software of the Microcad system the recordings are exported as bitmap files. By exporting the images the actual height value information is lost, the bitmap files that are imported in Matlab only contain gray values therefore all calculations performed in Matlab return results in terms of gray values. The software included in the Microcad measuring system calculates the maximum and minimum height values of a recorded object with respect to the reference plane used in the calibration. These values are referred to as Z_{max} respectively Z_{min} and are necessary to determine the conversion factor that was used for the representation of the height profile in gray values. This factor C indicates the height difference between consecutive gray values.

$$C = \frac{Z_{max} - Z_{min}}{255} = \frac{\Delta Z}{255} \mu m / grayvalue \qquad [15]$$

To be able to compare two tablets their recordings should have the same conversion factor. In case they are not the same they must be adjusted, there are several situations possible that might lead to differences in this factor. When the logos of two tablets are not as deep, their $\Delta Z's$ and thereby their $C's$ will not be the same. A reason for differences in gray value scaling between multiple recordings of the same tablet can be found in a non-horizontal base. Figure 64 shows what happens with the gray value scaling of the images when the tablets are rotated while placed on the tilted holder. Z_{max} and Z_{min} that are used to calculate the conversion factor are not constant in all rotated images of the tablet.

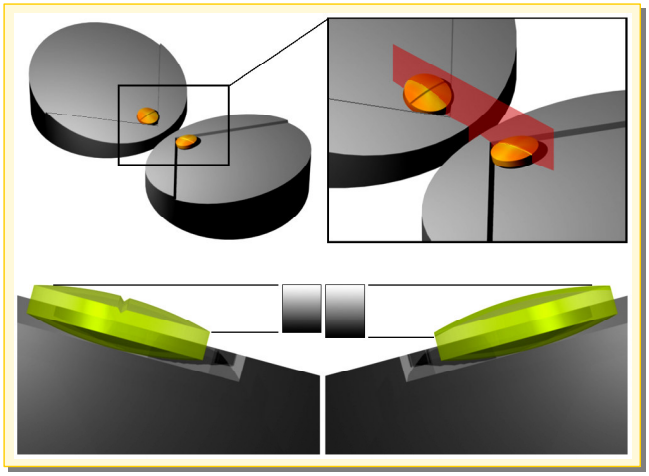

Figure 64 rotating the tablet will change the measured $\Delta Z's$

Thus instead of calculating the conversion factor C once for all rotated recordings, by using the tilted holder the conversion factor becomes dependant of $\Delta\varphi$ and will have to be calculated for

all recordings individually and adjusted so that all rotated recordings are converted to gray value images using the same scaling. Therefore before any kind of comparison can take place the first step always must be gray scale adjustment, to do so $Z_{max}(\Delta\varphi)$ and $Z_{min}(\Delta\varphi)$ values for each image must be registered and using following equation the correction factor $C^*(\Delta\varphi)$ for each image can be calculated

$$C^*(\Delta\varphi) = \frac{C(\Delta\varphi)}{C(0°)} = \frac{Z_{max}(\Delta\varphi) - Z_{min}(\Delta\varphi)}{Z_{max}(0°) - Z_{min}(0°)} \qquad [16]$$

When using the tilted holder these differences are always present and very well visible and even though they might be negligible or absent most of the time when the flat holder was used it should always be checked and corrected if necessary in both cases.

Step 2: Alignment

When the tilted holder is used the data will also have to be adjusted in order to remove the addition in height caused by the slope of the holder, the calculated height values will have to be corrected afterwards for the slope that is added because the tablets are tilted over 15 degrees.

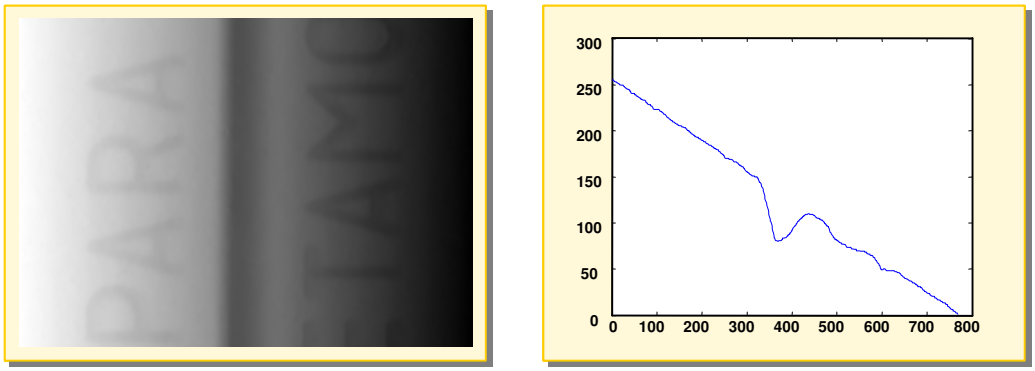

Figure 65 Example of recording and cross-section of a tablet recorded using the holder

The software included with the Microcad system contains an alignment procedure but instead of rotating the data it performs a projection. When the angles are very small, this approximation can be used but because in this case the data is rotated over an angle of 15 degrees this is no longer allowed. The figures below show what goes wrong when projection is used.

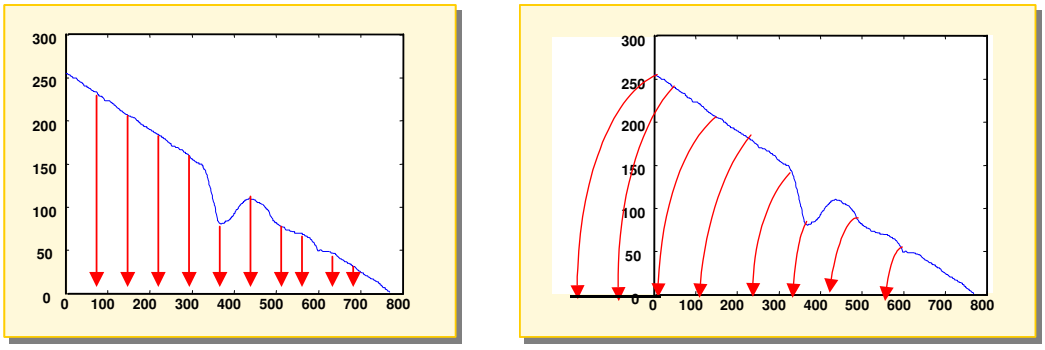

Figure 66 left: projection leads to distortion right: correct adjustment through rotation

So this alignment procedure cannot be used to adjust the data, it has to be done by hand afterwards. Therefore a Matlab algorithm was written which can be found in Appendix A: Matlab routines This algorithm calculates the slope in each recording separate instead of using a fixed angle of 15 degrees and performs a rotation on the data. To determine whether the algorithm rotates the data correctly several experiments were done with known objects. The staircase that was already described and used in earlier experiments was measured now while lying on the tilted holder. By rotating the staircase over several different angles and correcting the data afterwards could be determined that the algorithm works well under any angle. Figure 67 shows the results of both alignment procedures on a recording of the staircase

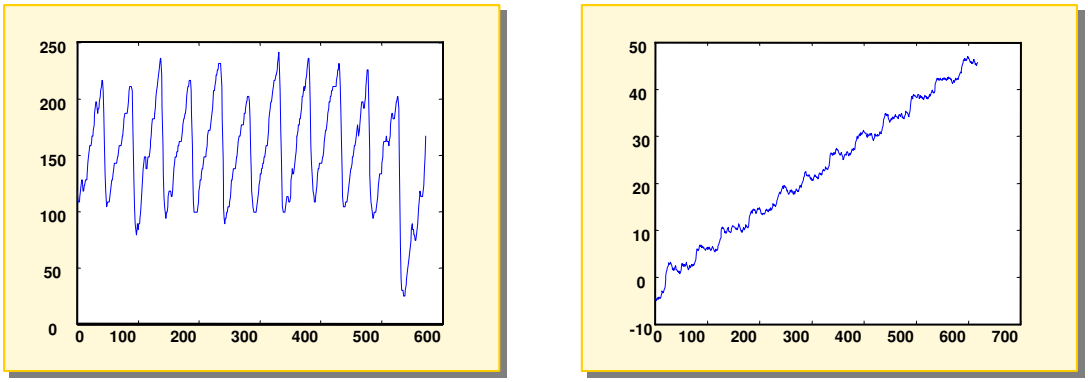

Figure 67 staircase aligned left: microcad software right: matlab algorithm

Step 3: Matching of the series of both tablets one by one.

As indicated in Figure 68 the images of both tablets in the same position are all matched separately. Using a Matlab routine that matches the Fourier-Mellin transforms of two images through symmetric phase-only matched filtering, the 0° images of both tablets are matched with each other, so are their 10° images, their 20°'s and 30°'s etc. A printout of this routine can be found in Appendix A: Matlab routines and for a more elaborate description of this technique and its performance [11].

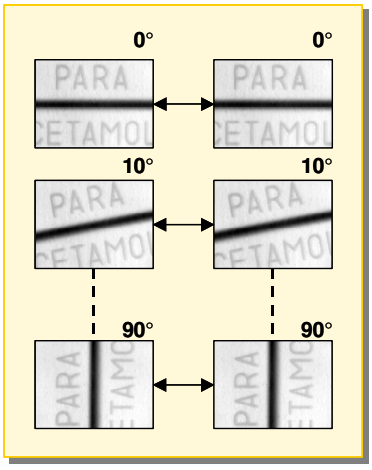

Figure 68 Matching for method one

This technique matches a two dimensional image to a translated, rotated or scaled reference image. The Fourier-Mellin invariant (FMI) descriptor of an image is translation invariant and represents rotation and scaling as translations in parameter space and is calculated as follows:

Given an image $s(x, y)$ that's a rotated, scaled and translated version of $r(x, y)$, where α is the rotation angle, σ the uniform scale factor and x_0 and y_0 parameters of the translation

$$s(x, y) = r\left[\sigma(x\cos\alpha + y\sin\alpha) - x_0, \sigma(-x\sin\alpha + y\cos\alpha) - y_0\right] \quad [17]$$

The Fourier transform $S(u, v)$ of image $s(x, y)$ contains the spectral phase term $\varphi_s(u, v)$ that depends on scaling, rotation as well as translation but the spectral magnitude on the other hand is translation invariant

$$\left|S(u, v)\right| = \sigma^{-2}\left|R\left[\sigma^{-1}(u\cos\alpha + v\sin\alpha), \sigma^{-1}(-u\sin\alpha + v\cos\alpha)\right]\right| \quad [18]$$

Equation 18 shows that rotation of the image rotates its spectral magnitude by the same angle and a scaling σ of the image by scales its spectral magnitude by σ^{-1}. By defining the spectral magnitudes of r and s in polar coordinates as $r_p(\theta, \rho)$ and $s_p(\theta, \rho)$ the rotation and scaling can be uncoupled and equation 18 becomes

$$s_p(\theta, \rho) = \sigma^{-2} r_p(\theta - \alpha, \rho/\sigma) \quad [19]$$

Thus rotating the image causes $s_p(\theta, \rho)$ to shift along the angular axis and a scaling of the image is now reduced to a scaling of the radial coordinate ρ and a magnification of the intensity by a constant factor σ^2. By using a logarithmic scale for the radial coordinate the scaling can further reduced to a translation as well.

$$r_{pl}(\theta, \lambda) = r_p(\theta, \rho) \quad [20]$$

$$s_{pl}(\theta, \lambda) = s_p(\theta, \rho) = \sigma^{-2} r_{pl}(\theta - \alpha, \lambda - \kappa) \quad [21]$$

In above polar-logarithmic representation of image $s(x, y)$ where $\lambda = \log(\rho)$ $\kappa = \log(\sigma)$ both rotation and scaling are reduced to translations and will appear as phase shifts in the Fourier transforms of these polar-logarithmic representations

$$S_{pl}(\upsilon, \varpi) = \sigma^{-2} e^{-j2\pi(\upsilon\kappa + \varpi\alpha)} R_{pl}(\upsilon, \varpi) \quad [22]$$

The Matlab routine now calculates first the FMI descriptor for both images of the tablets and then matches these descriptors using a symmetric phase-only matched filtering (SPOMF). Phase-only matched filtering (POMF) solves the problems due to noise and the dependency on the energy of images that limit the performance of the classical matched filters see [11]. Because the spectral phase of an image preserves the location of objects but is insensitive to image energy there will

be a much sharper peak than in classical matched filtering. By using the SPOMF- technique further improvement can be achieved because the output of the used non-linear filter reduces in absence of noise to a Dirac δ-function yielding an even sharper maximum than the POMF. For example given two images $s(x, y)$ and $r(x, y)$ again but now related as follows:

$$s(x, y) = r(x - x_0, y - y_0) + n(x, y) \qquad [23]$$

with $n(x, y)$ a zero-mean stationary random noise field, independent of $r(x, y)$. The classical matched filter maximizes the signal to noise ratio and if the noise has a flat spectrum with intensity n_ω the output function can be written as

$$q_0(x, y) = \frac{1}{|n_\omega|^2} \int \int_{-\infty}^{\infty} s(a,b) r^*(a - x, b - y) da db \qquad [24]$$

the position of the maximum (x_0, y_0) of this function determines the parameters of the translation. The transfer function of a phase-only matched filter is equal to the spectral phase of image $r(x, y)$ and leads to a much sharper peak that makes it easier to detect the maximum. But by extracting and correlating the phases of both images $s(x, y)$ and $r(x, y)$ the output of the filter is given by the inverse transform of the function:

$$Q(u,v) = \frac{S(u,v)}{|S(u,v)|} \bullet \frac{R^*(u,v)}{|R^*(u,v)|} = \exp[j(\varphi_s(u,v) - \varphi_r(u,v))] \qquad [25]$$

with $\varphi_s(u,v)$ and $\varphi_r(u,v)$ the spectral phases of $s(x, y)$ and $r(x, y)$. In the absence of noise this function reduces to

$$Q(u,v) = \exp[-j2\pi(ux_0 + vy_0)] \qquad [26]$$

of which the inverse Fourier transform a Dirac δ-function is centered at (x_0, y_0) yielding an even sharper maximum than the POMF.

Thus given two images $\mathrm{Im}1(x, y)$, $\mathrm{Im}2(x, y)$ to be matched the FMI-SPOMF algorithm consists of the following steps:

- compute the Fourier transforms of the FMI descriptors of both images and extract their phases.
- determine the output of the SPOMPF:

$$Q_0(\upsilon,\varpi) = \frac{\mathrm{Im}1_{pl}^*(\upsilon,\varpi) \bullet \mathrm{Im}2_{pl}(\upsilon,\varpi)}{|\mathrm{Im}1_{pl}(\upsilon,\varpi)| \bullet |\mathrm{Im}2_{pl}(\upsilon,\varpi)|} = \exp[-j(\varphi_{im1}(\upsilon,\varpi) - \varphi_{im2}(\upsilon,\varpi))] \qquad [27]$$

- compute the inverse Fourier transform

$$q_0(\theta,\lambda) = F^{-1}\{Q_0(\upsilon,\varpi)\} \qquad [28]$$

- locate the position (α,κ) of the maximum of $q_0(\theta,\lambda)$ and determine the rotation angle α and the uniform scale factor σ

$$\alpha = \theta_{\max} \quad \text{and} \quad \sigma = \exp(\kappa) = \exp(\lambda_{\max}) \qquad [29]$$

- re-scale and re-rotate $\mathrm{Im}2(x,y)$ and calculate the SPOMF between this re-rotated and re-scaled version of $\mathrm{Im}2(x,y)$ and $\mathrm{Im}1(x,y)$
- again locate the position of the maximum of the output and determine the parameters of the geometric transformation, the translation offsets x_0 and y_0

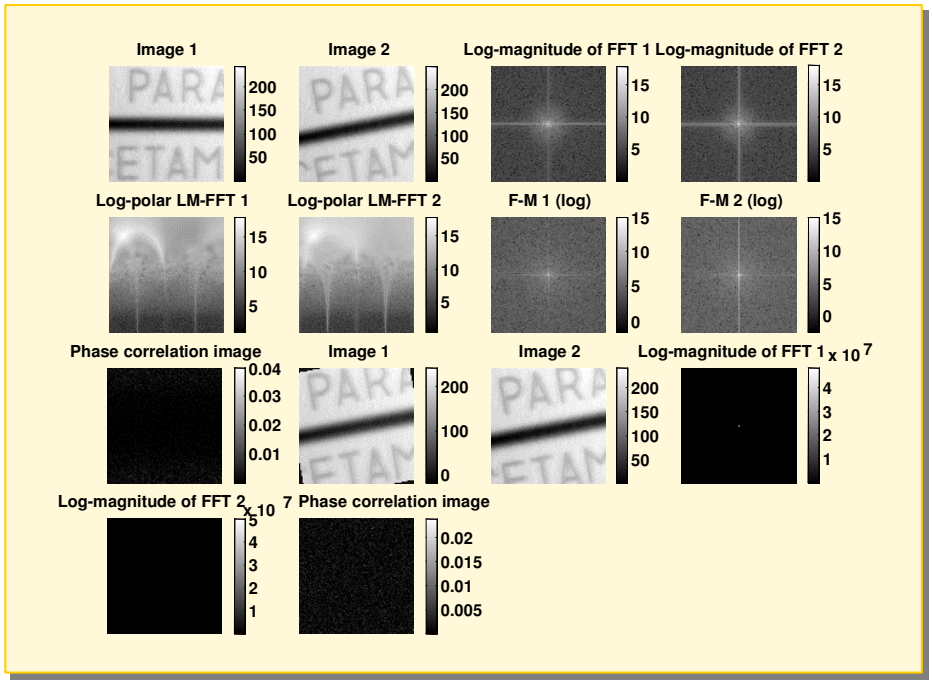

Figure 69 Example of the output of the fm-match routine

Figure 69 shows an example of the output figure of the fm-match routine. Following the subfigures from left to right, the first two show the two images to be matched, the next two are their spectral magnitudes on a logarithmic scale. The first two on the second row are the polar logarithmic representations and the next two are their Fourier transforms on a logarithmic scale again. The first subplot on the third row shows the phase correlation image of the two Fourier transformed FMI descriptors. The second and third subplots show respectively the rotated and re-scaled version of image 1 and the original image 2. In the last of the third and the first of the fourth row their spectral magnitudes are plotted and the final subplot shows their phase correlation image. In both of the phase correlation images the routine locates the maximum and calculates respectively the rotation, scaling and translation parameters and gives their values as output. By applying these transformations to $\mathrm{Im}2(x,y)$ and subtracting this transformed image of $\mathrm{Im}1(x,y)$ the comparison of the two can take place.

Experiments:

Tests method1:

- match two series of recordings of the same tablet
- match two series of recordings of two different tablets made with the same punch
- match two series of recordings of two different tablets made with different punches
- show necessity for multiple recordings in case of logos with rotational symmetry

4.2.2.2 Method 2

Step one and two, the gray scale adjustment and rotation correction in case of the tilted holder are the same as for method 1.

Step 3: matching the series of images of each of the rotated tablets

Thus instead of matching the recordings of both tablets in the same position now the whole series of recordings of the first tablet is matched with the $\varphi = 0°$ image of that tablet and the recordings of the second rotated tablet are all matched with their own $\varphi = 0°$ image. The same technique can be used to find the rotation, scaling and translation parameters as in method 1.

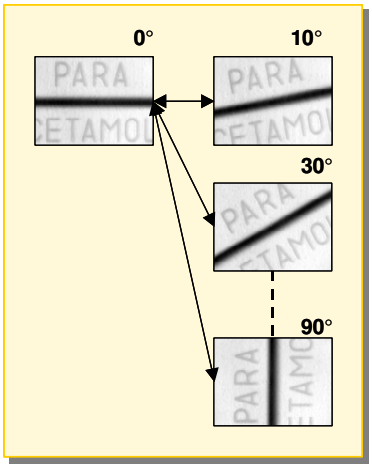

Figure 70 Matching for method two

Step 4: combine the matched images into one

Before doing the actual comparison of different tablets the series of matched images will be combined into one. In each of the recordings of the rotated tablet only part of all pixels is imaged correctly. Figure 71 shows what orientation was imaged optimally in each of the recordings, if the logo contains for example the letter A, the gray values for the horizontal stripe must be taken from the $0°$ recording while the values for the left leg are more reliable in the $60°$ or $80°$ recordings, same hold for the right leg the gray values for those positions are determined best in the $100°$ or $120°$ recordings.

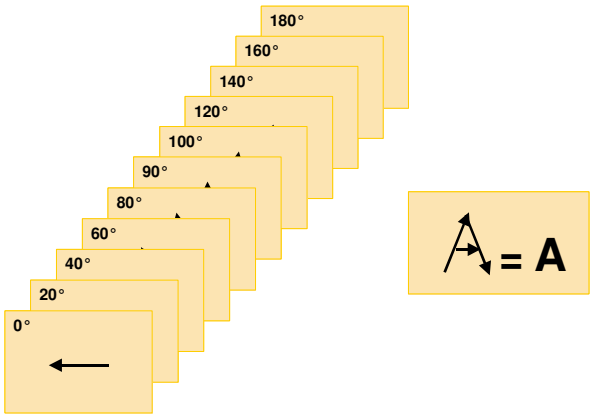

Figure 71 optimal imaged orientations for the different recordings

By using only those pixel values from each of these recordings to build up the combined image, this new image will contain only pixels that were in the right orientation while they were recorded. So it will be one 'perfect' image of the tablet, the height values will be reliable on every position of the tablet. The selection of pixels that can be used in each of the recordings is done based on their orientation. These orientation values can be determined by using the structure tensor $\overline{G}$ [12]:

$$\overline{G} = \overline{\nabla f \cdot \nabla f^{t}} = \overline{\begin{pmatrix} f_x \\ f_y \end{pmatrix} \cdot \begin{pmatrix} f_x f_y \end{pmatrix}} = \begin{pmatrix} \overline{f_x^2} & \overline{f_x f_y} \\ \overline{f_x f_y} & \overline{f_y^2} \end{pmatrix} = \begin{pmatrix} \overline{f_u^2} \equiv \lambda_1 & 0 \\ 0 & \overline{f_y^2} \equiv \lambda_2 \end{pmatrix} \qquad [30]$$

Figure 72 graphically shows the transformation to the principal axes u and v.

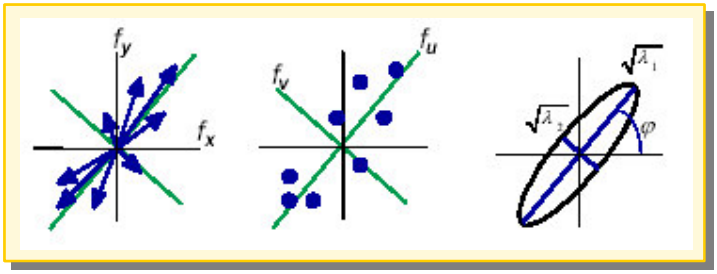

Figure 72

The orientation value for all pixels is given by

$$\varphi = \tan^{-1}\left(\frac{2\overline{f_x f_y}}{\overline{f_x^2} - \overline{f_y^2}} \right) \qquad [31]$$

The figures below show examples of 'orientation pictures' of the paracetamol recordings. Now the gray values are replaces by the orientation of a pixel as calculated with the gradient structure

tensor. To make the combined image, pixels that have orientation $|\varphi| = \frac{\pi}{2}$ are selected. In the figures below these pixels are highlighted in red.

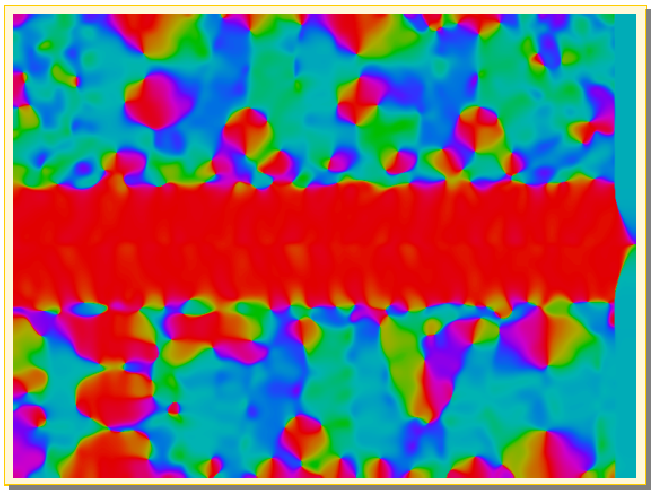

Figure 73 Orientation image of 0° recording of a paracetamol tablet

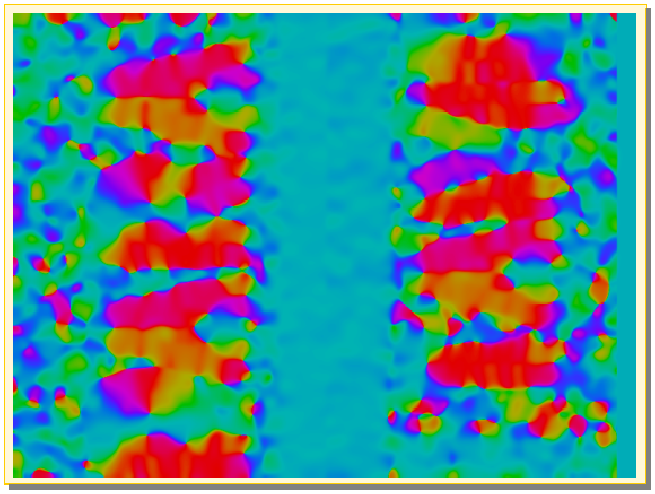

Figure 74 Orientation image of 90° recording of a paracetamol tablet

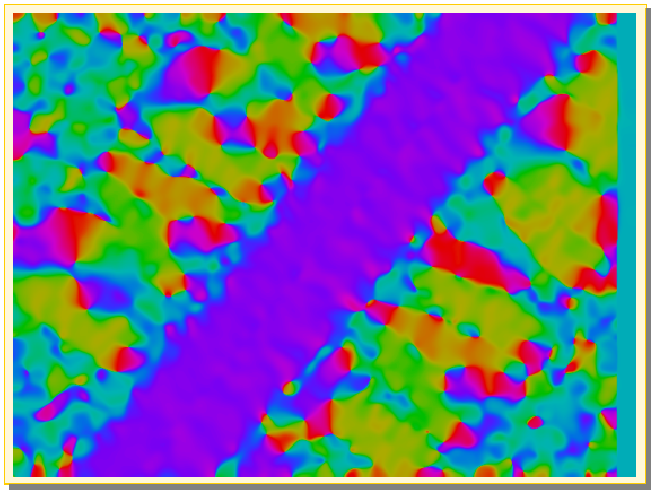

Figure 75 Orientation image of 50° recording of a paracetamol tablet

Step 5: matching the combined images of the tablets that must be compared

Finally the combined images of both tablets under investigation must be matched with each other and based on that match the comparison of the two can be done. Dependent on the results of that match a conclusion can be drawn whether it's possible that the tablets were made with the same punch. Again the Fourier-Mellin method can be used to do the matching.

Experiments:

Test method 1:

- match a series of recordings of a rotated tablet with the zero degree recording
- explore the possibility of the combined image

3.2.3 Phase 3: comparison

In this last phase the results of the matching process are investigated. The MSE value of two matched images is an indication for the measure of their resemblance. In case of large differences cross-sections can be made to visualize the cause of these differences. Besides comparing the entire depth-images several features of the imprints as described in chapter 2 can be determined and compared.

5 EXPERIMENTS

Most experiments described in this chapter are performed on paracetamol tablets. This is done while these tablets have imprints containing logo and break line on one side of the tablet.

5.1 Determination of minimal number of required recordings

To determine the number of recordings that is needed to image the entire tablets properly the following experiments were done. A paracetamol tablet was recorded in 18 different positions, it was rotated over a range of $-90° \leq \varphi \leq 90°$ in steps of 10 degrees. Cross-sections perpendicular to the break line were taken at the same location on the tablet in each recording as is indicated in Figure 76. The cross-sections in the recordings of the rotated tablets were compared to the one that

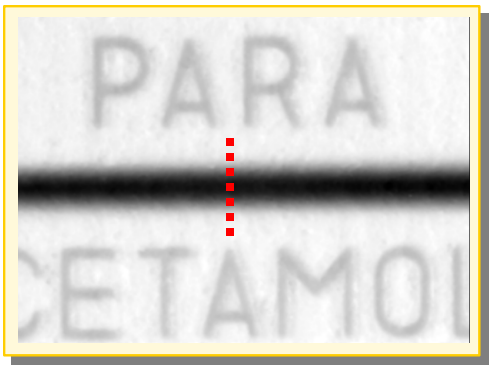

Figure 76 Location of cross section (in red)

was taken of the tablet when it was in the position that images the break line correctly, the $\varphi=0°$ position. To rule out accidental deviations, the gray values in the cross-sections shown in the following figures are the mean values of 10 neighboring pixels. By comparing the cross-sections of the rotated images to the 'correct' one it becomes clear at which rotation angle the deviation in height values becomes so large that they cannot be used anymore as reliable values in the comparison process. Figure 77 shows an example of this deviation.

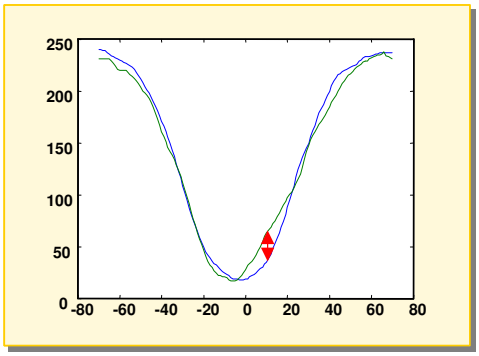

Figure 77 Example of deviation caused by occlusion

To decide at which angle of rotation the deviation is no longer acceptable following procedure was used. An error signal ε_φ was calculated for each rotation angle φ by subtracting each of the curves, l_φ from the $\varphi = 0°$ curve, $l_{0°}$.

$$\varepsilon_\varphi = l_{0°} - l_\varphi \qquad [32]$$

Figure 78 shows an example of the resulting error curve for the $\varphi = 90°$ cross-section.

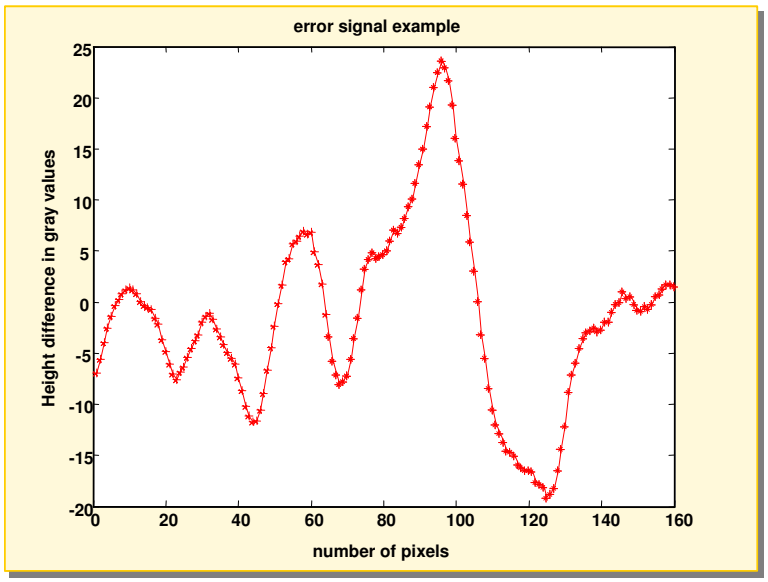

Figure 78 Resulting error curve for the $\varphi = 90°$ cross-section

As can be seen in Figure 79 the cross-sections are divided into four areas A,B,C and D. The parts A and D both contain 50 pixels and B and C each take up 30 pixels.

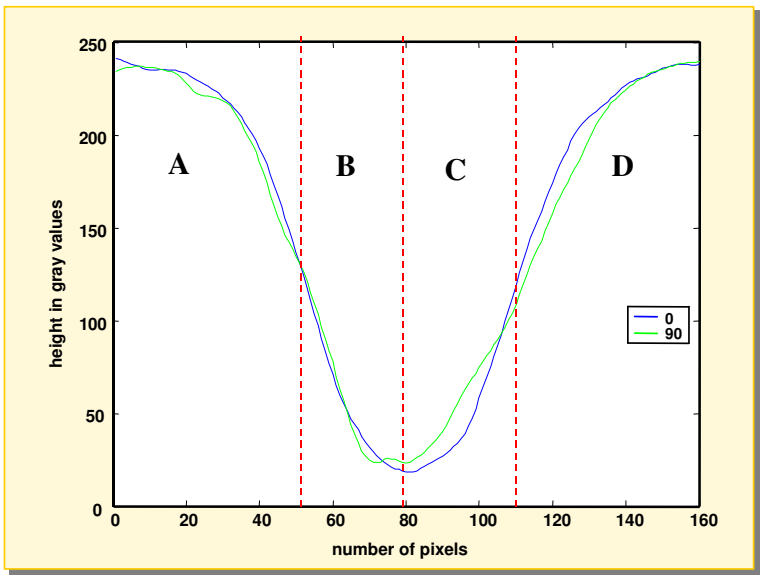

Figure 79 cross-sections divided in four areas

For each rotation angle φ the area between the two curves l_φ and $l_{0°}$ is calculated. By integrating the error signals ε_φ over these different areas, the mean error E in each of the four areas separately and for the total curve as well as the two half curves, A+B and C+D can be calculated.

$$E_A = \frac{\int_A |\varepsilon| dx}{\int_A dx} \qquad E_B = \frac{\int_B |\varepsilon| dx}{\int_B dx} \qquad E_C = \frac{\int_C |\varepsilon| dx}{\int_C dx} \qquad E_D = \frac{\int_D |\varepsilon| dx}{\int_D dx}$$

$$E_{AB} = \frac{\int_{A+B} |\varepsilon| dx}{\int_{A+B} dx} \qquad E_{CD} = \frac{\int_{C+D} |\varepsilon| dx}{\int_{C+D} dx} \qquad E_{tot} = \frac{\int_{A+B+C+D} |\varepsilon| dx}{\int_{A+B+C+D} dx} \qquad [33]$$

Before subtracting them the curves are shifted so that they overlap with the $l_{0°}$ curve as much as possible. To determine the shift that results in this best match, the curves were first subjectively placed onto each other by hand. Using this as start position the curves were then shifted 3 pixels up, down, to the left and to the right. By calculating the total mean error E_{tot} for each possible

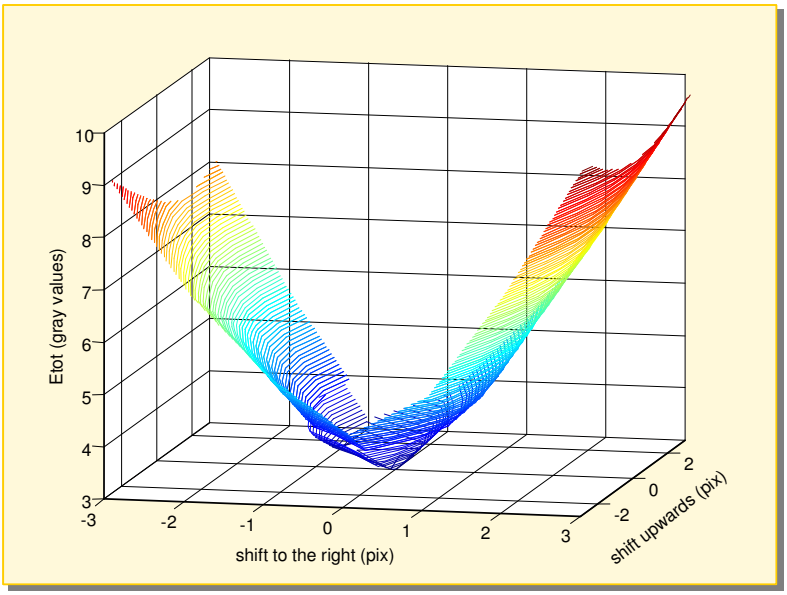

Figure 80 Variation in E_{tot} for $\varphi = 30°$

combination of shifts and applying the one that results in the minimal total error, an objective best match was found. In Figure 80 and Figure 81 examples of the effect of shifting the curves in the four directions on the total error E_{tot} is shown for $\varphi = 30°$ and $\varphi = 90°$.

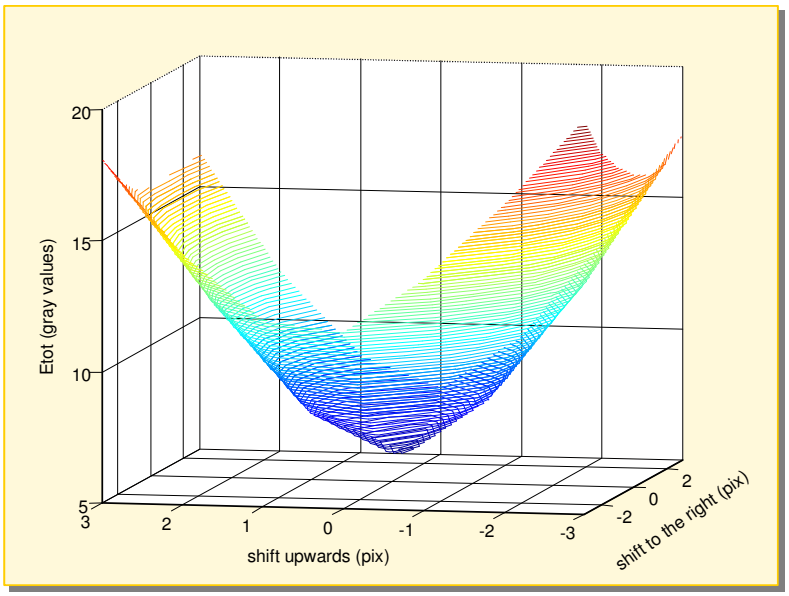

Figure 81 Variation in E_{tot} for $\varphi = 90°$

In order to find out whether the number of necessary recordings can indeed be reduced by using the tilted holder, the series of 18 recordings of the tablet were done using the flat holder as well as the tilted one. The results of both series are presented in the following sections. In both series the projection came from the right. The FH or TH in the subtitles of the figures indicate whether the cross-sections are part of the series in which the flat holder respectively the tilted holder was used. The numbers represent the angle of rotation $\Delta\varphi$ with respect to the $\varphi = 0°$ curves.
The minimal total errors as well as the belonging errors for the separate areas were calculated for $\varphi = 0°,10°..90°$ and plotted versus the angle of rotation. Both error curves for the flat as well as the tilted holder are plotted in the same figures so the effect of the tilt on these errors can best be determined.

5.1.1 Cross-sections flat holder

In Figure 82-Figure 87 the blue curves are the cross-sections of the $\varphi = 0°$ recording and the green curves are cross-sections in the recordings of the rotated tablets. In all figures the height is plotted in gray values, to convert these values to actual heights, the conversion factor C for the results of the flat holder is $C = 1.69\,\mu m/grayvalue$

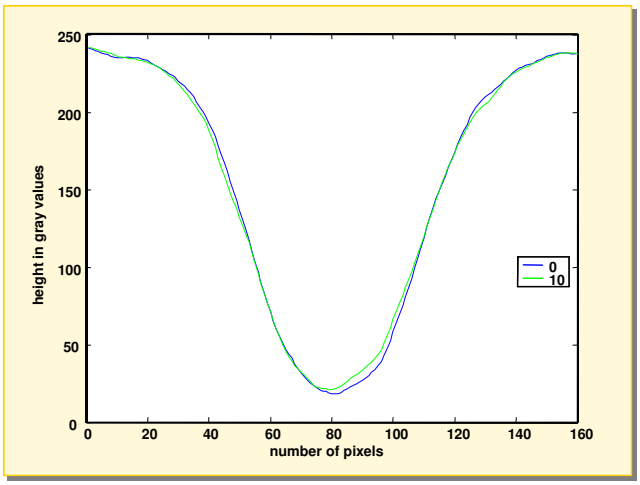

Figure 82 FH 10

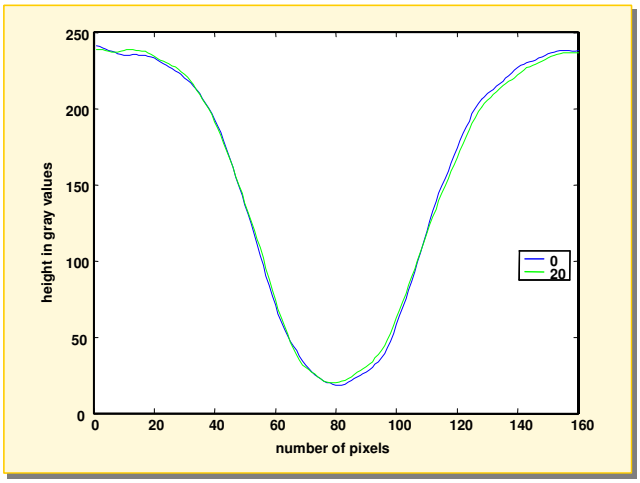

Figure 83 FH 20

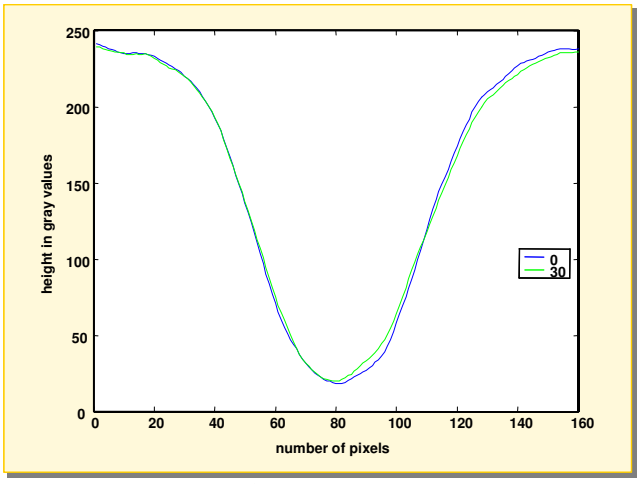

Figure 84 FH 30

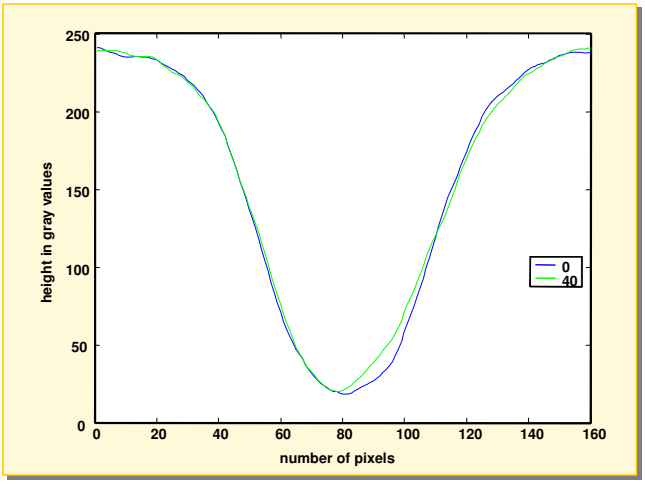

Figure 85 FH 40

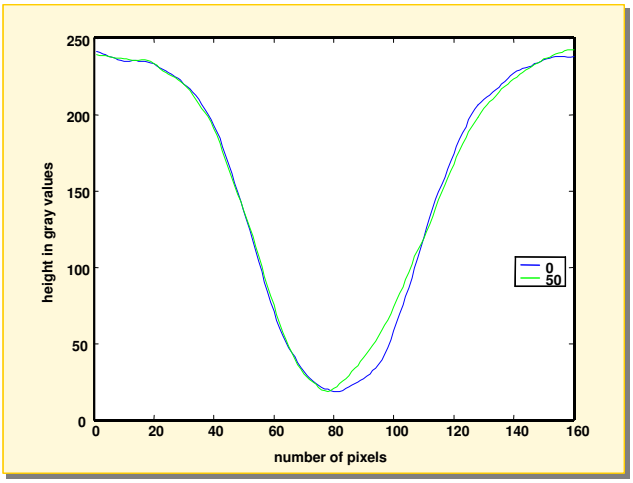

Figure 86 FH 50

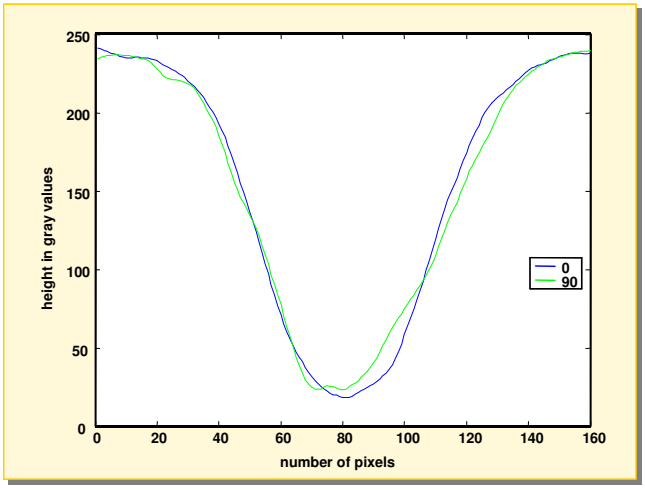

Figure 87 FH 90

5.1.2 Cross-sections tilted holder

In Figure 88-Figure 93 the blue curve is the cross-section of the $\varphi = 0°$ recording and the red curves are cross-sections in the recordings of the rotated tablets. At first sight the differences between both curves seem to be a lot smaller in the following figures but that's because they are not plotted on the same scale as the curves of the flat holder. The conversion factor C for the results of the tilted holder is $C = 9.176 \mu m / grayvalue$

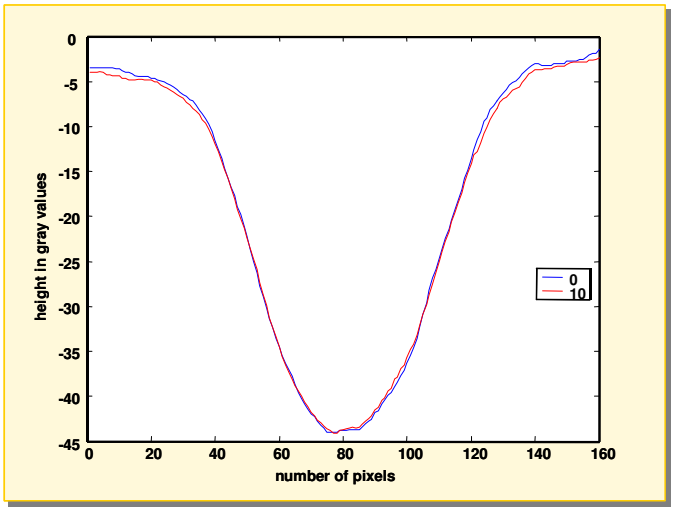

Figure 88 TH 10

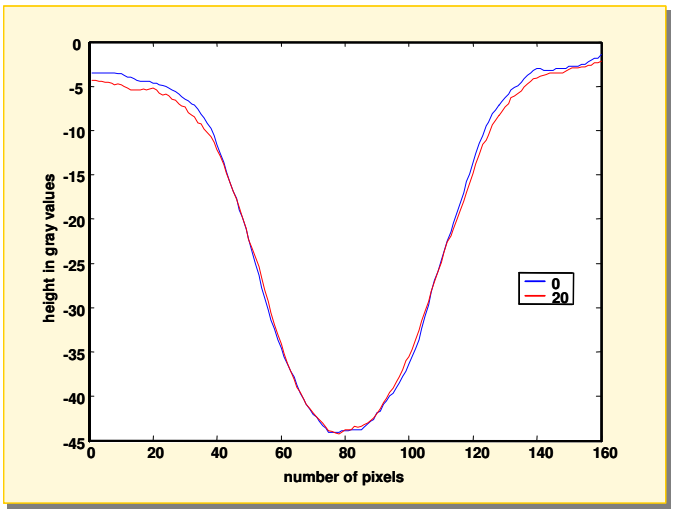

Figure 89 TH 20

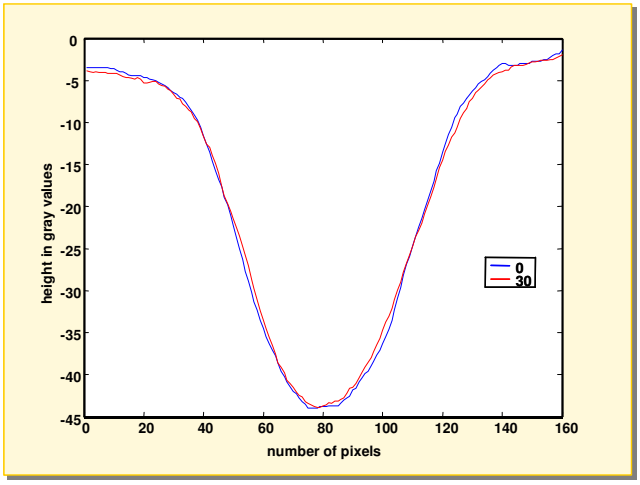

Figure 90 TH 30

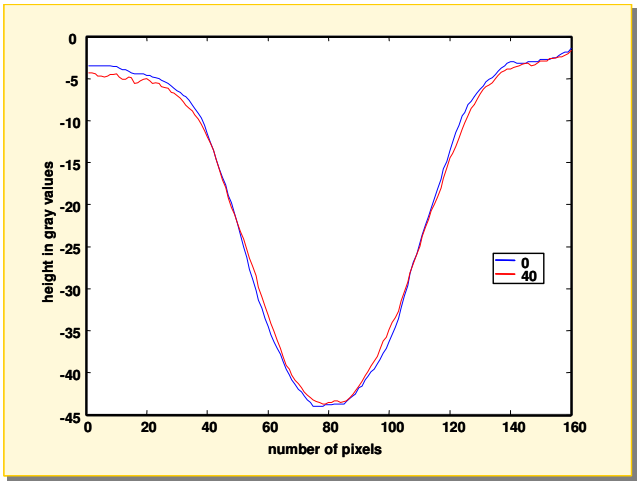

Figure 91 TH 40

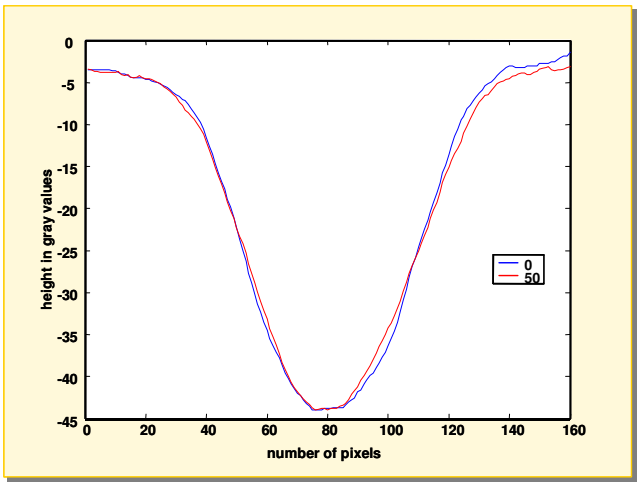

Figure 92 TH 50

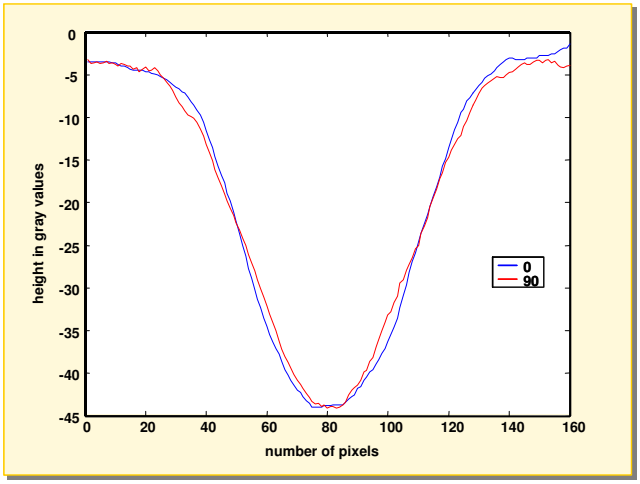

Figure 93 TH 90

5.1.3 Error curves

The minimal total errors as well as the belonging errors for the separate areas were calculated for $\varphi = 0°,10°..90°$ and plotted versus the angle of rotation. Both error curves for the flat as well as the tilted holder are plotted in the same figures so the effect of the tilt on these errors can best be determined. In Figure 94-Figure 100 the blue curve represents the errors found using the flat holder and the green curve shows the errors for the tilted holder recordings. To demonstrate the effect of shifting the curves as was shown already for the total errors in Figure 80 and Figure 81, for $\varphi = 30°$ and $\varphi = 60°$ the other errors were also calculated for a one-pixel shift in all four directions. The maximum and minimum errors that were found are presented respectively by the upper and lower limits of error bars in the graphs. All errors are determined in gray values the scaling for the recordings of the tilted holder was adjusted to match the scale of the flat holder recordings. Therefore the gray values in the error graphs can be converted to height values using the same conversion factor $C = 1.69\,\mu m/grayvalue$

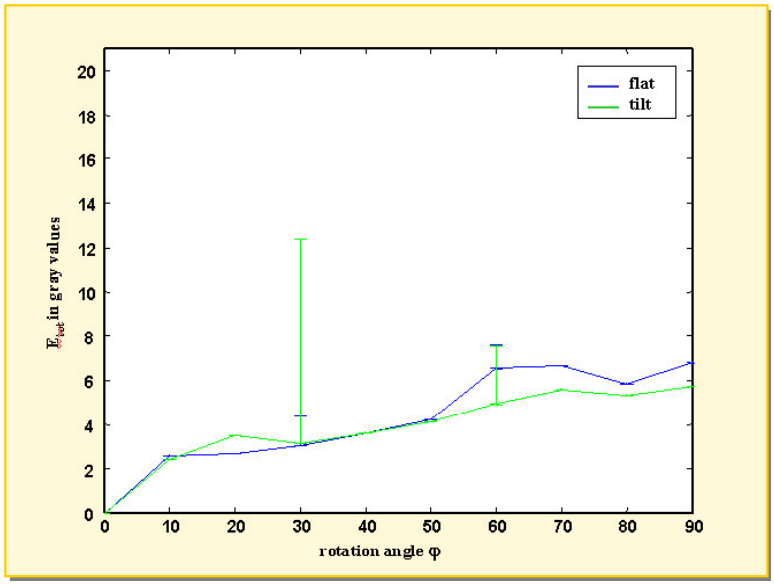

Figure 94 E_{tot} for both holders

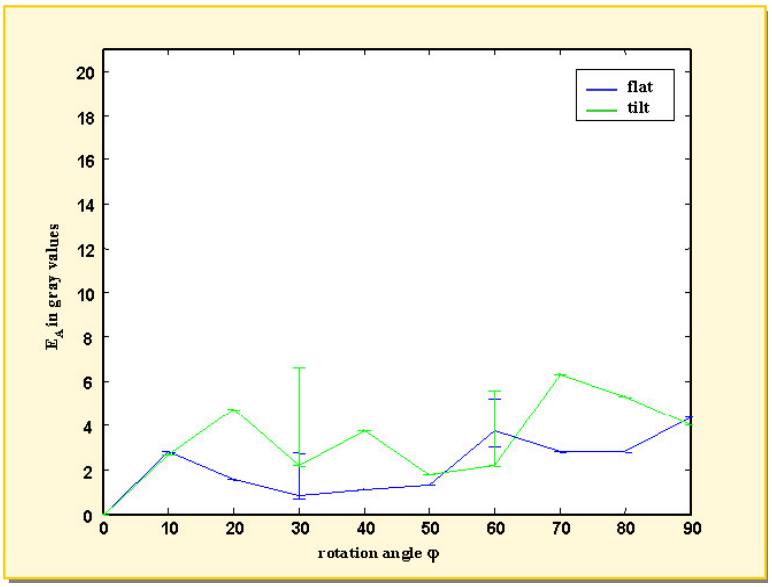

Figure 95 E_A for both holders

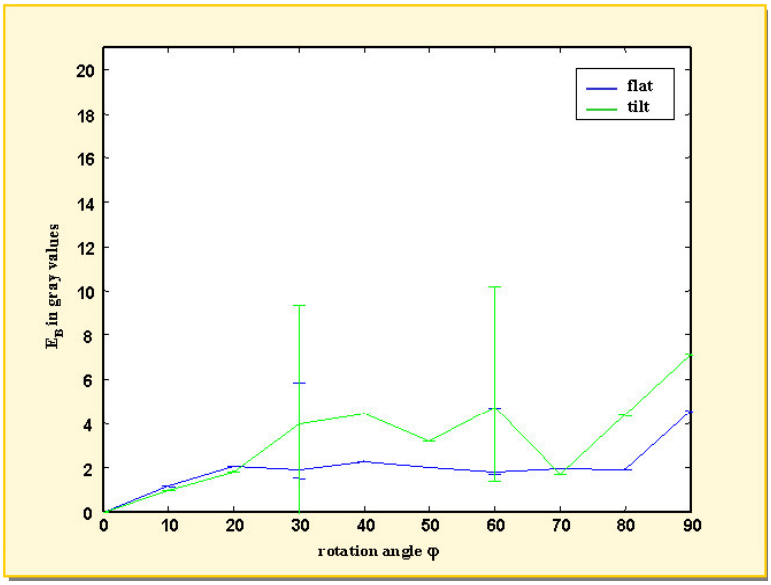

Figure 96 E_B for both holders

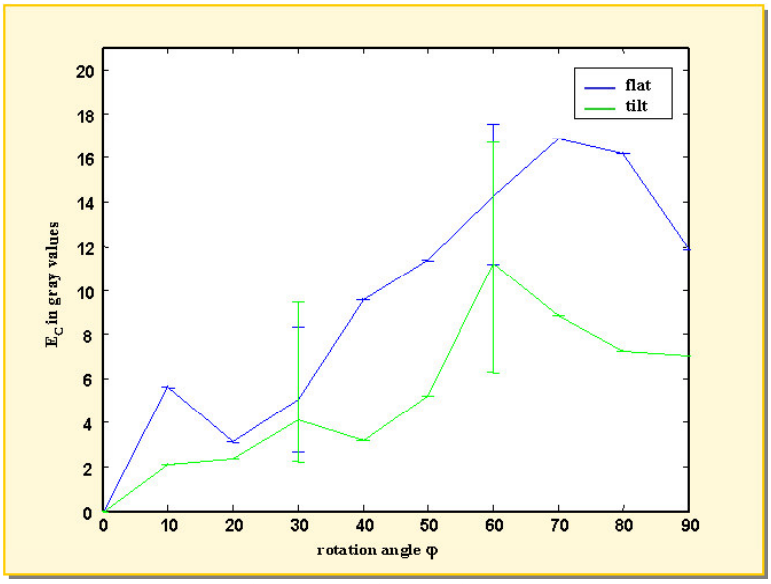

Figure 97 E_C for both holders

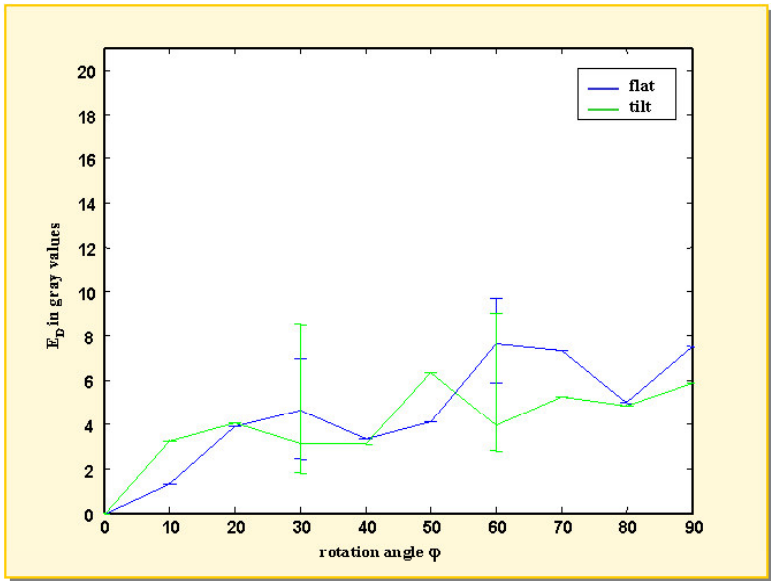

Figure 98 E_D for both holders

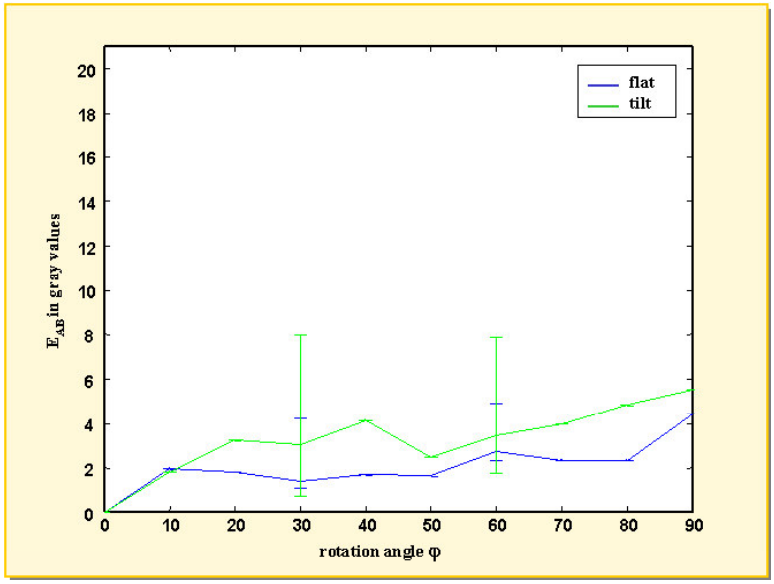

Figure 99 E_{AB} for both holders

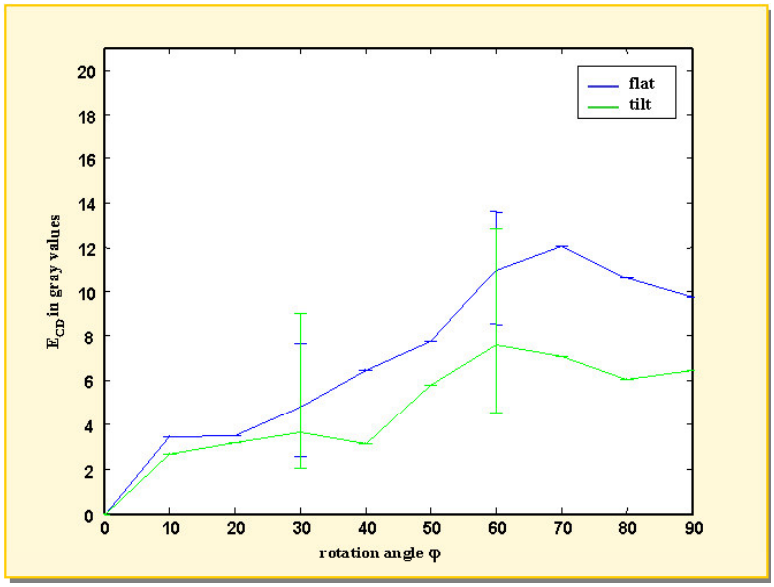

Figure 100 E_{CD} for both holders

5.1.4 Conclusion

Figure 82-Figure 93 show a clear tendency, the measurement error in the problem area CD increases with increasing rotation angle as was expected. To decide at what angle the errors are still acceptable the real height values were examined. Even though this experiment only represents one realization of the problem it is a good indication of what happens to the measurement error for increasing rotation angle. Up to 20 degrees the mean error in all areas stays below 7 µm but as can be seen from the error bars for the 30° and 60° angles these errors are very sensitive to matching, shifts of one pixel can easily double or even triple these values. These errors depend obviously also on the angle of the break line of the tablet that is being examined. The results of this experiment on a paracetamol tablet argue for steps of 20° between subsequent recordings of the rotated tablet and an quick examination of a series of different XTC tablets show that they contain break lines of comparable angles as this paracetamol tablet. Thus in most cases similar results are expected for XTC tablets but to be sure before recording a tablet, the angle should be measured and in case it is much smaller or larger a choice can be made to make respectively more or less recordings. Figure 94 shows that for rotation angles up to 50 degrees the tilted holder did not lead to smaller measurement errors. For greater angles the results show some improvements but considering the extra steps that were introduced by using this holder they are not significant enough to balance out. In an attempt to profit from the improvement of the holder on the measurements without having to deal with its drawbacks one other recording method was examined. The same series of measurements was done only this time the tilted holder was also used as reference plane during the calibration. When the height values are calculated with respect to the tilted holder the rotation algorithm as well as the gray scaling correction are no longer necessary. Therefore using this holder as reference plane would be a very useful option but for unknown reasons the MicroCad seems not to be able to handle tilted reference planes. At first sight it appeared to be possible, the pixel sizes were adjusted correctly and the recordings seemed to be accurate. Unfortunately after taking a closer look at the results of the experiments unexplainable things were found leading to the conclusion that it is not working

correctly. Figure 99 and Figure 100 show that the tilted holder does work as was expected it divides the measurement errors caused by occlusion over both sides of the break line. Measurements in the “problem area” CD improve for all angles but while the other side of the break line is now occluded as well because the tilted holder leads to a symmetrical set up, the error in this area AB becomes larger and as a result the total error is not reduced significantly. This effect can also be seen in the cross-sections plots the ones with the tilt do not match for both sides of the break line while the curves of the flat holder fit well on the left side for all angles but the right sides diverge more and more.

5.2 Detection of scratches on V-profiles

To determine the dimensions of the minimal detectable scratches a second test object was designed. As was mentioned earlier the punches are most likely to be damaged on the sharp edges of the logos and break line, in order to simulate this situation a punch containing a break line was manufactured and deliberately damaged. Several damages were made on top of the break line and on one of the flat sides of the punch as can be seen in Figure 101. The holes in this picture are not on scale but enlarged to make them visible.

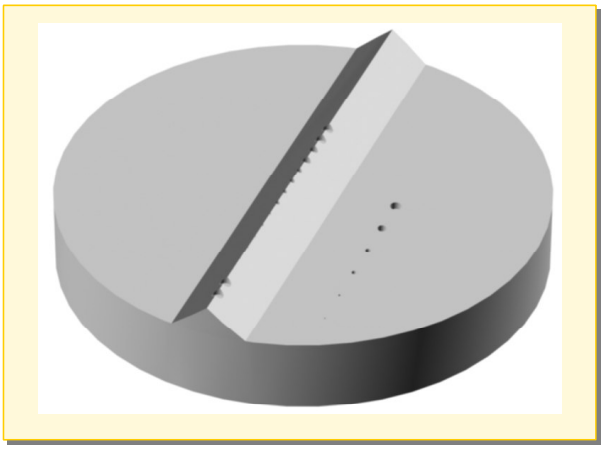

Figure 101 Damages on break line and flat sides of punch

These holes were made using laser drilling. The diameter of the holes is adjustable. The laser shoots 5 times per second creating a hole of approximately 200 nm deep per shot therefore the desired depth can be achieved by adjusting the time that the laser is working. For example to create a hole of 50 micrometer deep the laser must be on for 50 seconds. The exact resulting depth per shot depends on the material that is used. Above calculations are based on results of experiments done by the chemical department of the Forensic Institute on plastic objects and the depth created in the material used for the punch is expected to have similar properties resulting in comparable depths. Several holes with known and growing dimensions were made on top of the V-shaped break line and on the flat part of the punch. The exact number of holes on both locations and their dimensions are listed in Table 5-1 and Table 5-2

Table 5-1 dimensions of holes on top of the break line

number	diameter (µm)	depth (µm)
1	50	100
2	50	100
3	4	10
4	4	10
5	6	10
6	6	10
7	10	20
8	10	20
9	20	20
10	20	20
11	25	20
12	25	20
13	40	30
14	40	30
15	50	50
16	50	50

Table 5-2 dimensions of holes on flat side

number	diameter (µm)	depth (µm)
1	4	10
2	6	10
3	10	10
4	20	20
5	25	20
6	40	20
7	50	20

Using Silmark low viscosity gray a casting of the damaged punch was made. The scratches that were created on the punch will result in bumps on the break line in the casting thereby simulating the resulting bumps in a tablet. The cast was inspected with the Microcad and the results are shown in the following section.

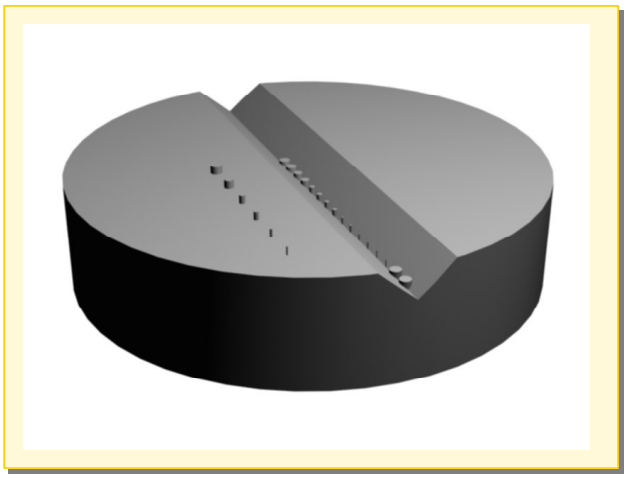

Figure 102 Bumps on the cast resulting from damages on the punch

5.2.1 Results

The break line was recorded while positioned parallel to the direction of projection therefore only one recording was sufficient to properly image the region of interest. In order to improve precision in detection of the bumps 12 recordings of the cast were made and averaged. Figure 103 shows one of these recordings, they were all made in one series without moving the cast or changing the adjustments in between.

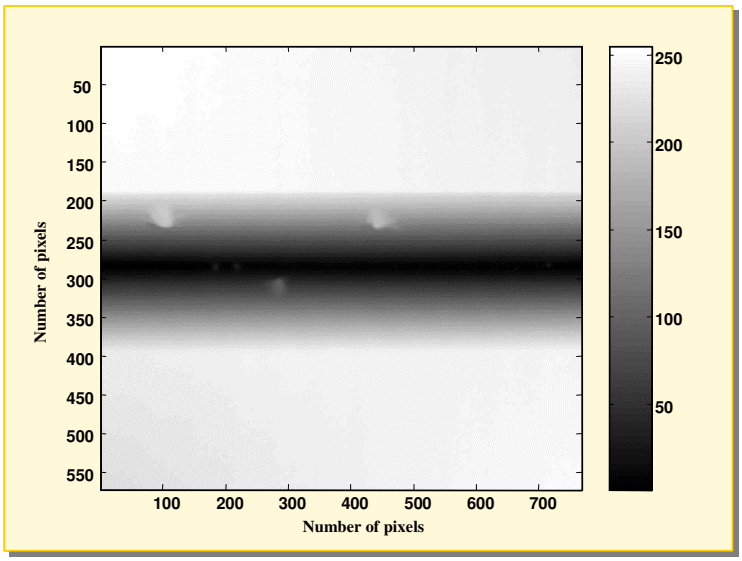

Figure 103 Example of recording of the cast

The large white spots in Figure 103 are larger bumps on the cast caused by damages on the punch that were made earlier with a milling machine during manufacture. They were used in preliminary research but the results will not be further discussed in this report.
Figure 104 and Figure 105 show both areas containing the bumps that were indeed used for this experiment.

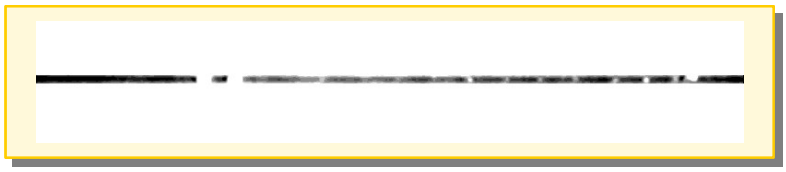

Figure 104 Zoom of series of bumps in break line

Figure 105 Zoom of series of bumps on flat side of cast

Figure 106-Figure 109 show cross-sections perpendicular to the break line in one of the recordings. The blue lines in all figures are the cross-section taken just a few pixels to left of each of the bumps and the red lines are cross-sections taken through the middle of the bumps. The gray values of the blue lines are the mean values of 5 neighboring pixels in all figures but the number of neighboring pixels used to calculate the gray values of the red lines is not the same for all figures. It depends on the diameter of each of the bumps how many pixels were used. The conversion factor C for these series of measurements is $C = 3.56 \mu m / grayvalue$. The large bulge on the left side of the break line in Figure 106 is caused by one of the bumps created by milling mentioned above, the bumps of interest are the ones in the tip of the V-profiles.

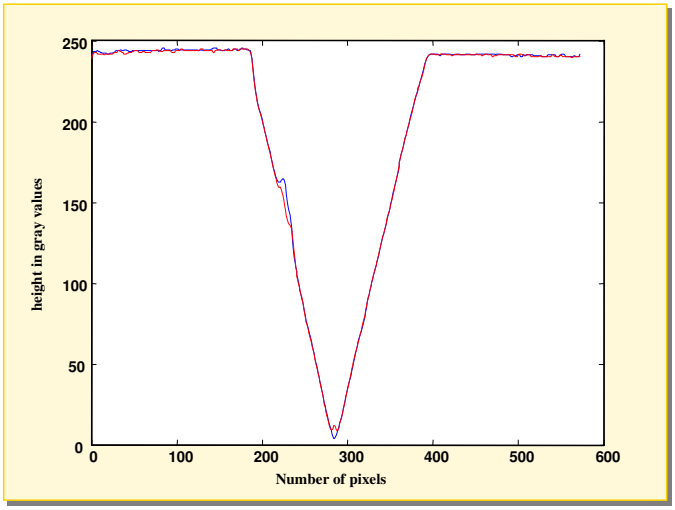

Figure 106 Bump diameter of 20 µm

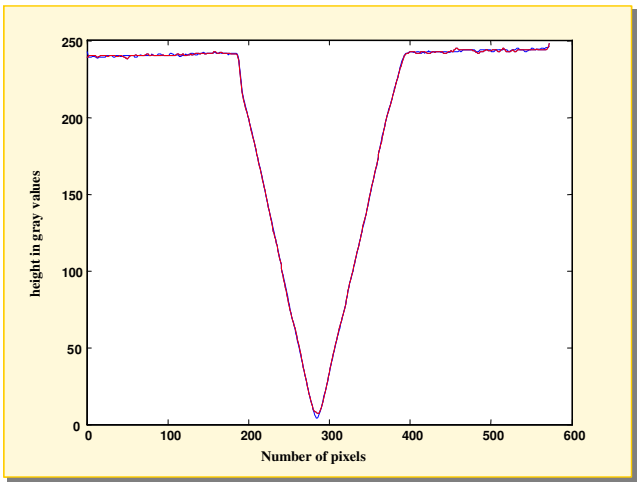

Figure 107 Bump diameter of 25 µm

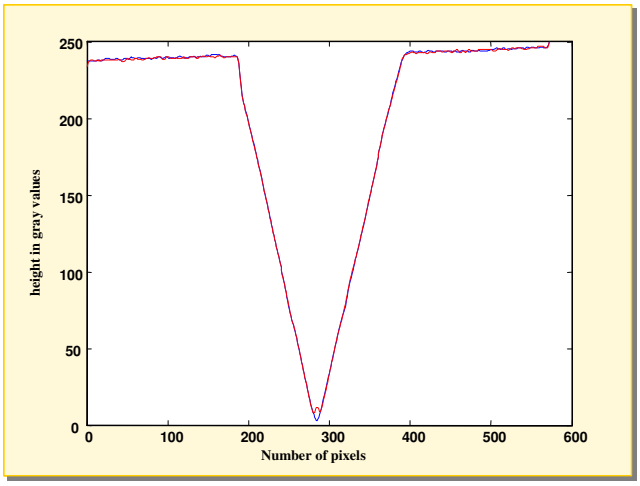

Figure 108 Bump diameter of 40 µm

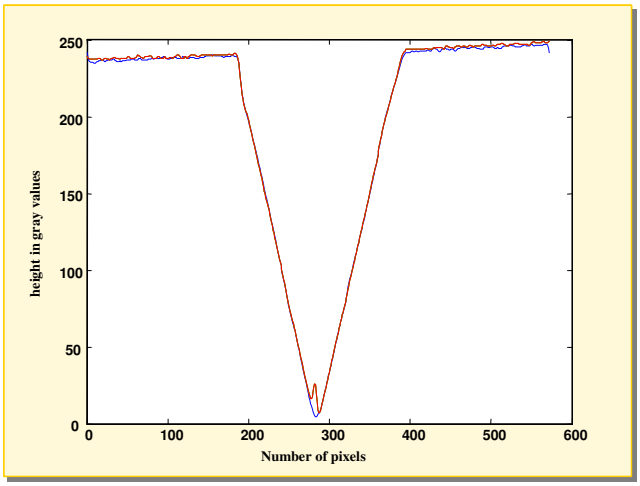

Figure 109 Bump diameter of 50 µm

For the series of bumps in the break line as well as the one on the flat side cross-sections were taken right through the series of bumps and a few pixels to the left of them. The cross-sections in the break line from all twelve recordings are plotted in Figure 110 and Figure 111.

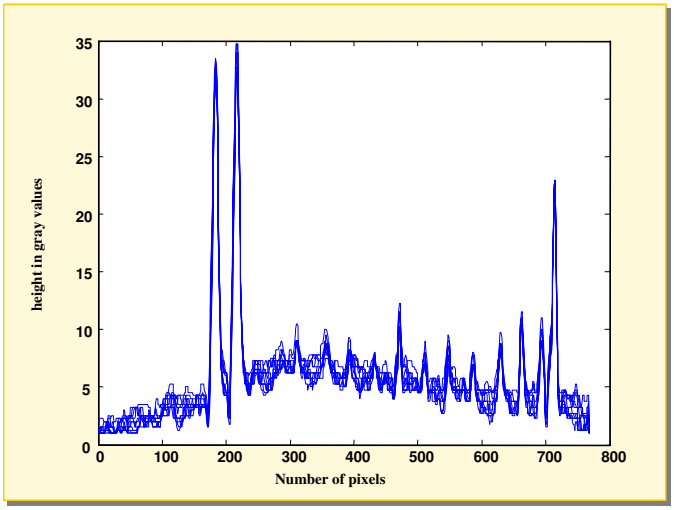

Figure 110 Twelve cross-sections through the bumps

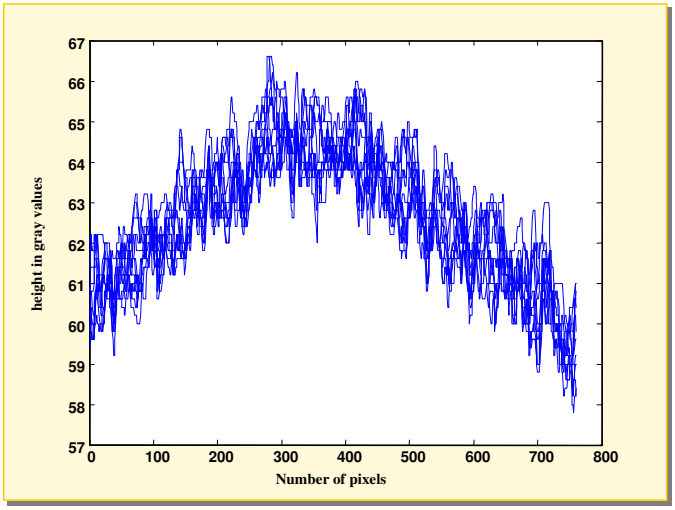

Figure 111 Twelve cross-sections next to the bumps

The twelve cross-sections for the other series of bumps are plotted in Figure 112 and Figure 113.

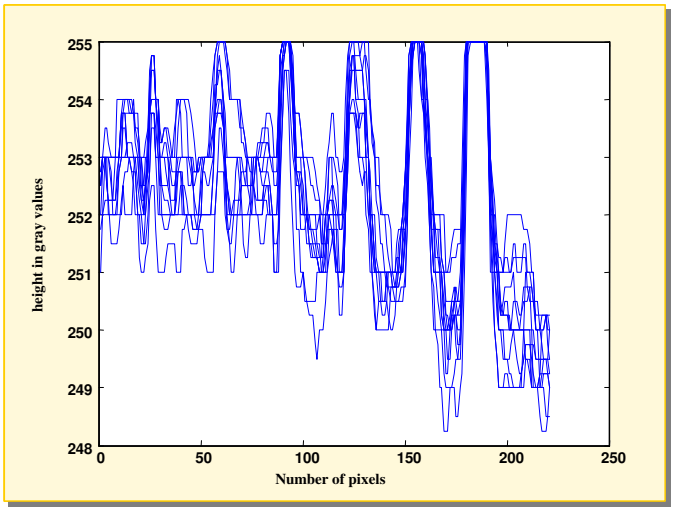

Figure 112 Twelve cross-sections through the bumps

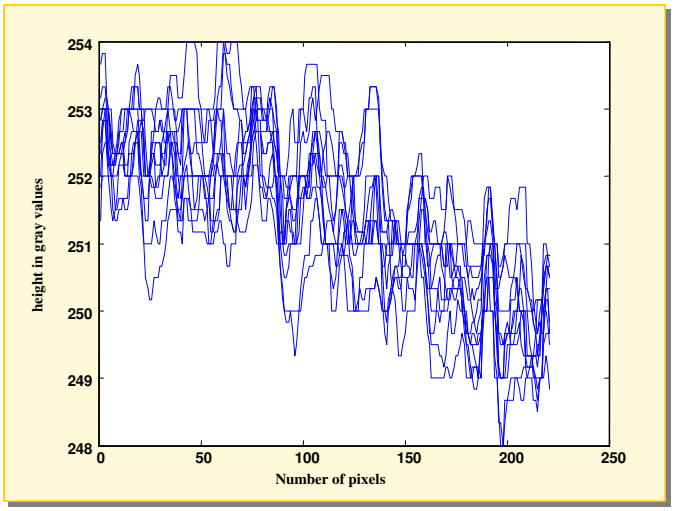

Figure 113 Twelve cross-sections next to the bumps

To determine whether a height difference in the plot can be classified as an actual bump the mean and standard deviation for the bumps as well as the areas in between the bumps are calculated. In Figure 114-Figure 119 the mean and standard deviation values are plotted for both series of bumps. The mean values for the cross-sections taken right next to the bumps are plotted in the same figures as the green curves.

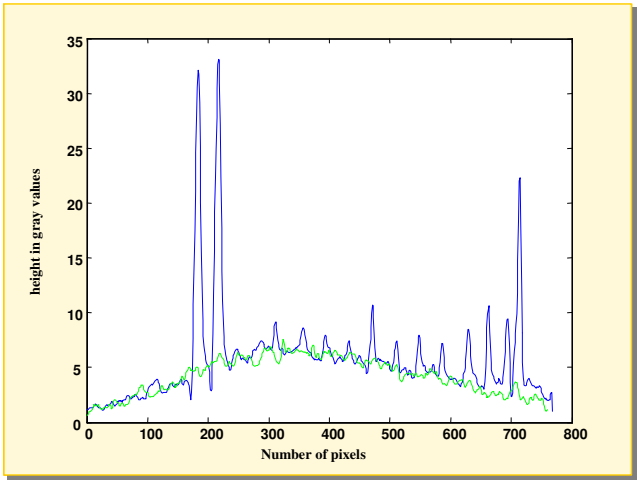

Figure 114 Two means of the twelve cross-sections in the break line

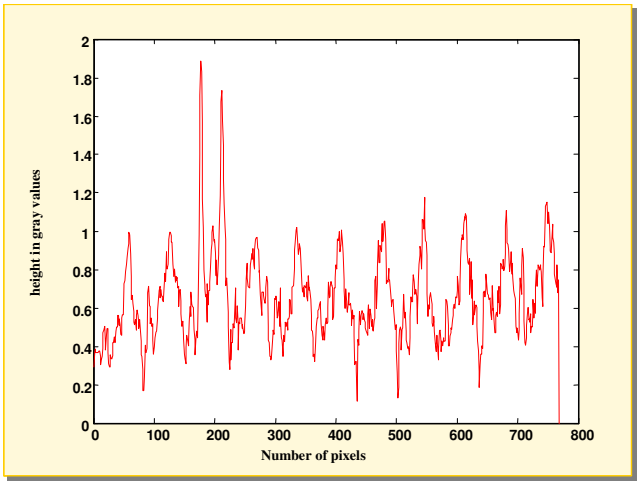

Figure 115 Standard deviation of the bumps

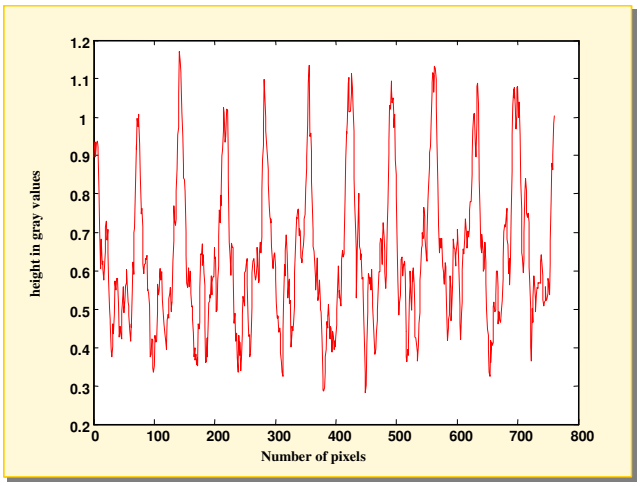

Figure 116 Standard deviation next to the bumps

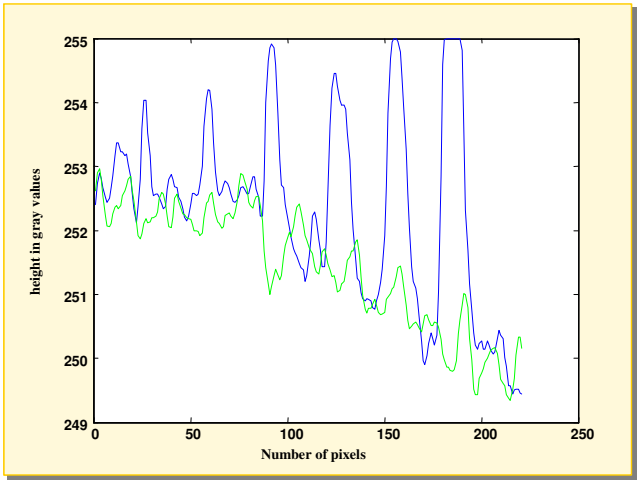

Figure 117 Two means of the twelve cross-sections on the flat side

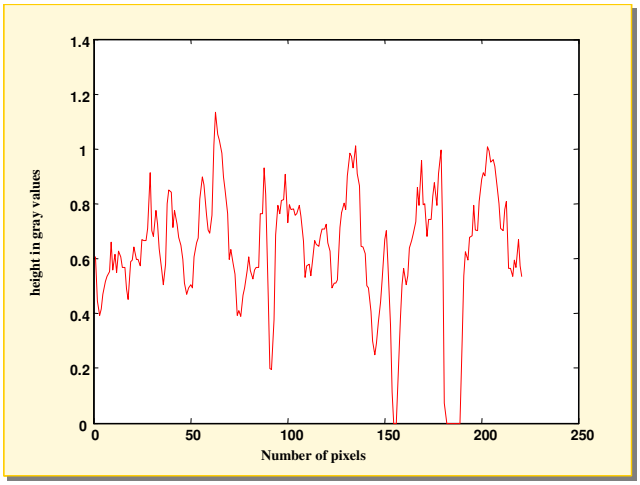

Figure 118 Standard deviation of the bumps

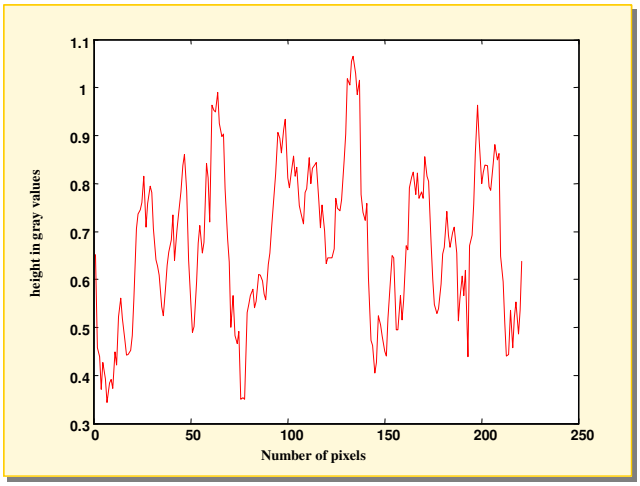

Figure 119 Standard deviation next to the bumps

For each of the height differences can be checked whether they fall within the range of imprecision of the measurements or that they are actual height differences using the following definition for the 95% confidence interval, see [13].

$$\bar{x} \pm t_{0.5*\alpha,n-1} * \frac{s}{\sqrt{n}} \qquad [34]$$

$$\beta = 100(1-\alpha) \qquad [35]$$

In equation $\bar{x}$ represents the mean value of the twelve measurements and s is the belonging standard deviation. The student-t factor $t_{0.5*\alpha,n-1}$ that is used in this equation can be found in table 2 of [13]. This factor depends on the number of measurements n that is done and the percentage of confidence β that is desired. In this case for a 95% interval, α=0.05 and together with n=12 a value of 1.796 was found for the student-t factor.

$$\bar{x} \pm 1.796 * \frac{s}{\sqrt{12}} \qquad [36]$$

Calculations of all confidence intervals proved that there is no overlap between the intervals of the bumps and the areas in between, except for the bump with a diameter of 4µm.

5.2.2 Conclusions

As can be concluded from the results above only the smallest bumps with a diameter of 4 µm can not be classified as actual height differences they can not be distinguished from the fluctuations in height due to noise. The fact that not all bumps that were created by holes of the same depth, have the same height is probably the result of the founding-process. The material that was used to make the mould probably did not fill all holes as deep, the ones with a smaller diameter are harder to fill as deep as the ones with a larger diameter. Another reason can be that the material that is ablated by the laser does not always leave the hole on time before the next shot so that part of the lasers energy is absorbed by this ablated material. Especially when the diameter of the hole is small compared to the desired depth this can cause the holes to become less deep then planned.

5.3 Tests method 1:

5.3.1 FM-routine performance tests

Before doing the actual experiments with the series of recordings of the rotated tablets the performance of the FM-match routine was tested on several test images. When matching a rotated and translated version of an image with its original the routine finds the used parameters without any problems. The angle of rotation can be estimated with an accuracy of 1 degree and the translations in both directions are determined in integer numbers of pixels, it is not possible to match on a sub-pixel level with this routine. After matching an image with its rotated and translated version using the fm-routine, the MSE-value of both images was determined as MSE =

0.0027. Repeating this test for several rotations, translations and different images resulted in comparable MSE values.
When matching two recordings of a tablet that was translated over known distances in between by moving the x-y table the translation parameters were also easily detected by the routine even though the images were not exactly the same now anymore.
Problems occurred when the tablet was rotated in between recordings, for small rotations that unavoidable lead to small translations as well because the tablet has to be moved, the output parameters were zero in many cases. For larger rotations the parameters were not zero anymore but in most cases far from correct. The reason for these poor results is not that the routine has trouble with rotations but in the second test more was changed besides the 2D transformation. The difference between both tests is that by translating the tablet through movement of the x-y table the tablet does not move with respect to the ground but when the tablet is picked up and put down again in a different position in between recordings the tablet does move in relation to the ground. Therefore when the surface where the tablet lies on is not exactly horizontal in the second test there is also a change in the z-direction between the two recordings. This situation was also described in 4.2.2.1. Because the flat holder has to be pressed onto the MicroCad's measuring plane it is practically impossible to do this in a way that it lies exactly horizontal. To minimize these effects in the following experiments the system was calibrated using the flat holder as reference plane, thereby simulating a horizontal ground. This improved the results, but might not be a real workable solution in all situations in future measurements. For instance when tablets must be compared to tablets that were recorded months ago under different calibration another approach is necessary.
The unwanted slopes in the measurements that disturb the matching can be treated as shading in the gray value images. Two different ways to deal with this shading were tested. The first approach was to remove the shading from the images before trying to match them. This was done by estimation of the background of the images and subtracting that background from the original images. To estimate the background a closing operation was applied. A gray-level closing consist of a maximum filter followed by a minimum filter of the same size, in these tests a filter size of 100 was used and the fm-matching gave good results. A major drawback of this technique is the appearance of the 'circles' in the resulting difference-images with the size of the used filters.

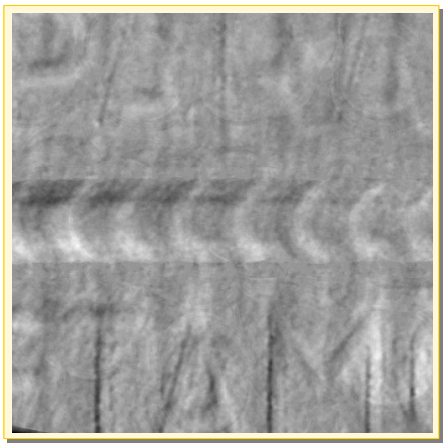

Figure 120 Example of circles due to shading correction using max en min filters

The second approach that was tested and indeed used in the following experiments is avoiding the problem by representing the images by their Laplacian-filtered versions and use those for the

matching. The Laplacian is a scalar second-derivative operator that is used to detect edges and is defined as

$$\nabla^2 f(x,y) = \frac{\delta^2}{\delta x^2} f(x,y) + \frac{\delta^2}{\delta y^2} f(x,y) \qquad [37]$$

Second derivatives produce an abrupt zero crossing at an edge and because the transfer function of the Laplacian is zero at the origin of frequency space it will suppress large slowly varying components of the image [14].
Thus by filtering the images with a Laplacian filter and use the output images for the matching, the fm-routine will try to match on the edges of the logos. The slopes caused by a non-horizontal ground that ruined the matching before are no longer present. This approach gave the best results and therefore the results of the experiments in following sections are shown in form of Laplacian-filtered images. Figure 121 shows an example of such a Laplacian-filtered image. This image as well as the ones in all following experiments was contrast stretched for display purposes, the 5 % of the pixels with the lowest gray-values are all mapped to 0, the highest 5% to 255 and all other values are mapped linearly in between.

Figure 121 example of Laplacian-filtered image of a paracetamol tablet

5.3.2 Two series of recordings of the same tablet

For this experiment a paracetamol tablet was rotated and recorded in the positions $\varphi = 0°$, $\varphi = 10°$, $\varphi = 20°$ … $\varphi = 90°$. This series was succeeded by a second using the same tablet and the same positions. The tablet's positions in the two series are never exactly the same though, for the placements of the tablet are done by hand. Z_{max} and Z_{min} values were registered for all recordings and used to adjust their gray level scaling. The Laplace operator was applied to all images before they were matched. The Laplacian-filtered images were matched as pairs using the fm-routine and the results for several positions are shown below. The Laplacian-filtered images of the second series were transformed using the output of the fm-routine and then subtracted from the Laplacian-filtered images of first series. The resulting images for the $\varphi = 0°, \varphi = 20°, \varphi = 30°, \varphi = 40°, \varphi = 50°$ and $\varphi = 80°$ image pairs are shown in Figure 122.

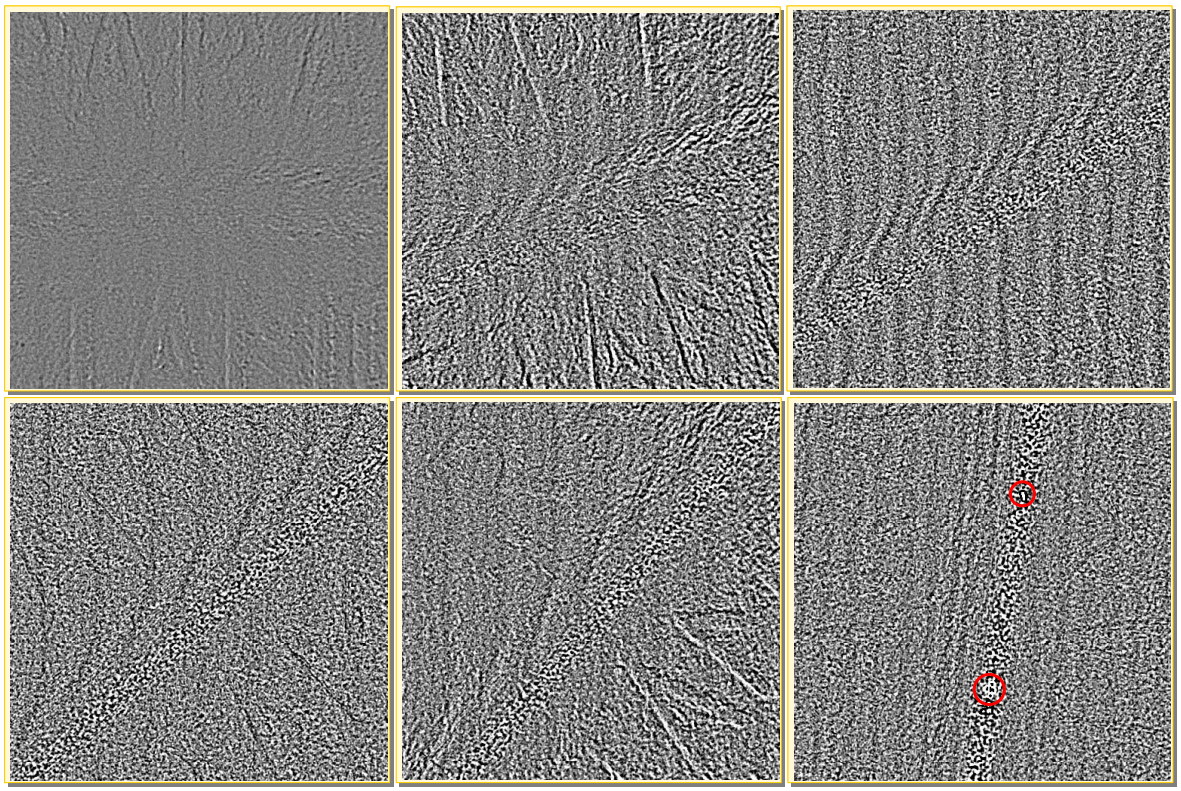

Figure 122 top row left to right: results for $\varphi = 0°$, 20°, 30° bottom row $\varphi = 40°$, 50° and 80°

The last image for $\varphi = 80°$ is not exactly the direct result from the fm-routine. Not all output parameters were applied in this case, the calculated translation parameters were so large that obviously something went wrong. The red circles in the $\varphi = 80°$ image indicate the position of occluded areas. These occluded areas that result in extreme values in the image cause problems because instead of matching on the edges of the logo the routine now tries to match the occluded areas of both images. Since the occluded areas are on different positions of the tablet in both $\varphi = 80°$ recordings this will never work. Occluded areas are always on the same side of the break line but when the tablet is moved just a little bit the location, size and shape can be a lot different. The presented image proves that ignoring the determined translation gives a good result the estimation of the rotation angle was apparently not influenced by the occluded areas.

The results are not satisfying for all positions in some images the logo is still visible indicating that the match could be better. The performance tests of the fm-routine proved that rotation angles smaller than $1°$ are not detected therefore for further improvement the estimation of the rotation angle must be refined. To do so another Matlab routine was written that rotates the second image over a range of $-1° \le \varphi \le 1°$ in steps of $0.1°$ subtracts the resulting image from the one of the first series and calculates their MSE. The output of this brute-force routine is the rotation angle that leads to the minimal MSE, the value of this MSE and the belonging difference image. The improvement on the images of $\varphi = 0°, \varphi = 20°$ and $\varphi = 50°$ is shown in Figure 123.

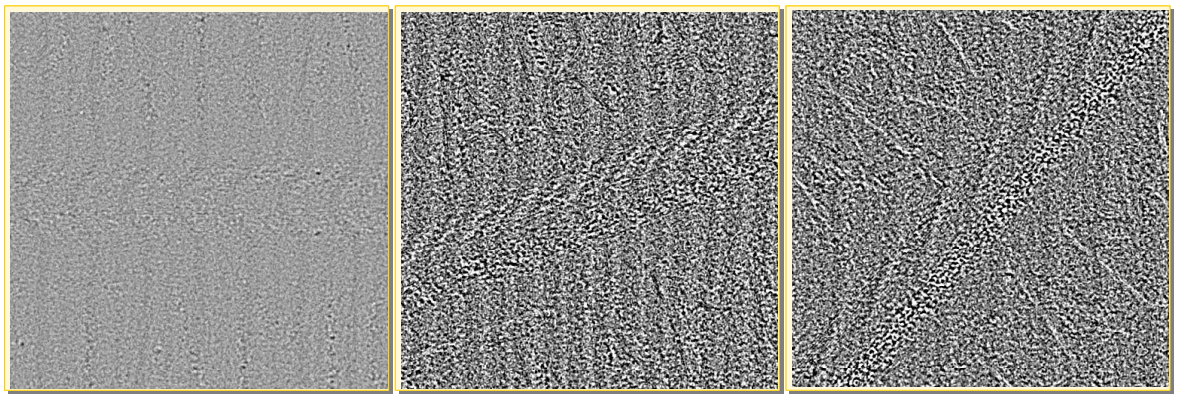

Figure 123 improved results after brute-force matching for $\varphi = 0°$, 20° and 50°

The rotation angles that were calculated by this brute-force method (BF) are given in Table 5-3 together with the belonging minimal MSE values. The MSE values for all other positions are given as well

Table 5-3: rotation angles calculated by brute force method and MSE values for all positions

position φ	rotation angle° (BF)	MSE (gray values)
0	0.3	0.081
10	--	0.090
20	-0.5	0.097
30	--	0.083
40	0.5	0.090
50	0.3	0.112
60	--	0.087
70	--	0.520*
80	0.9	2.164*
90	0.5	0.127*

To be able to evaluate these final results reference images and MSE values are needed, therefore the tablet was also recorded 10 times in the $\varphi = 0°$ position without moving it in between. Two of the resulting difference images are presented below in Figure 124 these two were chosen to show the spread in the results. The MSE values for both image sets are respectively 0.079 and 0.086 The fact that they contain the stripes as well indicates that their presence in the images above is not a result of poor matching.

* High value due to occlusion, corrected values for φ = 70°, 80° and 90° respectively: 0.0704, 0.1910 and 0.0926

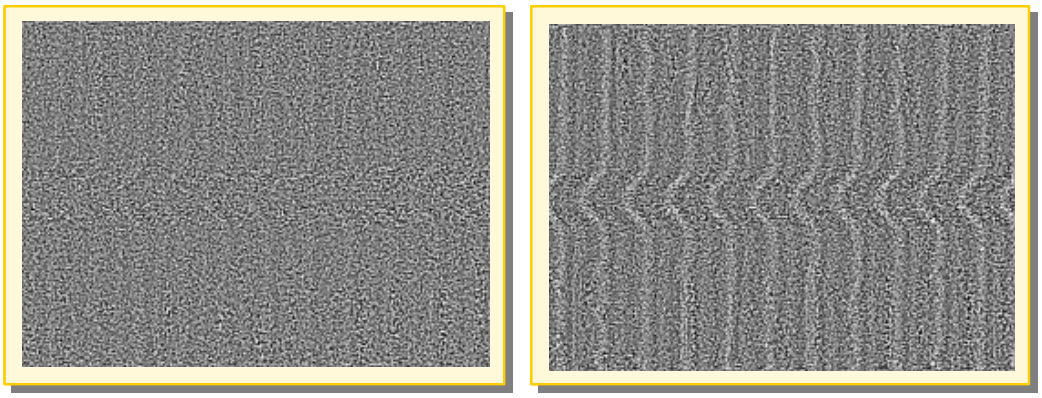

Figure 124 two examples of the difference between two recordings of the same tablet without moving it in between

That the matching is not optimal in all images is obvious but the extreme high MSE values for the $\varphi = 70°$, $\varphi = 80°$ and $\varphi = 90°$ images are the result of the occluded areas which not only ruin the matching but lead to a distorted notion of the MSE values as well. A solution for this situation can be to try and match the images without the occluded areas and calculate the MSE for a part of the image that does not contain these extreme values either. The second part of this approach was indeed tested and resulted in following reduced MSE values: 0.0704, 0.1910 and 0.0926.

5.3.3 Two series of recordings of two different tablets made with different punches

The set of tablets used for this experiment consists of the same paracetamol tablet as the one used in experiment 1 and another paracetamol tablet from a different box. When there is no further information about the manufacture of the two tablets it's impossible to be a 100 % sure upfront that they were made with different punches. But to increase the probability they were taken from different boxes that were bought a year apart and in different parts of the country. Another important clue that they were not made with the same punch was found by checking the position of the logo on the upper side with respect to the position of the one on the bottom. They are not the same for both tablets and even though there is always a possibility that the lower punch was replaced in the time between the manufacturing of both tablets while the top one was not in this experiment we will assume that they were made with different punches. A similar series of recordings was made of this second tablet. Again the tablet was placed in the same positions a well as possible by hand. After adjusting the gray value scaling and applying the Laplace operator on these images they were matched with the ones from the first series of the tablet from the first experiment. This series contained some unsatisfying results as well therefore the brute-force method was used on the positions $\varphi = 20°$ $\varphi = 50°, \varphi = 60°$ in order to improve the matching. The final results for the positions $\varphi = 10°, \varphi = 20°, \varphi = 50°$ $\varphi = 60°, \varphi = 70°$ $\varphi = 90°$ are given in Figure 125

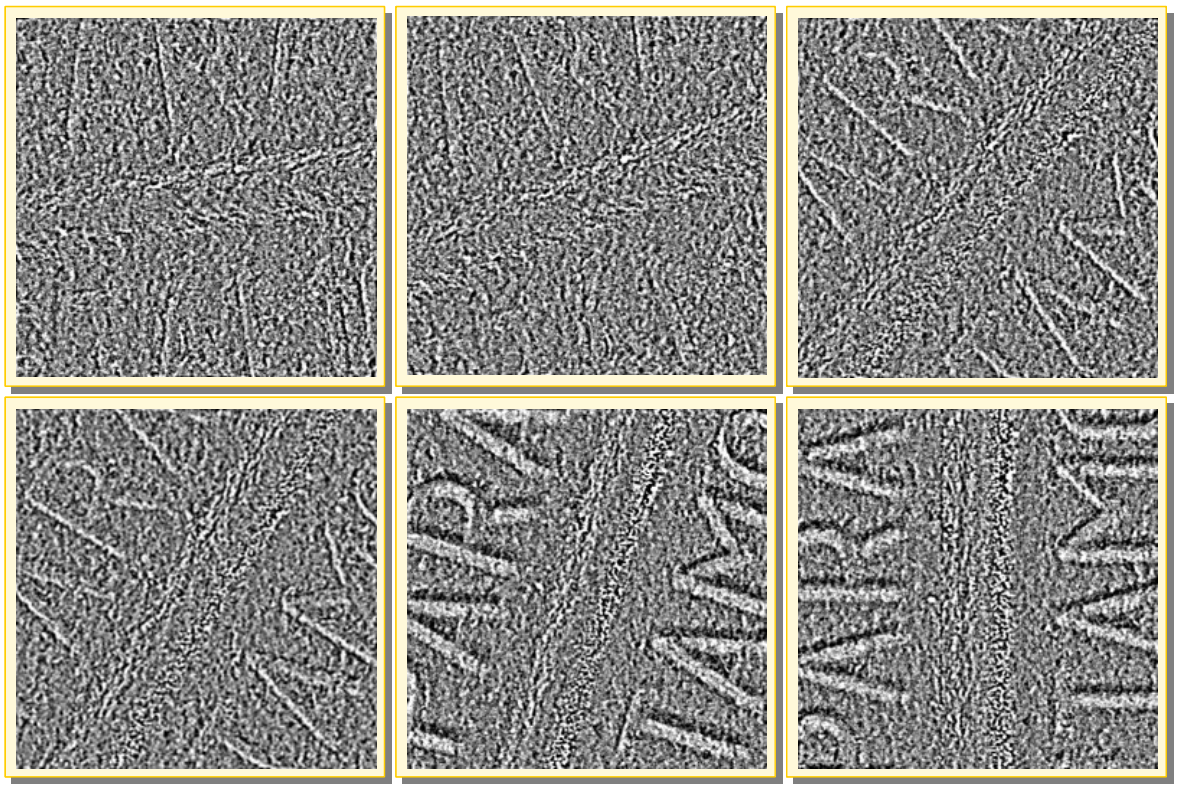

Figure 125 top row left to right: results for φ=10°, 20°, 50° bottom row φ= 60°, 70° and 90°

The MSE values that were calculated for all matched recordings are given in Table 5-4

Table 5-4 MSE values for all positions

Position	MSE (gray values)
10	0.295
20	0.287
30	0.309
40	0.333
50	0.332
60	0.344
70	0.648*
80	1.570*
90	0.437*

The MSE values for this series are much higher than the ones for the series of the first experiment. While in this case both tablets are known to be different, these high values are expected to be the result of differences in depth and shape of the imprints. To verify that this is indeed the case and the differences are not simply due to poor matching, cross-sections in several matched sets of images of both series were examined. The original images were matched using the parameters that were calculated with the FM-and BF- routines and the cross-sections of each image of a set were plotted together in the same figure. All sets of images were rotated into the

* High value due to occlusion, corrected values for φ = 70°, 80° and 90° respectively: 0.404, 0.497 and 0.395

same position to assure that the cross-sections of image sets of different positions were taken at roughly the same location on the tablet. This way the break lines were positioned horizontal in all images and the cross-sections were taken perpendicular, respectively parallel to it.

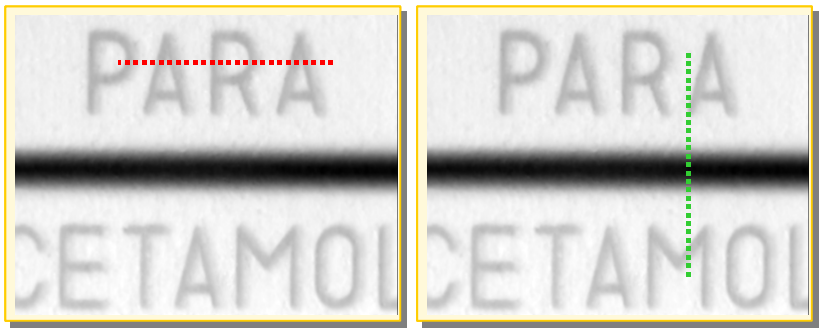

Figure 126 positions of the cross-sections

Figure 127 and Figure 128 show two sets of cross-sections from the first experiment. The blue lines in these and all following figures are the curves of the first series of the first tablet. In Figure 127 and Figure 128 the red lines are the curves for the second series of the first tablet and in Figure 129-Figure 130 they are for the second tablet.

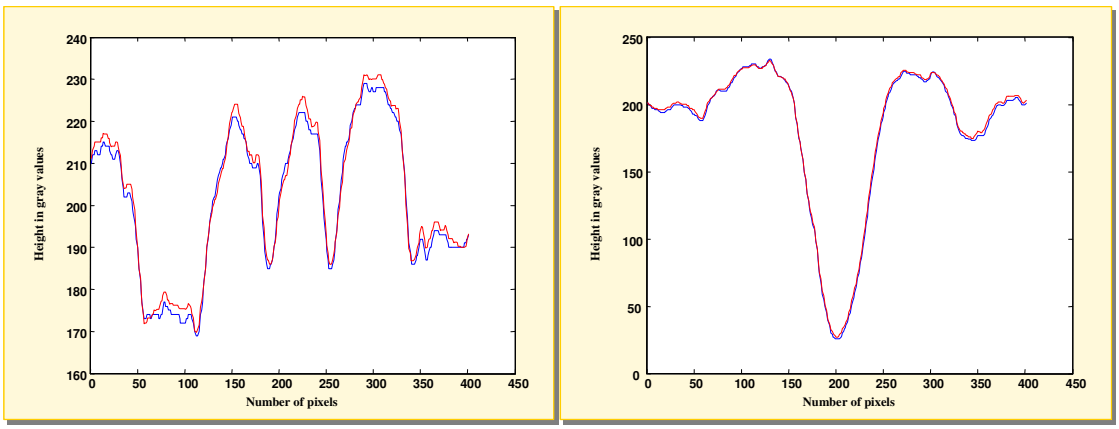

Figure 127 cross-sections in two matched φ=0° recordings of the same tablet, C = 2.07 µm/gray value

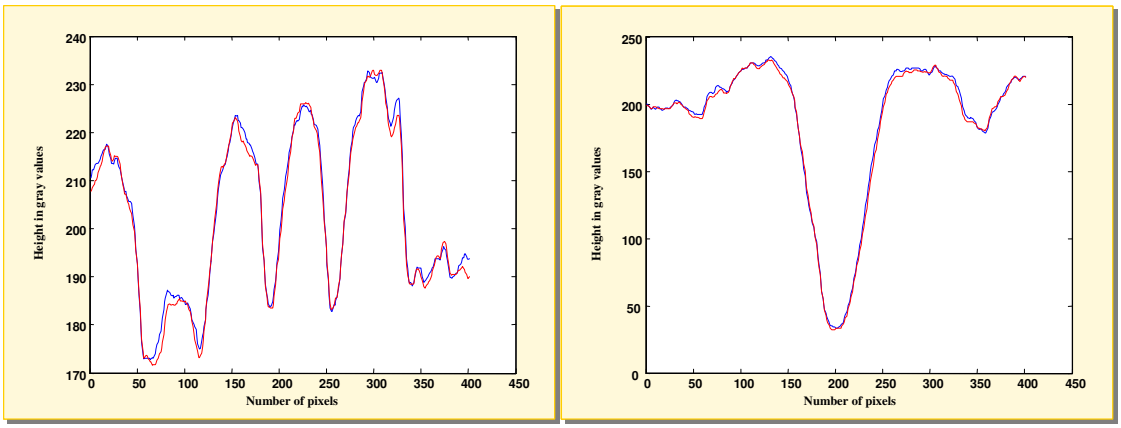

Figure 128 cross-sections in two matched φ=20° recordings of the same tablet, C = 2.07 µm/gray value

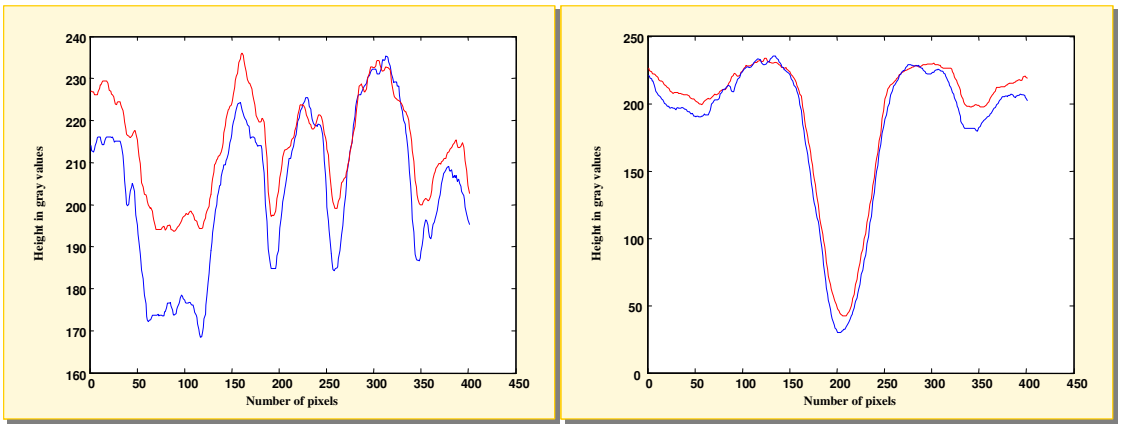

Figure 129 cross-sections in two matched φ=10° recordings of two different tablets, C = 2.07 µm/gray value

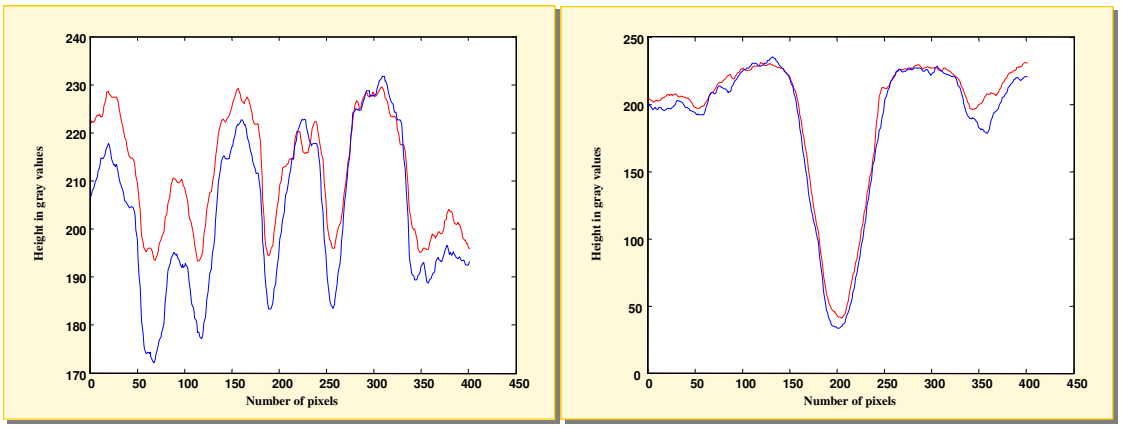

Figure 130 cross-sections in two matched φ=20° recordings of two different tablets, C = 2.07 µm/gray value

These four sets of cross-sections are a good representation of the situation and expose the cause for the large differences in MSE values between the images of the first and second experiment. The quality of the matching is comparable for both experiments, the differences are obviously caused by the fact that the images are simply not the same in the second experiment. Whatever matching method is used to improve these results they will never be as good as in experiment 1

because the curves simply do not fit. The ΔZ values that were used to adjust the gray value of the gray scaling of this series to the one of the first tablet indicate a significant difference in depth of both logos. The cross sections in Figure 129 and Figure 130 clearly confirm this. Whether this can lead to the conclusion that these tablets were not made with the same punch will be discussed in chapter 5. From the original data can be concluded that the tablets did not have the same thickness. This offset in Figure 129 and Figure 130 was removed to make the difference in depth and shape of the imprints more visible. The value of this offset was 35 gray values, or 72.5 µm. With an average thickness of a paracetamol tablet of approximately 4 mm this difference is in the order of 2 % .

5.3.4 Recordings of several different tablets made with the same punch

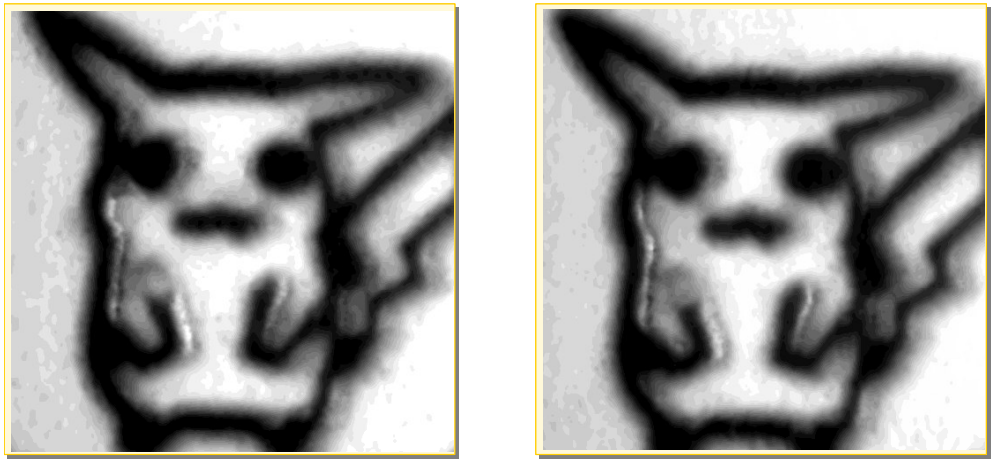

Figure 131 Recordings of two of the tablets used in this experiment

Since there is no way of knowing whether two paracetamol tablets were made with the same punch if they were not taken directly from the tabletting machine, for this test XTC-tablets from an actual case were used. Even though the only way to be a 100% sure is to use self-made tablets, the tablets used for this experiment are the closest to a sure thing as possible in this project. They were confiscated at a crime scene together with the tabletting machine and the punches. Besides the fact that they were found together which is not 100 % proof but a very strong clue, the tablets were also analyzed chemically and labeled as very likely to originate from the same source of manufacture. Another indication was found by examining the logos of the tablets and the punches with a microscope. The tablets were made using 7 punches simultaneously and the batch of tablets that was found next to the machine contained tablets with different characteristics that could be traced back to the seven individual punches. All above arguments together plea for an "on certainty bordering probability" label. Anyhow 6 tablets from this sample were measured in the same position, $\varphi = 0°$ and tablets 2-6 were all compared to the first tablet. Again their Laplacian-filtered images were matched using the fm-match routine and an example of the resulting difference images after the transformations were applied is presented below.

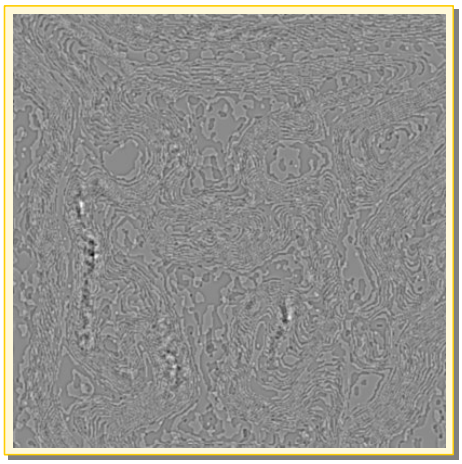

Figure 132 result for two tablets pressed with the same punch

Figure 131 shows that the recordings of the tablets in this experiment suffer from occlusion in several parts of the arms of the pikachu figure. The occluded parts did not disturb the matching in this case but they obviously lead to high MSE values. Using the same procedure as in earlier experiments these values were corrected and presented in Table 5-5. To determine the MSE value due to system noise and the matching procedure, the first tablet was recorded twice and these to images were matched as well.

Table 5-5 MSE values for tablets pressed with the same punch

Tablet numbers	MSE (gray values)
1 & 1	0.0143
1 & 2	0.0266
1 & 3	0.0242
1 & 4	0.0221
1 & 5	0.0257
1 & 6	0.0216

The difference between the first and the rest of the values in Table 5-5 shows that there is a variation in tablets that were manufactured using the same punch. To determine whether this variation is too large to be able to distinguish tablets pressed with different punches from different tablets pressed with the same punch a second experiment was done with tablets manufactured with different punches.

5.3.5 Second test with different tablets made with different punches

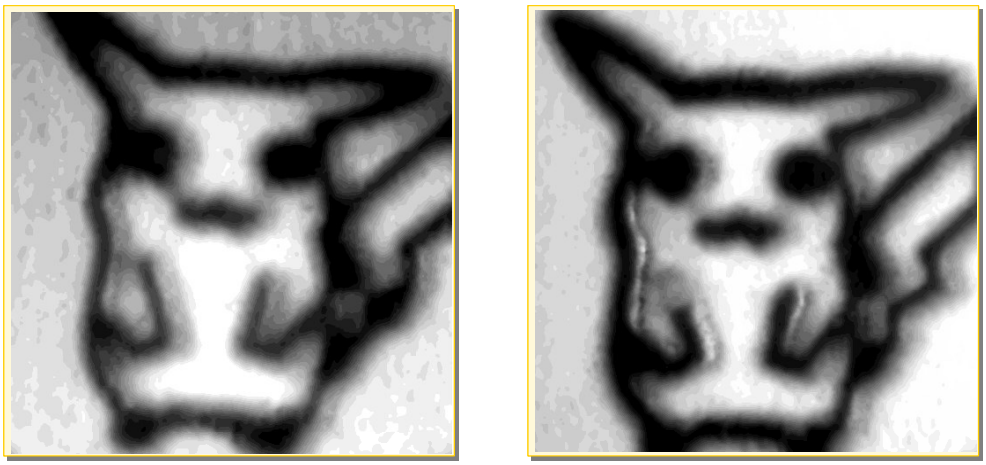

Figure 133 Recordings of two of the tablets used in this experiment

Another set of tablets was taken from the same case as the ones used in the previous experiment. But now one of the tablets was taken from a batch that was confiscated on another time at another place but contains tablets with a at first sight similar logo. They were brought in for analysis to determine whether it was possible that they were manufactured at the same location using the same punches as the tablets mentioned above. Chemical analysis showed that their composition was not the same and examination of the logos with a microscope indicated that only one of the characteristics of one of the seven punches was found on all tablets. The fact that all the tablets of the sample appear to be manufactured with one punch does not make it very likely that were made with the seven-punch tabletting machine cause it is not very likely that they were sorted out and distributed separately. Thus by taking one tablet from the sample that was labeled as belonging to the punches and one from the sample that was labeled as most likely to be not, we've got another set for this experiment. Again it's not waterproof but it's as good as it gets for this project. This experiment was done using 5 different sets, the procedure for the experiment is the same as for the previous one and the results are presented below. Numbers 1-5 are the same tablets as in the previous experiment, numbers 7-11 are the five tablets from the other batch.

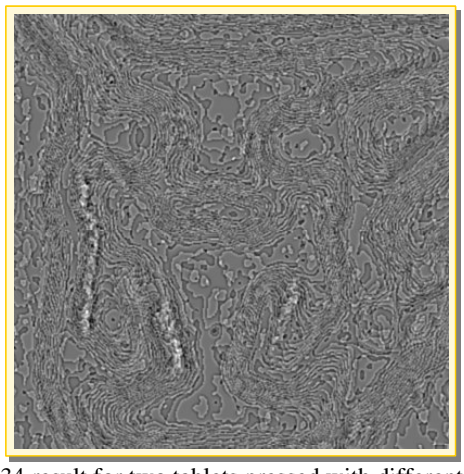

Figure 134 result for two tablets pressed with different punches

Figure 133 shows that the pikachu's in the recordings of the new series of tablets do not suffer from occluded armpits. The grooves of these imprints are apparently less steep then the ones from

the first series. The recordings reveal several other differences in the imprints as well. The left arm of the pikachu on the left is clearly longer than the one of the pikachu on the right of Figure 133 and the grooves in their tales are visibly different as well. Whether these differences lead to significantly higher MSE values was further examined in the same way as described in the experiments with the paracetamol tablets. The calculated MSE values are given in Table 5-6 and several cross-sections were made to reveal the difference between the values in this experiment and the ones from the experiment with the tablets that were manufactured with the same punch.

Table 5-6 MSE values for tablets pressed with different punches

Tablet numbers	MSE (gray values)
1 & 7	0.0443
2 & 8	0.0477
3 & 9	0.0395
4 & 10	0.0392
5 & 11	0.0412

These MSE values were corrected for the occluded areas in the recordings too. They are all higher than the ones in Table 5-5 and their spread is larger as well. This difference in spread is probably caused by the fact that in the first experiment one of the tablets was the same in each matching while in the second experiment both tablets are different for each pair. Using different sets decreases the chance that the results are dominated by possible accidental deviations of the one tablet that is used in each test, the results are more general. In the first experiment this was not done while there were only five tablets available.

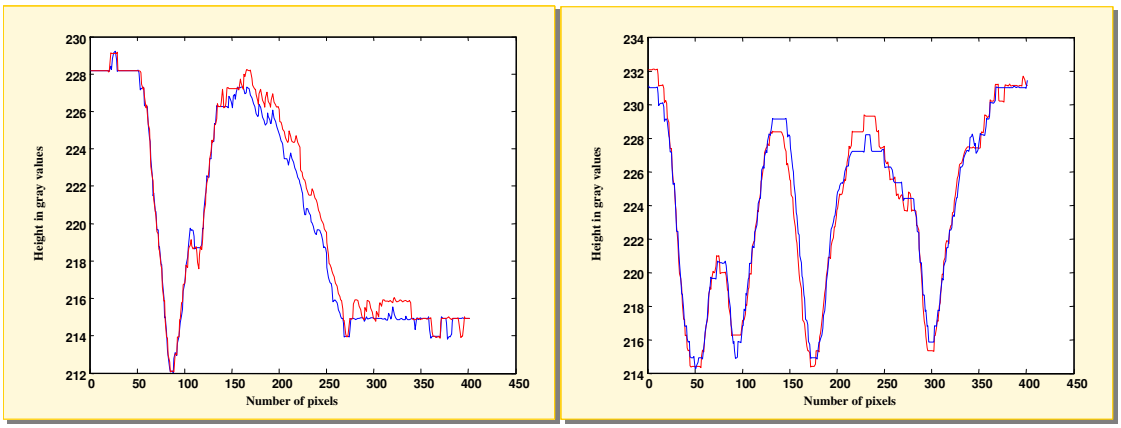

Figure 135 cross-sections in matched recordings of two tablets made with the same punch, C = 17µm/gray value

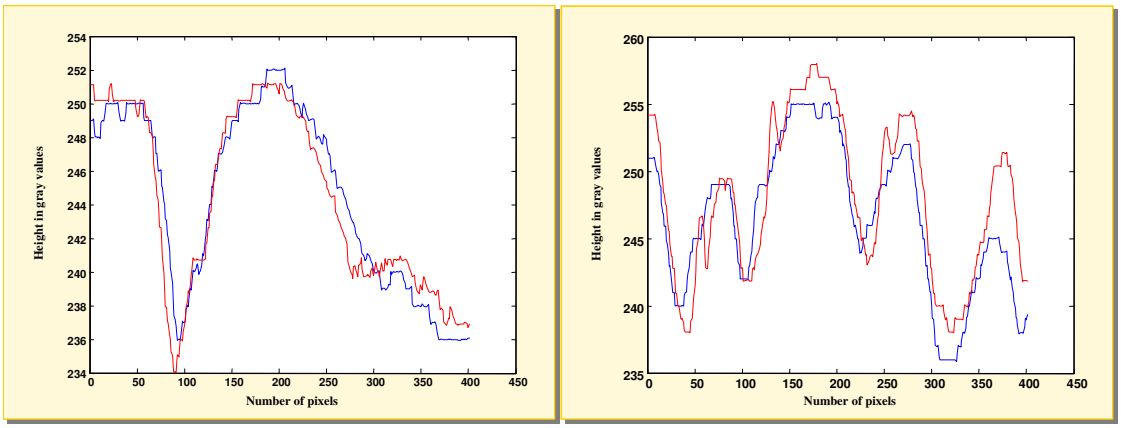

Figure 136 cross-sections in matched recordings of two tablets made with different punches, C = 17 µm/gray value removed off-set = 26 gray values

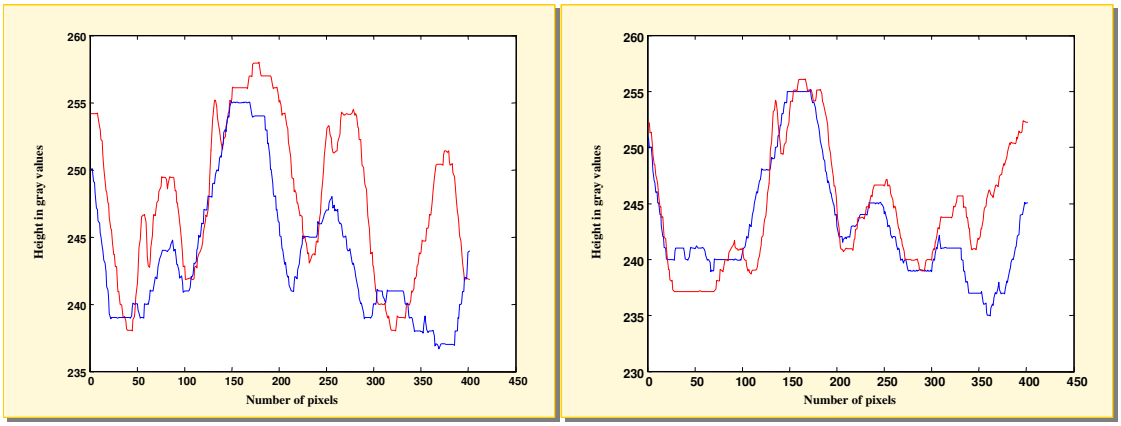

Figure 137 cross-sections in matched recordings of two tablets made with different punches, C = 17 µm/gray value removed off-set = 26 gray values

The red curves in Figure 136 and Figure 137 were shifted upwards for visibility purposes. An off-set of 26 gray values means in this case a difference in thickness of the tablets of 440 µm. The cross-sections in Figure 137 are taken at the locations in the recordings where they were visibly different, through the left arm and through the tale. They show that the curves will never overlap whatever matching techniques are used. The differences are significant while a deviation of 5 gray values in this situation means a height difference of 85µm that cannot be accounted for by noise. The cross-sections in Figure 136 were taken at the same positions in the recordings as the ones in Figure 135 and show that the differences are not as large in the rest of the images.

Conclusions

The difference between the first and the other 5 MSE values in Table 5-5 indicate that the tablets manufactured with the same punch do differ significantly. However there is no overlap with the values in Table 5-6 therefore it can be concluded that in spite of the large variation between the pikachu tablets that were manufactured with the same punch they can be distinguished from the ones that were manufactured using another punch.

5.3.6 Tablets containing rotational symmetric logos

For this experiment a paracetamol tablet from a different brand was recorded. The tablets of this brand do not have both letters and break line on the same side. The imprints on one of the sides only contain a single break line making them symmetrical. The tablet that was used for the experiment has a bump on one of the sides of its break line and is therefore well suitable to demonstrate the necessity for multiple recordings in case of symmetrical logos. A recording of the tablet in the $\varphi = 0°$ position is matched with a second one in the same position as well as with one of the tablet in the $\varphi = 180°$ position. It was also matched with recordings of another tablet in these same two positions. Whether this tablet was made with the same punch is unknown, it came from the same box but that is no argument since these tablets are made with tabletting machines that can stamp up to 32 tablets simultaneously and collected together before they are put into boxes. There is clear difference between the two though, making them useful for this experiment, the second tablet does not contain the bump. The matching for this experiment was done solely by matching the Laplacian-filtered versions of the recordings with the fm-routine, the results are shown in Figure 138.

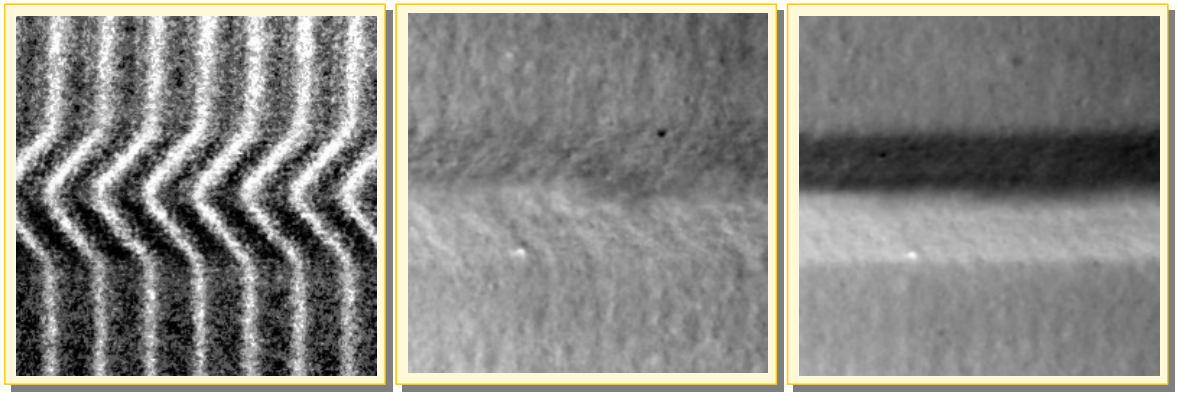

Figure 138 left to right results of matching with the same tablet for φ=0°, gray range = 8, φ=180°, gray range = 42 and with a different tablet, gray range = 74 and C = 3.82µm/gray value

These three difference images are here shown in original instead of their Laplacian-filtered versions for visibility purposes. The first image is obviously the result for the correct match its Laplacian filtered version has an MSE value of 0.050. The second image can be identified as the result of a $180°$ mismatch because the bump on the lower side of the break line is not just still visible indicating that it was only present at that position in one of the two matched images, its negative is also present at the opposite side. This mirrored version indicates that the second image does contain the same bump but was recorded in the $\varphi = 180°$ position instead of the $\varphi = 0°$. The last image is the result of a match with one of the recordings of the second tablet and shows that the bump was indeed only present on the first tablet cause its still visible in the difference image but its negative on the opposite side is no longer present. Considering the MSE values for the Laplacian-filtered versions of the last two images which are respectively 0.098 and 0.200 it seems that a $\varphi = 180°$ mismatch leads to a high MSE value but its still significantly lower than a mismatch between two tablets. Naturally these results alone are not enough to draw any hard conclusions because they are the outcome of just one experiment, they do however confirm the necessity for multiple recordings in case of symmetrical logos that was proposed in section 4.1.4

5.4 Tests method 2

To explore the second method in which all recordings of the rotated tablets will be combined into one perfect image, the fm-match algorithm was used to try and match all recordings of one tablet with its $\varphi = 0°$ recording. For this experiment the series that was used to determine the number of required recordings in section 5.1 was used again. The fm-routine was able to find rotation and translation parameters that were approximately correct for the $\varphi = 10°$, $\varphi = 20°$, $\varphi = 30°$ $\varphi = 40°$ images but for the $\varphi = 50°, 60°\ldots$ $\varphi = 90°$ the output parameters were clearly so far off that there was no use in applying them and check the results. Though by using the available foreknowledge in the second attempt the results were far more satisfying.

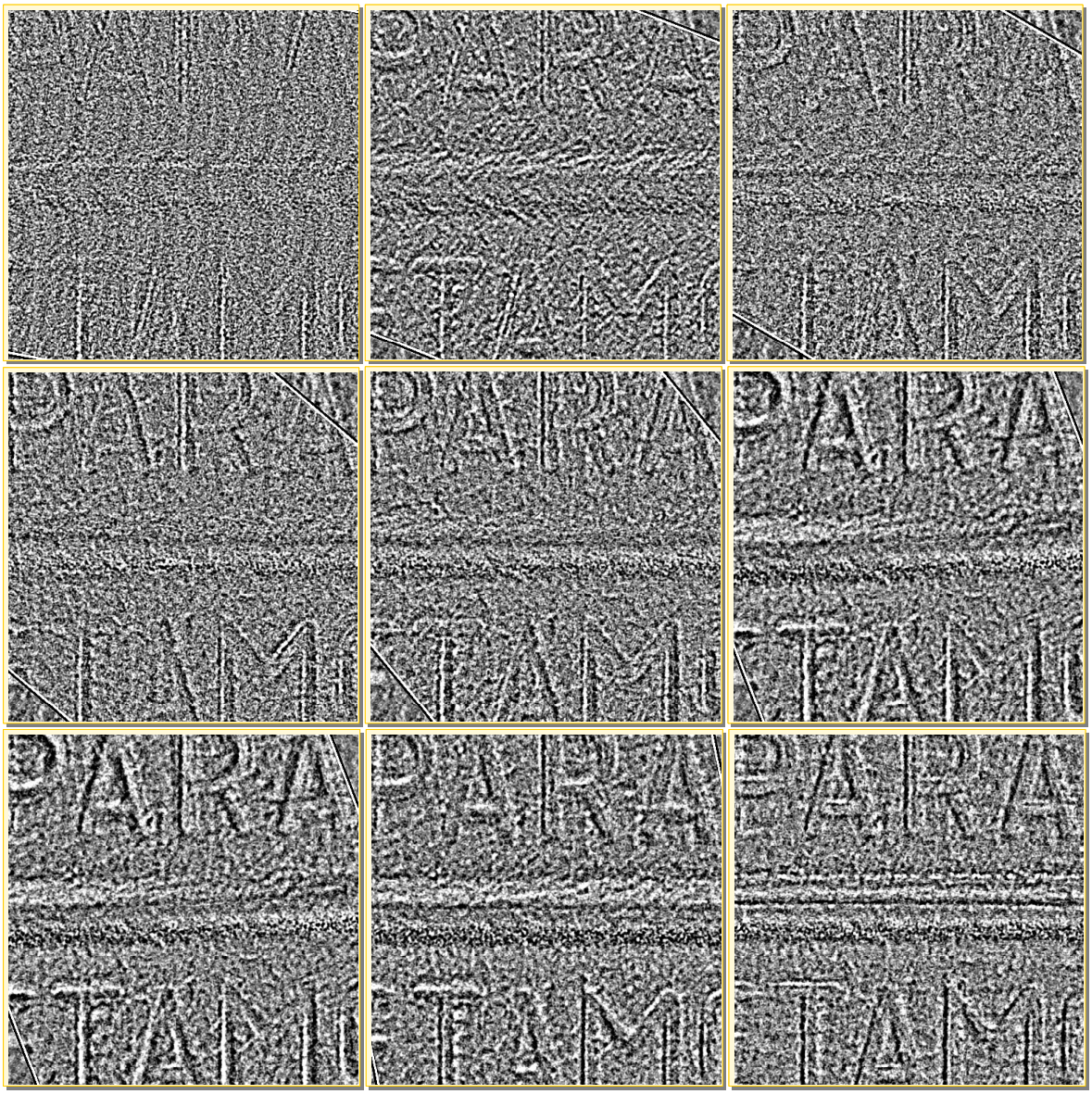

Figure 139 top row left to right: results for φ = 10°, 20°, 30° second row = 40°, 50°, 60° bottom row = 70°, 80°, 90°

While the rotation between the different images is approximately known they can be pre-matched roughly by rotating them before the final more accurate matching takes place. The results of this second attempt are presented for all rotation angles in Figure 139.
The MSE values for all positions were calculated and are given in Table 5-7. The images that were matched in this experiment do not each hold entirely the same part of the tablet. As a result parts of the images in Figure 139 do not contain reliable values because they are not the difference between the $\varphi = 0°$ image and the rotated one but solely the values of the $\varphi = 0°$ image because those parts were not recorded in the other position. The sizes of the images in Figure 139 are all 500x500 pixels and the above-mentioned parts are clearly visible cause they are bounded by black and white transition lines. The MSE values in Table 5-7 were therefore calculated over a square part of 350x350 pixels in the middle of each image.

Table 5-7 MSE values for all positions

Position	MSE (gray values)
10	0.1094
20	0.2045[1]
30	0.1285
40	0.1524
50	0.1789
60	0.1866
70	0.2571[2]
80	0.2630[2]
90	0.2780[2]

As could be expected from the images in Figure 139 these MSE values are much higher then the ones in the first experiment with the two series of the same tablet. To expose the reason for these poor results similar sets of cross-sections were made for these images as well. The locations of these cross-sections are the same as for experiments 1 and 2 and were given in Figure 126. Figure 140 shows the cross-sections for the matching of the φ=0° with the φ=10° recordings. Figure 141 and Figure 142 present the ones for respectively the φ=0° with φ=20° and φ=0° with φ=60° matching.

[1] High value due to poor matching
[2] High values due to occlusion

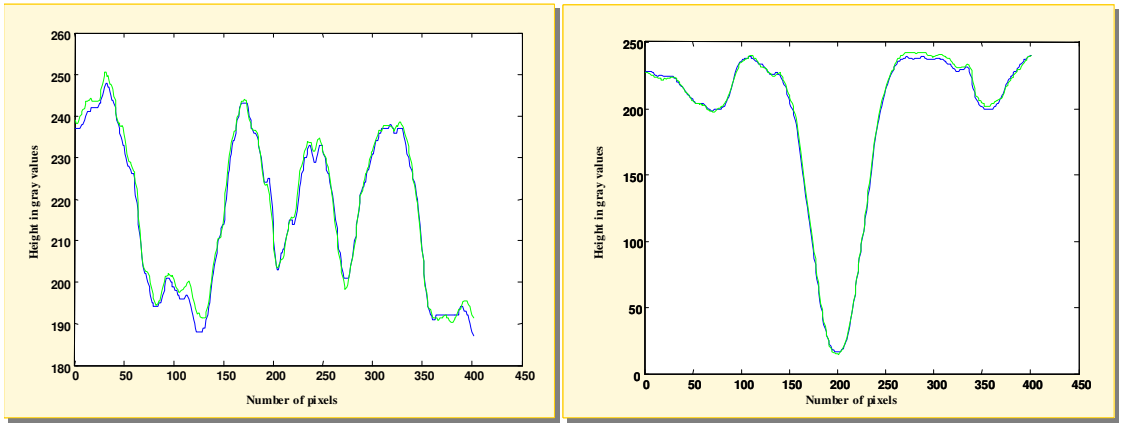

Figure 140 cross-sections in the well matched $\varphi = 0°$ and $\varphi = 10°$ recordings of the same tablet
C = 1.69 µm/gray value

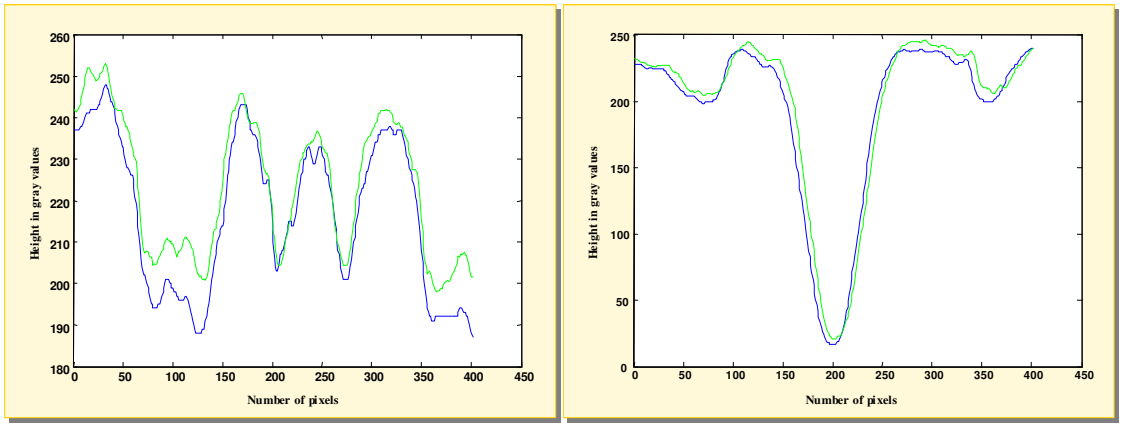

Figure 141 cross-sections in the not optimally matched $\varphi = 0°$ and $\varphi = 20°$ recordings of the same tablet
C = 1.69 µm/gray value

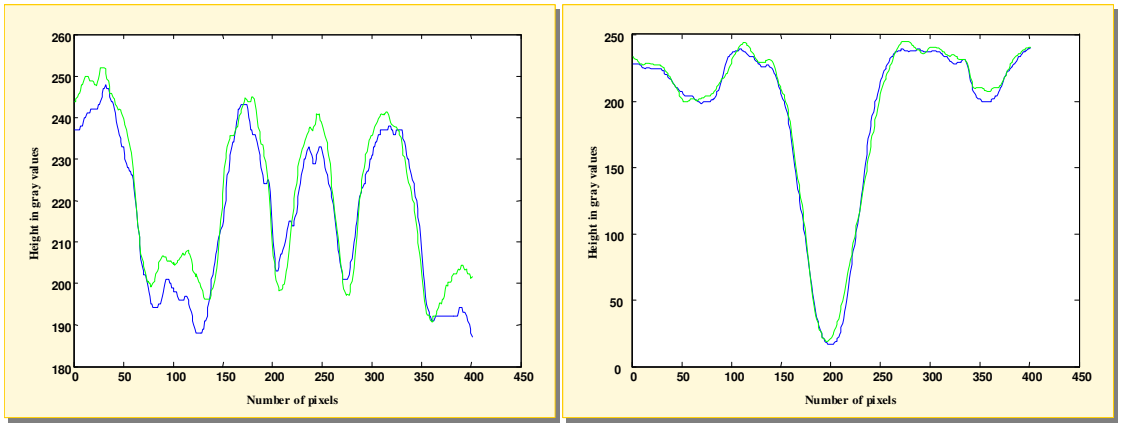

Figure 142 cross-sections in the well matched but too different $\varphi = 0°$ and $\varphi = 60°$ recordings of the same tablet
C = 1.69 µm/gray value

The cross-sections as well as the MSE values show a relation between an increasing rotation angle and increasing deviations. This relation was already discovered earlier in section 5.1. The

poor results are not caused by matching but simply by the fact that the images to be matched are not the same. The fact that they are not the same was also already predicted by the theory in section 4.1.2 about occlusion and is the reason why the multiple recordings are necessary in the first place. Similar cross-sections perpendicular to the break line were already shown in the experiment in 5.1 in Figure 82-Figure 87. Therefore the results in this experiment are not surprising. The extra high MSE value for the $\varphi = 20°$ image though is due to poor matching as well, as can easily be seen in Figure 141. Despite the fact that the two curves are indeed not exactly the same they still could be matched better causing the MSE value to drop and probably fit in with the others in Table 5-7.

Conclusions

Even though there are still options to improve the results, as there is for instance partial matching, this method doesn't seem to be the way to go. Partial matching means dividing the images in several parts match them separately and put them back together afterwards, by doing so not the entire image will suffer from certain parts that might be distorted due to occlusion. Combining the rotated recordings into one perfect image may sound as the most graceful way to do the comparison but due to this poor matching possibilities and the fact that there are several extra steps that may introduce more errors and certainly complicate the procedure it looses on practicality from method number 1.

6 CONCLUSIONS

- Due to occlusion it is not always possible to obtain a reliable depth image of the entire tablet in a single recording. The number of required recordings depends on the angles that are present in the imprint of the tablet. Experiments on paracetamol tablets proved that for imprints containing a break line with an angle of approximately 100 degrees, recording the rotated tablets with steps of 20 degrees is sufficient. Examination of a large number of XTC tablets shows that they contain break lines with similar or larger angles therefore 20 degree steps are sufficient for the average XTC tablet as well.

- In case of rotational symmetric logos multiple recordings are necessary as well while it is impossible to determine the $\varphi = 0°$ reference position.

- The tilted holder does not improve the image quality enough to counter balance the extra image processing steps that its use brings to the comparison process.

- The Mirocad system is able to detect bumps with diameters from 6 µm and heights from 10 µm in the break line or on any other part of the tablet.

- To examine whether the depth-images can be used to exclude the possibility of common sources of manufacture a number of experiments were conducted to determine the differences between depth images in several situations. After being matched using the FM- and possibly the BF-routine images are compared by calculation of the MSE-values of their Laplacian-filtered versions. By using the Laplacian filtered versions the matching is not disturbed by unwanted gradients caused by an uneven ground. Furthermore the MSE- values will not be dominated by differences in thickness of the tablets these differences should be reported but are not interesting for the identification of the used punch while the thickness of the tablets can be adjusted independent of the punches. Several experiments on paracetamol tablets and XTC tablets resulted in a series of MSE values for different situations that all showed no overlap. The situations that were examined are

  MSE due to matching (error due to interpolation and limited possibilities of the FM-routine)
  MSE due to system noise
  MSE due to system noise + matching
  MSE due to system noise + matching + variation in tabletting (different tablets made with the same punch)
  MSE due to system noise + matching + different punches

- The fact that there was no overlap between the different situations indicates that this procedure to detect mismatches using depth- images has potential and should be further investigated.

7 RECOMMENDATIONS

- The next step in this research is to translate differences between depth-images or extracted features of tablets into conclusions about the used punch. Considering all the aspects that play a role in determining the relevance of the features, it turns out to be impossible to draw meaningful conclusions based on the results from measurements on a few tablets. At least several punches are needed to examine the differences between them and to use statistics. It is also impossible to conclude anything when there are no tablets of which is known for certain that they were made with those punches. Therefore in order to continue this research it is necessary to have access to a tabletting machine, more then one punch that fits this machine and a large supply of XTC powder

- While the next step involves lots of recording and matching it is recommended to simplify the recording of the tablets as well as the matching by designing a new holder. This holder should contain a stepping motor that rotates the tablet over the desired angles and it should pinch the tablets somehow during rotation thereby eliminating unwanted translations. When the rotating is no longer done manually and translations are eliminated the matching will probably be improved as well.

- In further research on the determination of the source of detected bumps it is recommended to cooperate with the department of tool marks while this is obviously their field and their knowledge of production techniques and their forensic implications is needed to answer the questions involving the uniqueness of found damages.

- If a large 3D image database is available statistics on the characteristics of XTC tablets and punches can improve the knowledge on variations in these characteristics for forensic identification. It is therefore recommended to continue the development of such a database in cooperation with the group Intelligent Sensory Information Systems of the University of Amsterdam.

8 BIBLIOGRAPHY

[1] P.J.Gomm, I.J.Humphreys and N.A.Armstrong, “Physical Methods for the Compasion of Illicitly Produced Tablets”, Journal of Forensic Science, 16, 283, 1976.

[2] M.J.Vellekoop, P.W. Verbeek and J.J.Gerbrands, Sensorsystemen voor robottoepassingen, diktaat ET 4131 TU delft, faculteit ITS, Jan 1999.

[3] K. Sato, S. Inokuchi, “Three Dimensional Surface Measurement by Space Encoding Range Imaging”, Journal of Robotic Systems, 2, pp. 27-39, 1985.

[4] K. Creath and J.C. Wyant, “Comparison of interferometric contouring techniques”, SPIE Opt Test. Met. II, Vol 954, pp. 174-182, 1988.

[5] G. Sansoni, M. Carocci and R. Rodella, “Three-dimensional vision based on a combination of gray-code and phase-shift light projection”, J. App. Optics, vol 38-31, 1999.

[6] GFMesstechnik GmbH, Optical Measurement Coding Analyzation, 1998.

[7] www.ph.tn.tudelft.tudelft.nl/Diplib/

[8] T. Young, J.J.Gerbrands, L.J.van Vliet, Fundamentals of imaging processing, version 2.2, TU delft, 1998.

[9] D.E. Zaal, 3D Moire project, thesis, Netherlands Forensic Institute,1998

[10] K. Hyun, L.A. Gerhardt, “The use of laser structured light for 3D surface measurement and inspection”, IEEE Trans. Comp. Int. mfg. Aut. tech., 1994.

[11] Q. Chen, M. Defrise and F. Deconinck, “Symmetric Phase-Only Matched Filtering of Fourier-Mellin Transforms for Image Registration an Recognition”, Trans. Pattern Analysis Machine Intelligence, vol 16-12, Dec. 1994.

[12] www.ph.tn.tudelft.tudelft.nl/~lucas/education/et4085/2002/MultiDimImAnalysis.pdf

[13] C. Chatfield, Statistics for Technology, Third edition, Chapman & Hall, Londen, 1983.

[14] K.R.Castleman, Digital image processing, Prentice Hall Upper Saddle, 1996.

[15] A.H.Tillson and D.W. Johnson, “identification of Drug Tablet and Capsule Evidence as to Source”, Journal of Forensic Science, 19, 873, 1974.

9 APPENDIX A: MATLAB ROUTINES

9.1 Fmdemo.m

```
% [ES, ET, ER] = FMDEMO (IM, SCALE, TRANSLATION, ROTATION, DISPLAY, VERBOSE)
%
% Scale, translate and rotate IM and re-find these transforms using the
% Fourier-Mellin transform. Returns estimated scaling ES, translation ET and
% rotation ER.
%
% SCALE (default 1.0), TRANSLATION (default [0 0]) and ROTATION (default 0.0)
% specify the transforms. Note that TRANSLATION and ER should be (2,1)-
vectors.
%
% If DISPLAY=1, images will be shown (default 0); if VERBOSE=1, status
% messages will be displayed (default 0).

function [e_scale, e_translation, e_rotation] = ...
                                    fmdemo (im, scale, translation, rotation,
display, verbose)

      if (nargin < 6)
            verbose = 0;
      end;
      if (nargin < 5)
            display = 0;
      end;
      if (nargin < 4)
            rotation = 0.0;
      end;
      if (nargin < 3)
            translation = [ 0 0 ];
      end;
      if (nargin < 2)
            scale = 1.0;
      end;

      if (verbose)
            fprintf (1, 'Step 0: Transforming image by given parameters\n');
      end;

      [im1, im2] = transform (im, scale, translation, rotation);

      [e_scale, e_translation, e_rotation] = fmmatch (im1, im2, display,
verbose);

return
```

9.2 Fmmatch.m

```
% [ES, ET, ER] = FMMATCH (IM1, IM2, DISPLAY, VERBOSE)
%
% Match IM1 and IM2 invariant under scaling, rotation and translation,
% using the Fourier-Mellin transform. Returns estimated scaling ES,
translation
% ET and rotation ER of IM2 w.r.t. IM1.
%
% If DISPLAY=1, images will be shown (default 0); if VERBOSE=1, status
% messages will be displayed (default 0).
```

```
function [e_scale, e_translation, e_rotation, c] = ...
                                    fmmatch (im1, im2, display, verbose)

      if (nargin < 4)
            verbose = 0;
      end;
      if (nargin < 3)
            display = 0;
      end;

      if (display)
        f = 1; fx = 4; fy = 4; figure(1); clf;
      end;

      size_x = size(im1,1); size_y = size(im1,2); N = size_x;

      if (display)
            subplot (fx, fy, f); f = f + 1; imagesc (im1); axis off; colorbar;
colormap gray; axis square; title ('Image 1');
            subplot (fx, fy, f); f = f + 1; imagesc (im2); axis off; colorbar;
colormap gray; axis square; title ('Image 2');
      end;

      % STEP 1: LOG-MAGNITUDE OF FFT

      if (verbose)
        fprintf (1, 'Step 1: Take log-magnitude of FFT\n');
  end;

  fft_1 = fftshift(fft2(im1)); fft_1 = abs(fft_1); fft_1 = log(fft_1);
  fft_2 = fftshift(fft2(im2)); fft_2 = abs(fft_2); fft_2 = log(fft_2);

      if (display)
            subplot (fx, fy, f); f = f + 1; imagesc (abs(fft_1)); axis off;
colorbar; colormap gray; axis square; title ('Log-magnitude of FFT 1');
            subplot (fx, fy, f); f = f + 1; imagesc (abs(fft_2)); axis off;
colorbar; colormap gray; axis square; title ('Log-magnitude of FFT 2');
      end;

      % STEP 2: HIGHPASS FILTER

      if (0 == 1)
            if (verbose)
              fprintf (1, 'Step 2: Highpass filtering of LM-FFT\n');
      end;

        [xi,eta] = meshgrid(-size_x/2+1:1:size_x/2);
            X        = cos(pi*xi/size_x)+cos(pi*eta/size_x);
            H        = (1-X)*(2-X);
            fft_1        = H .* fft_1;
            fft_2    = H .* fft_2;

            if (display)
                  subplot (fx, fy, f); f = f + 1; imagesc (abs(fft_1)); axis
off; colorbar; colormap gray; axis square; title ('Highpass filtered LM-FFT
1');
```

```
              subplot (fx, fy, f); f = f + 1; imagesc (abs(fft_2)); axis off;
colorbar; colormap gray; axis square; title ('Highpass filtered LM-FFT 2');
            end;
      end;

      % STEP 3: LOG-POLAR CONVERSION

      if (verbose)
        fprintf (1, 'Step 3: Converting to log-polar coordinates\n');
      end;

      M = N; K = N;

  lp1 = logpolar(fft_1, M, K);
  lp2 = logpolar(fft_2, M, K);

  if (display)
            subplot (fx, fy, f); f = f + 1; imagesc (abs(lp1)); axis off;
colorbar; colormap gray; axis square; title ('Log-polar LM-FFT 1');
            subplot (fx, fy, f); f = f + 1; imagesc (abs(lp2)); axis off;
colorbar; colormap gray; axis square; title ('Log-polar LM-FFT 2');
      end;

      % STEP 4: PHASE CORRELATION

      if (verbose)
            fprintf (1, 'Step 4: Phase correlation\n');
      end;

      out_1 = fftshift(fft2(lp1));
      out_2 = fftshift(fft2(lp2));

  if (display)
            subplot (fx, fy, f); f = f + 1; imagesc (log(abs(out_1))); axis
off; colorbar; colormap gray; axis square; title ('F-M 1 (log)');
            subplot (fx, fy, f); f = f + 1; imagesc (log(abs(out_2))); axis
off; colorbar; colormap gray; axis square; title ('F-M 2 (log)');
      end;

  cps = (out_1 .* conj(out_2)) ./ abs(out_1.*out_2);
  c   = ifft2 (cps);

      if (display)
            subplot (fx, fy, f); f = f + 1; imagesc (abs(c)); axis off;
colorbar; colormap gray; axis square; title ('Phase correlation image');
      end;

      c = abs(c);

      [dummy,ix] = max(c);
      [dummy,iy] = max(dummy);      ix = ix(iy);

      e_rotation        = 180-(iy-1)/K * 180;
      if (ix < M/2)
            e_scale                 = (M-1).^((ix-1)./(M-1));
      else
            e_scale                 = 1./((M-1).^((M-ix+1)./(M-1)));
      end;
```

```
      e_rotation    = e_rotation * 2;                % !!!!!!!!!!!!
?????????????
      e_translation = [ 0 0 ];

      if (verbose)
            fprintf (1, 'Maximum at (%d,%d) => scale = %f, angle = %f\n', ...
                                                ix, iy, e_scale, e_rotation);
  end;

      if (verbose)
            fprintf (1, 'Step 5: Rescaling/rotating original image\n');
      end;

      [dummy, im1] = transform (im1, e_scale, [0 0], e_rotation);

% !!!!!
fprintf (1, '        REMOVING BORDERS!\n');
im1 = im1(25:end-25,25:end-25);
im2 = im2(25:end-25,25:end-25);

      size_x = size(im1,1); size_y = size(im1,2); N = size_x;

      if (display)
            subplot (fx, fy, f); f = f + 1; imagesc (im1); axis off; colorbar;
colormap gray; axis square; title ('Image 1');
            subplot (fx, fy, f); f = f + 1; imagesc (im2); axis off; colorbar;
colormap gray; axis square; title ('Image 2');
      end;

      % STEP 6: LOG-MAGNITUDE OF FFT

      if (verbose)
        fprintf (1, 'Step 6: Take log-magnitude of FFT\n');
  end;

  fft_1 = fftshift(fft2(im1));
  fft_2 = fftshift(fft2(im2));

      if (display)
            subplot (fx, fy, f); f = f + 1; imagesc (abs(fft_1)); axis off;
colorbar; colormap gray; axis square; title ('Log-magnitude of FFT 1');
            subplot (fx, fy, f); f = f + 1; imagesc (abs(fft_2)); axis off;
colorbar; colormap gray; axis square; title ('Log-magnitude of FFT 2');
      end;

      % STEP 7: HIGHPASS FILTER

      if (0 == 1)
            if (verbose)
              fprintf (1, 'Step 7: Highpass filtering of LM-FFT\n');
      end;

        [xi,eta] = meshgrid(-size_x/2+1:1:size_x/2);
            X        = cos(pi*xi/size_x)+cos(pi*eta/size_x);
            H        = (1-X)*(2-X);
            fft_1        = H .* fft_1;
            fft_2    = H .* fft_2;
```

```
            if (display)
                  subplot (fx, fy, f); f = f + 1; imagesc (abs(fft_1)); axis
off; colorbar; colormap gray; axis square; title ('Highpass filtered LM-FFT
1');
              subplot (fx, fy, f); f = f + 1; imagesc (abs(fft_2)); axis off;
colorbar; colormap gray; axis square; title ('Highpass filtered LM-FFT 2');
            end;
      end;

      % STEP 8: PHASE CORRELATION

      if (verbose)
            fprintf (1, 'Step 8: Phase correlation\n');
      end;

  cps = (fft_1 .* conj(fft_2)) ./ abs(fft_1.*fft_2);
  c = ifft2 (cps);

      if (display)
            subplot (fx, fy, f); f = f + 1; imagesc (abs(c)); axis off;
colorbar; colormap gray; axis square; title ('Phase correlation image');
      end;

      c = abs(c);

      [dummy,ix] = max(c);
      [dummy,iy] = max(dummy);      ix = ix(iy);

%     if (ix > (size(im1,1)/2)), ix = size(im1,1)-ix; else, ix = ix-1; end;
%     if (iy > (size(im1,2)/2)), iy = size(im1,2)-iy; else, iy = iy-1; end;
      if (ix > (size(im1,1)/2)), ix = -size(im1,1)+ix-1; else, ix = ix-1; end;
      if (iy > (size(im1,2)/2)), iy = -size(im1,2)+iy-1; else, iy = iy-1; end;

      e_translation = 2 * [ ix iy ];

      if (verbose)
            fprintf (1, 'Maximum at (%d,%d) => translation = (%d,%d)\n', ...
                                                ix, iy, e_translation);
  end;

return
```

9.3 Logpolar.m

```
% OUT = LOGPOLAR (IN, M, K)
%
% Performs a Cartesian to log-polar transform of image IN trough bi-linear
% interpolation. The OUT image will have size M x K, regardless of the size
% of IN.
%
% NOTE: Uneven sizes do not work yet, so IN should be square and M should be
% equal to K.

function out = logpolar (in, M, K)
```

```
  N = size(in,1);

  out = zeros (M,K);

      % Some abbreviations.

  c1 = (N/2-1)/(M-1);
  c2 = N/2-1;                                    % Used to be N/2

      % Min and max possible values.

  mins = zeros(M,K);
  maxs = ones(M,K)*(N-1);

      % Log-polar grid.

  [mm,kk] = meshgrid(1:M,1:K);

      % Find Cartesian (U,V) for log-polar grid [mm,kk].

  U = c1 .* (M-1).^((mm-1)./(M-1)) .* cos(2.*pi.*(kk-1)./K) + c2; U = U';
  V = c1 .* (M-1).^((mm-1)./(M-1)) .* sin(2.*pi.*(kk-1)./K) + c2; V = V';

      % For each position, find four neighbouring pixels. Clip at borders.

  F_U = min(max(floor(U),mins),maxs);
  F_V = min(max(floor(V),mins),maxs);
  C_U = max(min(ceil(U), maxs),mins);
  C_V = max(min(ceil(V), maxs),mins);

      % Now use neighbour coordinates as indices in original 'in' image.

      rin = reshape(in,1,N*N);
      G1 = reshape(rin(reshape(F_U,1,M*K)+N*(reshape(F_V,1,M*K))+1),M,K);
      G2 = reshape(rin(reshape(C_U,1,M*K)+N*(reshape(F_V,1,M*K))+1),M,K);
      G3 = reshape(rin(reshape(F_U,1,M*K)+N*(reshape(C_V,1,M*K))+1),M,K);
      G4 = reshape(rin(reshape(C_U,1,M*K)+N*(reshape(C_V,1,M*K))+1),M,K);

      % Calculate distances from position to each neighbour.

  D1 = 1-(U-F_U);
  D2 = 1-(C_U-U);
  D3 = 1-(V-F_V);
  D4 = 1-(C_V-V);

      % To avoid jumps...

  D1(U==F_U) = 0; D2(U==F_U) = 1;
  D1(U==C_U) = 1; D2(U==C_U) = 0;
  D3(V==F_V) = 0; D4(V==F_V) = 1;
  D3(V==C_V) = 1; D4(V==C_V) = 0;

      % Bi-linear interpolation.

  out = D3.*(D1.*G1+D2.*G2)+D4.*(D1.*G3+D2.*G4);

return
```

9.4 Transform.m

```
function [im1, im2] = transform (im, scale, translation, rotangle)

      im1 = im;
      im2 = im;

      if (scale ~= 1.0)
%           im2 = imresize (im, scale, 'bicubic');
            im2 = double (resample (dip_image(im), [scale scale], [0 0], '4-
cubic'));
      end;
      if (rotangle ~= 0.0)
%           im2 = imrotate (im2, rotangle, 'bicubic');
    im2 = double (rotation (dip_image(im2), -rotangle * pi/180, 3));
      end;

      sx2 = size(im2, 1); sy2 = size(im2, 2);

      im2 = im2(max(1,translation(1)):min(sx2,sx2+translation(1)), ...
            max(1,translation(2)):min(sy2,sy2+translation(2)));

      sx1 = size(im1, 1); sy1 = size(im1, 2);
      sx2 = size(im2, 1); sy2 = size(im2, 2);

      if (sx2 > sx1)
            offset2 = ceil((sx2-sx1)/2);
            im2     = im2(offset2:offset2+sx1-1,:);
      end;

      if (sx2 < sx1)
            offset2 = ((sx1-sx2)/2);
            im2     = [zeros(floor(offset2),sy2); im2;
zeros(ceil(offset2),sy2)];
      end;

      sx1 = size(im1, 1); sy1 = size(im1, 2);
      sx2 = size(im2, 1); sy2 = size(im2, 2);

      if (sy2 > sy1)
            offset2 = ceil((sy2-sy1)/2);
            im2     = im2(:,offset2:offset2+sy1-1);
      end;

      if (sy2 < sy1)
            offset2 = ((sy1-sy2)/2);
            im2     = [zeros(sx2,floor(offset2)) im2
zeros(sx2,ceil(offset2))];
      end;

return
```

10 APPENDIX B: MICROCAD SOFTWARE FUNCTIONS

The EDIT menu

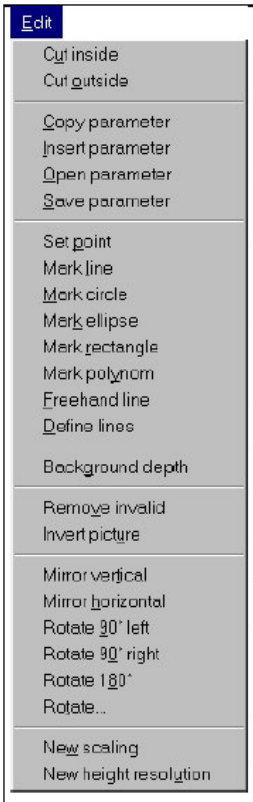

Cut inside	Cut out of a marked area of the height picture
Cut outside	Cut out of the height picture around a marked area
Copy parameter	Copy parameters of the marking (in the height picture) into the clip board
Insert parameter	Insert parameters of marking (into the height picture)from the clip board
Open parameter	Insert parameters of marking (into the height picture) from a marking file
Save parameter	Store parameters of the marking (in the height picture) in a marking file
Set point	Mark a point in the height picture
Mark line	Mark a line in the height picture
Mark circle	Mark a circle in the height picture
Mark ellipse	Mark an ellipse in the height picture
Mark rectangle	Mark a rectangle in the height picture
Mark polygon	Mark a polygon in the height picture
Freehand line	Mark a freehand line in the height picture
Define lines	Set lines with defined position in the height picture
Background depth	Change the background depth, i.e. background color of the height picture
Remove invalid	Assign of adjacent height value in case of absence of own height value for the measuring point
Invert picture	Inverts the height picture (calculation of the height picture print)
Mirror vertical	Mirror the height picture vertically
Mirror horizontal	Mirror the height picture horizontally
Rotate 90° left	Rotate the height picture 90° left
Rotate 90° right	Rotate the height picture 90° right
Rotate 180°	Rotate the height picture 180°
Rotate	Rotate the height picture a freely selectable angle
New scaling	Change the scaling of the height picture
New height resolution	Change the height resolution of the height picture

The MODIFY menu

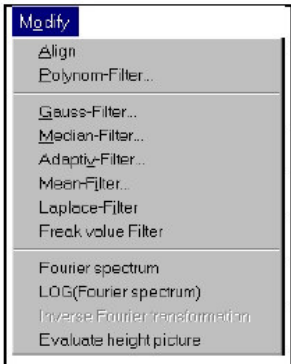

Align	Justify the height picture to its averaged plane
Polynom-Filter	Remove the deviation from a geometric form corresponding to selected class of polynom
Gauss-Filter	Apply a Gauss-Filter to the height picture
Median-Filter	Apply a Median-Filter to the height picture
Adaptiv-Filter	Apply a Adaptiv-Filter to the height picture
Mean-Filter	Apply a Mean-Filter to the height picture
Laplace-Filter	Apply a Laplace-Filter to the height picture
Freak value filter	Apply a freak value filter to the height picture
Fourier spectrum	Calculate the Fourier spectrum of the height picture
LOG (Fourier spectrum)	Calculate the logarithmic Fourier spectrum of the height picture
Inverse Fourier transformation	Calculate the height picture on basis of a Fourier spectrum
Evaluate height picture	Display a 3D picture of the color coded height picture

The EVALUATE menu

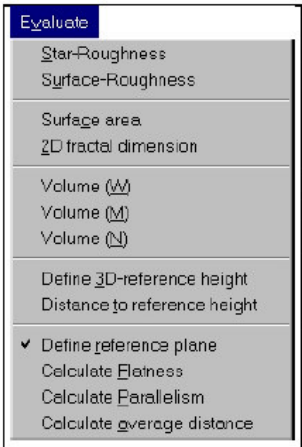

Star-Roughness	Determine star roughness parameters
Surface-Roughness	Determine area roughness parameters
Surface area	Determine "stretched" area of surface, marked before in height picture
2D fractal dimension	Fractal dimension is a parameter for description of surface structure
Volume (W)	Determine volume of height profile (or a part of it) below a reference plane
Volume (M)	Determine volume of height profile (or a part of it) above a reference plane
Volume (N)	Determine volume of height profile (or a part of it) below and above a reference plane
Define 3D reference height	Define the current height picture as reference height picture
Distance to reference height	Determine height difference of current height picture to height picture defined before as reference height picture
Define reference plane	Mark a reference area in the height picture
Calculate flatness	Determine the evenness of a connected height picture area. Outputs the max. macroscopic height difference after previous elimination of microscopic height variations by means appropriate filters. The concerning area should be defined before by means of the marking function.
Calculate parallelism	Determine the area parallelism of a selected part of height picture to a reference plane defined before. This function is available only after defining the reference plane. Outputs the max. height difference after aligning the marked areas parallel to reference area defined before.
Calculate average distance	Determine the average distance of marked areas of height picture to a reference area defined before.